Fabrication And Characterization of InP Semiconductor Ring Lasers

by

Raha Vafaei

B.Sc., The University of British Columbia, 2008

A THESIS SUBMITTED IN PARTIAL FULFILMENT OF
THE REQUIREMENTS FOR THE DEGREE OF

Master of Applied Science

in

The Faculty of Graduate Studies

(Electrical and Computer Engineering)

The University Of British Columbia

(Vancouver)

October, 2010

Abstract

This thesis investigates the fabrication of 1550 nm emitting InP semiconductor racetrack resonator lasers (SRLs) via wet etching techniques. The method of choice for SRL fabrication is reported to be via dry etching. Dry etching is a complex, time consuming and expensive process which leaves relatively rougher surfaces and sidewalls compared to wet etching techniques. In this thesis, coupling, racetrack resonators, and edge emitter laser theory were studied for the SRL design. Then, a fabrication process for the SRLs was developed via wet etching techniques. The light emitting diode (LED) characteristics of the fabricated devices were observed and successfully measured. The spectrum of the device was also measured with optical spectrum analyzer (OSA) and resonances were observed.

However, lasing was not observed. The cleaving process is a major limiting step in the fabrication and it is being improved. In parallel to the wet etching fabrication at UBC, dry etching (the common method for SRL fabrication) is being performed at the Centre de Recherche en Nanofabrication et Nanocaractérisation (CNR2) at the Université de Sherbrooke.

Preface

I am one of the co-authors in the Conference and Optics Letter titled, "Ring Resonator Reflector with a Waveguide Crossing" and "Design and Characterization of Microring Reflectors with a Waveguide Crossing" respectively. More specifically, I did the roundtrip loss value measurements and calculations, rebuilt and improved the SOI setup used for the measurements, performed some of the temperature measurements, wrote the curve fitting code which was modified by Wei Shi to fit his design and helped with the design procedure used to determine device parameters such as effective index, group index and coupling coefficients. The manuscript was written by Wei Shi.

I am one of the co-authors in the paper published in the Journal of Lightwaves titled, "Temperature Effects On Silicon-On-Insulator (SOI) Racetrack Resonators: a Coupled Analytic and 2D Finite Difference Approach". More specifically I did some of the design and analysis of the racetrack resonator, designed the SOI racetrack resonators that were fabricated and used to verify the design procedure and to study the temperature effects. I also did the quality factor analysis. The manuscript was written by Dr. Nicolas Rouger.

I am one of the co-authors in the SPIE paper titled, "Simulation of a 1550 nm InGaAsP-InP transistor laser", I researched the required p-type

contact composition for obtaining ohmic contact behaviour with the lowest reported resistance on the InGaAsP base contact layer. The manuscript was written by Wei Shi.

I am one of the co-authors in the poster titled, "SOI Nanophotonic Devices Analysis and Fabrication" presented at the Pacific Centre for Advanced Materials and Microstructures (PCAMM). More specifically I wrote the section on modelling and analysis of InP lasers, and provided the quality factor plot and the SOI racetrack resonator design.

The list of publications include:

1. Wei Shi, Raha Vafaei, Miguel Ángel Guillén Torres, Nicolas A. F. Jaeger, Lukas Chrostowski, "Design and Characterization of Microring Reflectors with a Waveguide Crossing", Optics Letters, vol. 35, issue 17, pp. 2901-2903, 09/2010.

2. Wei Shi, Raha Vafaei, Miguel Ángel Guillén Torres, Nicolas A. F. Jaeger, Lukas Chrostowski, "Ring Resonator Reflector with a Waveguide Crossing", 2010 International Conference on Optical MEMS and Nanophotonics, 09/08/2010.

3. Nicolas Rouger, Lukas Chrostowski, Raha Vafaei, "Temperature Effects On Silicon-On-Insulator (SOI) Racetrack Resonators: a Coupled Analytic and 2D Finite Difference Approach", Journal of Lightwave Technology, vol. 28, issue 9, pp. 1380–1391, 05/2010.

4. Wei Shi, Zigang Duan, Raha Vafaei, Nicolas Rouger, Behnam Faraji, Lukas Chrostowski, "Simulation of a 1550 nm InGaAsP-InP transistor

laser", Photonics and OptoElectronics Meetings, Proc. SPIE, vol. 7516, Wuhan, China, pp. 75160P-75160P-7, 08/2009.

5. Miguel Ángel Guillén Torres, Nicolas Rouger, Raha Vafaei, Shahrooz M. Amin, Robi Boeck, Behnam Faraji, Brendan Francis, Alina Kulpa, Juan Mario Michaan, Lukas Chrostowski, Nicolas Jaeger, Dan Deptuck, "SOI Nanophotonic Devices Analysis and Fabrication", Pacific Centre for Advanced Materials and Microstructures (PCAMM) Annual Meeting, 29/11/2008.

Table of Contents

Appendix

List of Tables

List of Figures

List of Abbreviations

- Semiconductor Racetrack Laser (SRL)

- Ridge Waveguide (RWG)

- Photoresist (PR)

- Infrastructure of Nanosctructures and Femtosciences (INRS)

- Centre de recherche en nanofabrication et nanocaracterisation (CNR2)

- Counter Clockwise (CCW)

- Clockwise (CW)

- Optical Injection Locking (OIL)

- Vertical Cavity Surface Emitting Laser (VCSEL)

- Finite Difference Time Domain (FDTD)

- Quantum Well (QW)

- Photoluminescence (PL)

- Ultraviolet (UV)

- Scanning Electron Microscope (SEM)

- Plasma Enhanced Chemical Vapor Deposition (PECVD)

- Electron Cyclotron Resonance (ECR)

- Reactive Ion Etching (RIE)

- Aspect Ration Dependent Etching (ARDE)

Acknowledgements

I would like to acknowledge the support, wisdom, leadership and friendship of my supervisor Dr. Lukas Chrostowski. In addition, I would like to acknowledge the support of all of my lab-mates, specially Wei Shi, Dr. Mark Greenberg, Dr. Nicolas Roger, Behnam Faraji and Miguel Ángel Guillén Torres for their daily discussions and brain storming sessions. I am very grateful to have had the chance to work along side them and to have had the opportunity to learn about optics in such a dynamic group.

Furthermore, I would like to acknowledge CMC Microsystems Inc. (Jessica Zhang, Dan Deptuck) for supporting the Silicon-On-Insulator racetrack resonator and InP semiconductor ring laser fabrication, and the Centre de Recherche en Nanofabrication et Nanocaractérisation (CNR2) at the Université de Sherbrooke (Vincent Aimee, Marie-Josée Gour, Jean-Francois Bedard, Etienne Grondin) for fabricating the semiconductor ring lasers via dry etching. I thank the BC Innovation Council for funding this research. Also, I would like to thank the committee (Nicolas A. F. Jaeger, Alireza Nojeh, S. Tang) for taking the time to read my thesis and provide me with their feedback.

I am very thankful to my family for all their love. My dad Masoud Vafaei, mom Sara Montazemi, sister Mina S. Vafaei and brother Rod Vafaei

have been continually supportive throughout my life and eduction. It is their unconditional love that has always been my biggest motivation for growth and learning.

I would also like to thank all of my great friends, for being there for me and supporting me.

Chapter 1

Introduction

1.1   Motivation

The continual advancement in communications has placed a growing demand on the innovation of optical communication systems to proceed to deliver integrated photonics and systems that are low cost, small sized and high bandwidth[4]. The region near 1550 nm emission is of interest, since optical fibers are available with losses as small as 0.15dB/km at this wavelength, making it a good candidate for long-distance optical communications [5]. Active ring resonators are desirable for optical monolithic integrated systems; they have been explored for applications such as optical amplifiers, optical flip flops (memory), optical digital processing (digital logic and switching), filters, and lasers. These active resonators can solve many drawbacks that passive resonators have been experiencing such as 1) lack of tune-ability 2) high insertion losses and 3) high optical switching powers [6]. One exciting area of interest is to use these active resonators as ring lasers for monolithic optically injection-locked laser systems, without the use of an isolator [4].

The modulation bandwidth (in GHz) of a directly modulated laser reveals the communication systems maximum achievable data rate (Gb/s). The best modulation bandwidths achieved by edge emitting lasers are up

to 40GHz [4]. Optical injection locking (OIL) can significantly improve the performance of directly modulated lasers. Using SRLs in OIL allows the removal of optical isolators by relying on the lasers' output asymmetry. Moreover, SRL cavity do not have any mirrors, gratings or cleaved facets; the rings' physical structure (i.e. width, height, radius) determines the optical modes. It is these inherent qualities of SRL that make it an exciting candidate for future optical interface technologies such as backplane and inter-chip communication [4].

1.2   Operating Principle

SRLs are made of two main components: 1) a straight bus waveguide and a 2) bent waveguide forming a closed loop. The region where the bus waveguide is close enough to the ring waveguide such that the fields in the two waveguides can interact is called the coupler region. The lasing action occurs in the bent waveguide resonator structure. Power is then coupled out of the resonator by the bus waveguide (power coupling factor affects the device performance and is a function of the coupler region design). To couple the power out of the bus waveguide, either a cleaved facet or a grating coupler is required.

Laser systems require three major components: 1) a pump (optical or electrical) to provide carriers required for light emission 2) an optical feedback to provide oscillation and 3) a gain region to provide amplification.

When current is applied to the ring/racetrack structure, lasing recombination takes place in the higher refractive index, active quantum well (QW)

region where spontaneous emission, stimulated emission and absorption are all happening simultaneously. When the laser is biased below threshold, only spontaneous emission can be observed. Laser threshold is reached once the device is biased at high enough currents such that the gain equals the cavity losses; the laser turns on at threshold. Increasing the bias current above threshold results in higher output power as long as the device is not overheating [5]. The wave-guiding layers provide orthogonal optical confinement. For a shallow etch design (where the waveguide structure is defined above the QWs), lateral confinement is defined by the air/wave-guiding layer refractive index contrast.

Laser oscillation in most laser systems such as in a Fabry-Perot Etalon laser, is achieved by the constructive interference of two counter propagating waves travelling between the two Fabry-Perot mirrors and forming a standing wave in the cavity. In the ring laser, the light is confined to circulate around the ring. However, two counter propagating waves can travel around the ring structure. One of the two counter propagating waves can be suppressed by experiencing higher losses and thus a unidirectional output can be obtained from the ring laser.

1.3 Literature Review

The preferred laser fabrication method used in industry for regular ridge waveguide (RWG) edge emitters and vertical Cavity surface emitting lasers (VCSELS) is wet etching or a combination of dry and wet etching. Wet etching techniques are preferred due to their lower processing costs, lower

processing time and lower optical losses [7–10]. To the best of our knowledge, there has been no reports of SRLs fabricated via wet etching techniques.
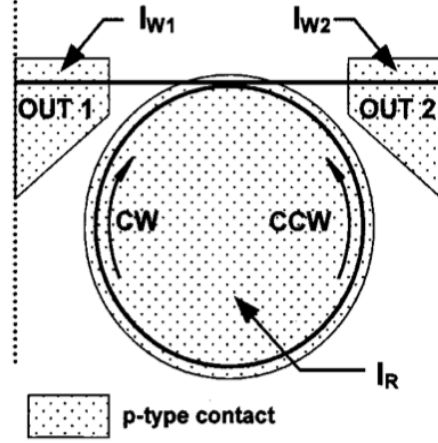
Figure 1.1: Geometry of the device showing the contact layout; I_R, I_{W1}, I_{W2} indicate the current biases applied to the ring and to the two output wave- guide contacts, respectively. The ring radius is 600 µm and the output waveguides are 800 µm long. Figure from Ref [11].

There are a few groups making SRLs in InP based materials, all with dry etching. In 2002, M. Sorel and P. J. R. Laybourn at the University of Glasgow and G. Giuliani and S. Donati at the University of Pavia published results on unidirectional bistability in large-diameter semiconductor ring lasers fabricated by CH_4H_2 reactive ion etching (RIE). Their design is shown in Figure 1.1 and had the following design parameters: ring radius of 600 µm, total length of the coupled waveguide of 1.6 mm, ring to output waveguide spacing of 1 µm, waveguide width of 2 µm [11]. They reported continuous wave measurements at room temperature exhibiting a threshold current of 125 mA. Figure 1.2 shows the optical spectrum of their device when biased
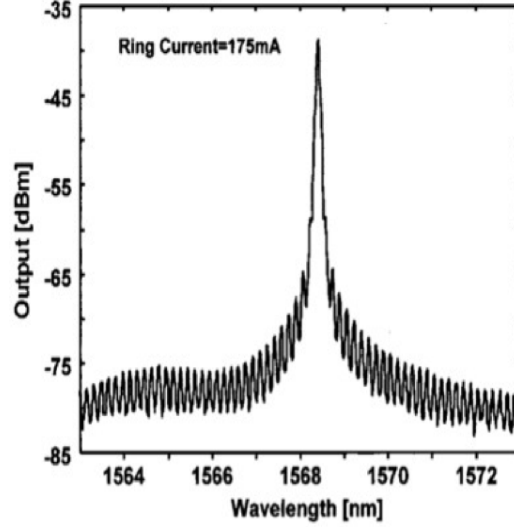
Figure 1.2: Showing a switching extinction ratio larger than 30 dB. The resolution of the optical spectrum analyzer is 0.1 nm. Figure from Ref [11].

at 175 mA.

L. Bach, J. P. Reithmaier, A. Forchel, J. L. Gentner, and L. Goldstein fabricated single-mode lasers by coupled micro-square resonators in GaInAsP-InP epitaxy; their stucture is shown in Figure 1.3. The devices were fabricated using Ar-Cl$_2$ electron cyclotron resonance (ECR)-RIE process and had width 4 μm, height 6 μm, radius 10-30 μm and threshold currents as low as 48 mA [12].

K. Amarnath, R. Grover, S. Kanakaraju and P. T. Ho from university of Maryland, published results on 0.8-1 μm wide, 20 μm radius, 5-10 μm long coupler length, deep etched, 1550 nm emitting microring lasers in 2005. Their design is shown in Figure 1.4. They were able to achieve threshold values as low as 12-20 mA [13].

5
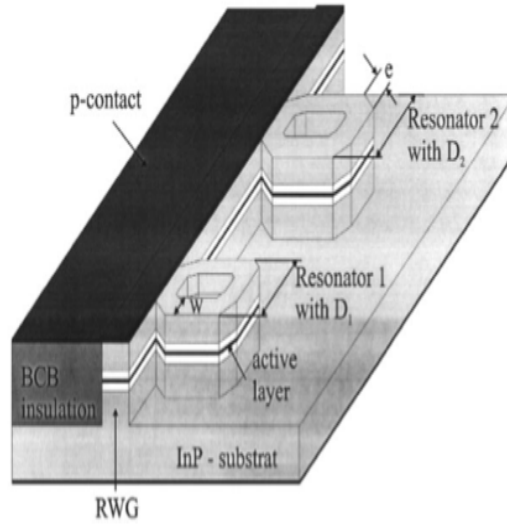
Figure 1.3: Schematic illustration of the device geometry with deeply etched RWG section and a strongly MMI-coupled pair of ring resonators with different diameters D_1 and D_2. The rings have square-like geometry with 45 C facets of width e. The resonators are also covered by BCB like the left side of the RWG. Figure from Ref [12].
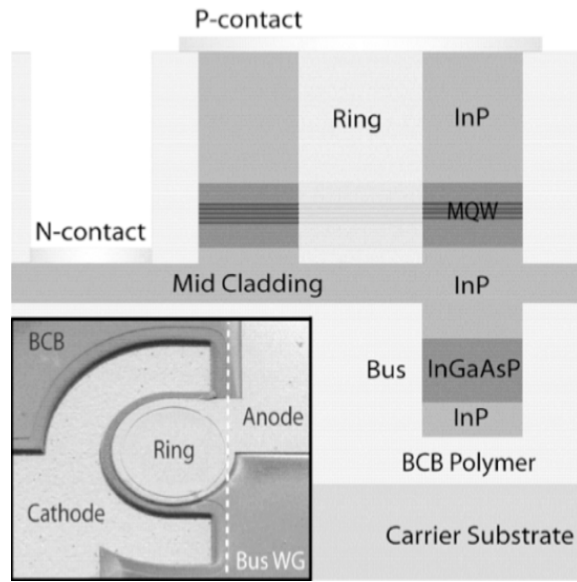
Figure 1.4: Schematic cross section of microring amplifier shoing the layer structure. Inset shows an SEM picture of a 20 μm radius microring device. The bus-waveguide (not visible) is shown as a dashed line. Figure from Ref [13].
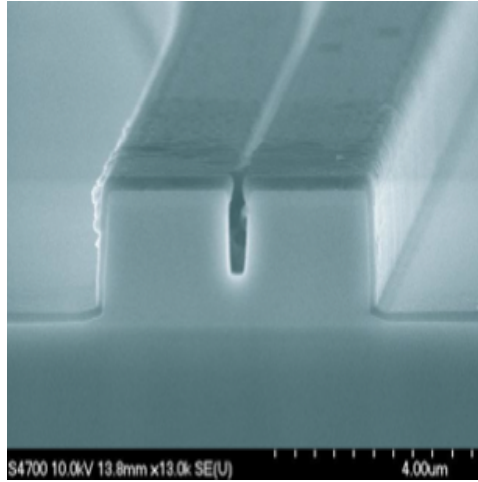
Figure 1.5: A cross sectional view in the coupling region of the waveguides etched down to the InAlAs layer and subsequently covered with 200 nm PECVD SiO2 (after removing the etching mask) for electrical passivation. The effect of small gaps on the etching: the coupler is not etched to the InAlAs layer. Figure from Ref [14]

S. Furst, M. Sorel, A. Scire, G. Giuliani and S. Yu Pavia published details on their high selectivity (between the upper cladding InP and the core layer AlInAs) RIE process in 2006. They achieved very smooth surfaces and a complete etch depth in the gap between the waveguide couplers [14]. Their dry etching recipe allowed precise control over the coupling (gaps as small as 0.5 μm) as well as reduction in losses resulting in a lower threshold current of 34 mA for a 150 μm ring radius for a structure emitting at 1300nm. They predicted theoretical values of 60 mA and 20 mA for rings of radii 100 μm and 170 μm correspondingly for an epitaxy emitting at 1550 nm [14]. Figure 1.5 shows the etching challenge of achieving a full etch depth in the gap region which was then solved by over etching with a selective recipe.

S. Park, S. S. Kim, L. Wang, and S. T. Ho published results on high-

density plasma etching of InP based SRLs using Cl_2-N_2 based gas mixtures. The addition of N_2 had an excellent effect on the InP reaction chemistry; it helped reduce the surface roughness and lateral etching. They fabricated SRLs with diameters 10 µm and 20 µm, gaps as low as 0.2 µm, waveguide width 0.8 µm, and threshold currents as low as 1.1 mA. In order to clear the 0.2 µm gap, the devices were over etched to achieve a 3 µm etch depth in the gap region and a 5 µm etch depth outside the gap region [15]. Figure 1.6 shows an SEM image of their fabricated SRL and Figure 1.7 shows the device spectrum.
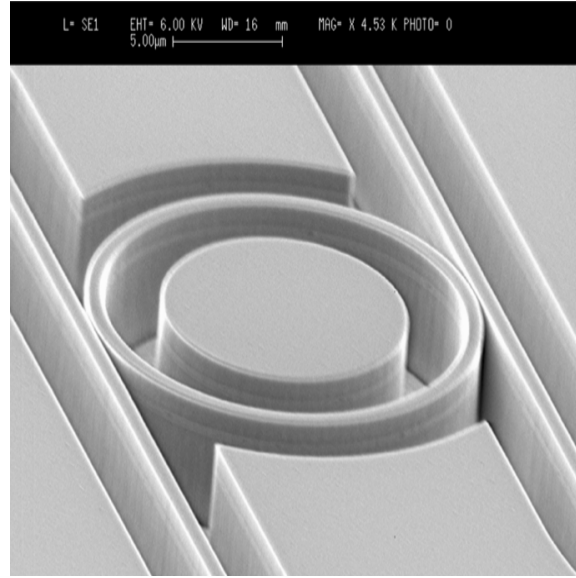
Figure 1.6: SEM image of a 0.8-µm-wide waveguide-coupled 20-µm-diameter ring resonator etched by ICP with 10/35/10 sccm Cl_2 N_2 Ar plasma at 200-W ICP power, 350-V dc bias, 2.3-mtorr pressure, 250 C temperature, and 400-nm/min etch rate. Figure from Ref [15].

A. W. Fang, R. Jones, H. Park, O. Cohen, O. Raday, M. J. Paniccia, and J. E. Bowers at the university of California reported a SRL integrated
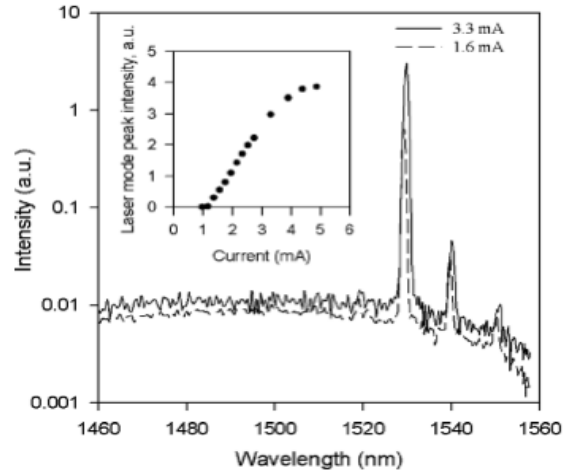
Figure 1.7: Spectra of scattered light from 20-µm-diameter microring laser and currentoptical output characteristics of a 20-µm-diameter microring laser (inset). Figure from Ref [15].
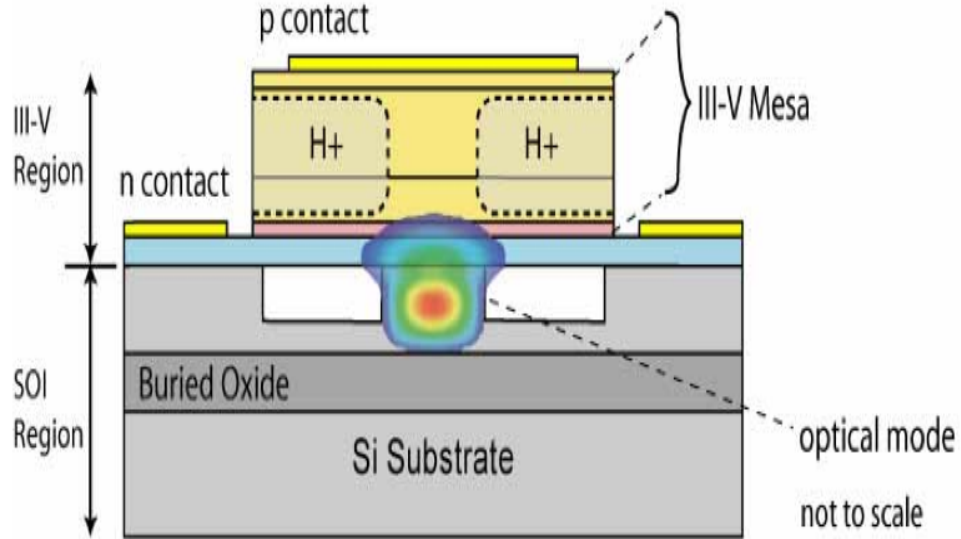
Figure 1.8: The hybrid silicon-evanescent device cross section structure. Figure from Ref [16].

with two photo-detectors on the hybrid AlGaInAs-silicon evanescent device platform. The SRL had a 200 μm radius, 0.5 μm gap, and 600 μm parallel coupler length. Running on continuous-wave at 1590 nm the laser had a threshold of 175mA, maximum total output power of 29 mW and a maximum operating temperature of 60 C [16]. The device cross section is shown in Figure 1.8.
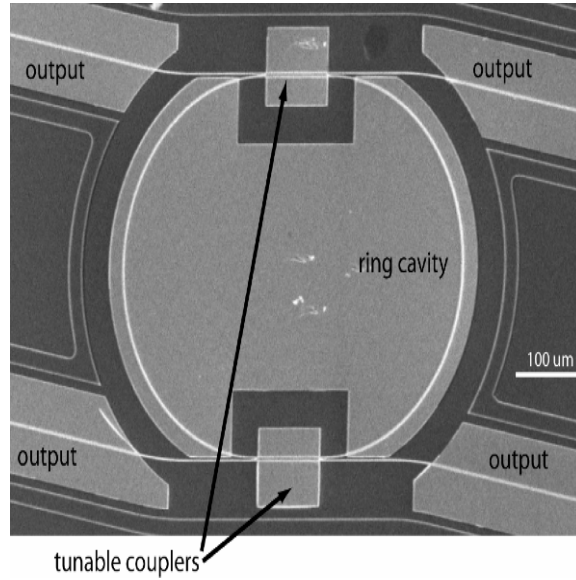
Figure 1.9: SEM image of fabricated SRL. Figure from Ref [14].

In 2008, Sorel and group made dry etched SRLs with tuneable evanescent couplers. Their fabricated design is depicted in Figure 1.9. They reported a coupler tuning ratio from 90% down to 10-20% with current injection values as low as 10 mA [14].

1.4   Objectives

The main objective of this thesis is to design, fabricate, and characterize SRLs in InP based materials. A large part of the project was invested in the fabrication of the SRLs. We aimed to develop a fabrication process for the SRLs via wet etching techniques.

1.5   Novel Contributions

The LED characteristics of the fabricated devices via wet etching were observed and successfully measured. The spectrum of the device was also measured with OSA and resonances were observed. The following were accomplished in the fabrication process:

1. A selective multiple step wet etch technique was developed to achieve InP waveguides with smooth surfaces, in-plane isotropy (equal etch rates in the x and y cross section), orthogonal to in-plane etch rate ratio of 2.

2. A planarization technique was developed using polyimide without any masking or plasma exposure.

1.6   Thesis Organization

SRL design was divided into 3 main sections:

1. Mode simulations were performed via Finite Difference Time Domain

(FDTD) mode solver to determine the main propagating mode, confinement factor, group index, crossover length and κ

2. Plots to summarize the dependency of output power and threshold current on cavity length, κ and propagation loss were obtained using Matlab.

3. Double bus passive resonators were designed in silicon on insulator (SOI), fabricated by Interuniversity Microelectronics Centre (IMEC) to further study the racetrack resonator, test the design process, and develop a parameter extraction method. The drop port output was successfully measured and the design parameters were extracted. The predicted design parameters matched the extracted parameters from the measurements, verifying the design method.

After the design section the devices were fabricated at the Advanced Materials and Process Engineering Laboratory (AMPEL) Nanofabrication facility in UBC. The following steps were taken and will be discussed in more detail:

1. The required mask was designed via a script and purchased. A commercial InP epi-wafer was purchased to eliminate epi-wafer design challenges.

2. A photolithography process was developed to successfully achieve a resolution better than 1 μm.

3. A selective multiple step wet etch technique was developed to achieve InP waveguides with smooth surfaces, in-plane isotropy (equal etch rates in the x and y cross section), orthogonal to in-plane etch rate ratio

of 2. A new planarization technique was developed using polyimide without any masking or plasma exposure.

4. Ohmic metal contacts with reasonably low resistance (roughly 1Ω) were found for the n-type and p-type contact layers.

5. SRL and RWG samples were fabricated via wet etching

6. A suitable setup was made for the measurements of edge emitting lasers. Matlab codes were written (some based on previously available codes) to automate most of the measurement process.

7. Devices were manually cleaved and the LED characteristics and optical spectrum were successfully measured.

8. Dry etching of SRLs were started in collaboration with CNR2 at the Université de Sherbrooke.

Chapter 2

InP Racetrack Laser Design

2.1   Purpose

The aim of this chapter is to study the laser theory and design the SRL physical parameters such as waveguide dimensions, coupling spacings and predict the threshold and output power.

2.2   Mode Calculation

The design is based on a conventional InP laser epitaxy commercially available from LandMark Optoelectronics Inc with details provided in Table 3.2. A simplified structure was used for FDTD mode simulations using Lumerical. Because the waveguiding layers are followed by relatively thicker InP layers, only the waveguiding layers (layers 4 to 7 in Table 3.2) were included in the simulated structure and the rest of the material was assumed to be that of bulk InP. The index values for the layers were calculated using the material information depicted in Table 2.1 and Equations 2.1 and 2.2, all provided by Crosslight (a commercial software used for laser/active optic simulations and design). For calculating the refractive index of the quantum well (QW) and barrier layers, initial guesses for the x and y compositions in

In$_{1-x-y}$Al$_y$Ga$_x$As, based on the following references [17] [18], were inputed into Equations 2.1 and 2.2 to achieve the material stress values of Table 3.2. The refractive index amplitude profile results are depicted in figure 2.1. The QWs and wave-guiding layers have higher refractive indices and lower band gaps compared to the InP n and p regions, thus, providing lateral optical confinement.

$$n_{InAlGaAs} = n_{InAs} + x(n_{GaAs} - n_{InAs}) + y(n_{AlAs} - n_{InAs}) \qquad (2.1)$$

$$a_{InAlGaAs} = a_{InAs} + x(a_{GaAs} - a_{InAs}) + y(a_{AlAs} - a_{InAs}) \qquad (2.2)$$

Table 2.1: Refractive Index and Lattice Constant Data

Material	Refractive Index	Lattice Constant
InP	3.164	5.8688
GaAs	3.65	5.65325
InAs	3.892	5.6605
AlAs	2.92	6.0584

The mode simulations via the FDTD mode solver showed 4 different possible modes; however, due to their distribution the higher order modes will be subjected to higher losses (i.e. scattering and bending). Eventually the other modes will lose and only the first order mode will be significant to the lasing. The main mode distribution is shown in Figure 2.2 (a) and the
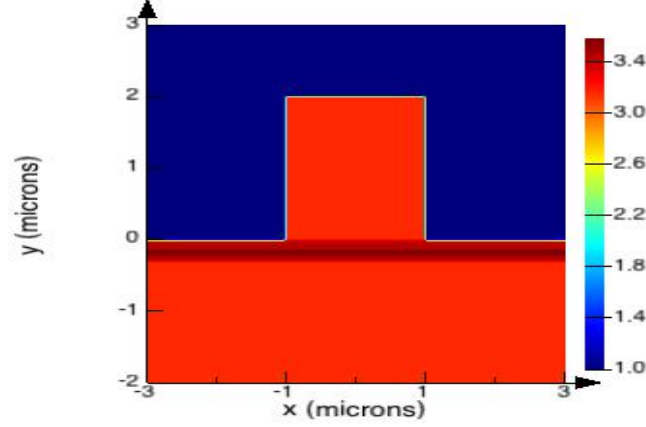
Figure 2.1: The index amplitude profile for $\lambda = 1550$ nm simulated in FDTD. The QW refractive index $= 3.5889$ with $In_{1-0.65-0.15}Al_0.15Ga_{0.65}As$. The barrier refractive index $= 3.5130$ with $In_{1-0.12-0.36}Al_0.36Ga_{0.12}As$. Taking x $= 0.03$ and y=0.44 as provided in Table 3.2, the upper $In_{0.53}Al_{0.44}Ga_{0.03}As$ layer's refractive index $= 3.4254$.

second order mode distribution is shown in Figure 2.2 (b). The portion of the mode in the active region will experience gain. The field intensity data was imported into Matlab in order to solve for the mode confinement factor Γ, for rectangular waveguides of width W and height H and trapezoidal waveguide of top width W_T and bottom width W_B:

- Rectangular waveguide: W = 2 μm, H= 2 μm $\Rightarrow \Gamma = 8.9\%$

- Rectangular waveguide: W = 3 μm, H= 2 μm $\Rightarrow \Gamma = 8.8\%$

- Trapezoidal waveguide: $W_T = 1$ μm, $W_B = 3$ μm, H = 2 μm $\Rightarrow \Gamma = 8.82\%$

The trapezoidal structure was considered to take into account the effect of wet etching during fabrication as it will be discussed later in the Fab-

17

rication chapter. However, it seems that the 3 considered structures have very similar mode confinement factors. The gain experienced by the mode varies with $1/t$, where t is the thickness of the active layer. The two main factors responsible for achieving low threshold in this semiconductor are: 1) confinement of injected carriers in the QW. and 2) confinement of optical mode in the QW.
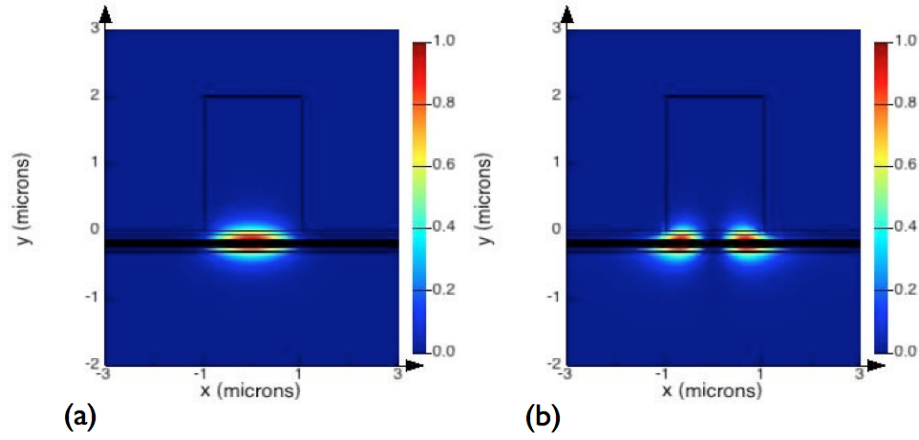
Figure 2.2: (a) First order mode distribution for $\lambda = 1550$ nm simulated in FDTD. It has an effective index of 3.276593. (b) Second order mode distribution for $\lambda = 1550$ nm simulated in FDTD. It has an effective index of 3.238451. This mode will not lase since it will experience higher losses (i.e. bending and scattering losses) relative to the first mode.

2.3 Racetrack Laser Coupler Design

The purpose of this section is to design the coupler of the semiconductor racetrack laser (SRL) and derive the coupling relationship with respect to the coupler's physical parameters such as waveguide width, height, length

and spacing.

The SRL output coupling loss (analogous to the mirror loss), is calculated using FDTD mode solver in combination with the super-mode coupling theory.

An exchange (coupling) of power between the modes of two waveguides occurs where the guided mode functions have a physical overlap region. Since the evanescent field has an exponential decay, there will always be some coupling between the guided modes, however at very large separation distances between the waveguides the suffers coupling significantly. The Power coupling between waveguides is dependent on many parameters such as the waveguide structure (waveguide dimensions, separation (s), and material), wavelength, and the distance (z) travelled by the electromagnetic wave along the waveguide [19].

The following assumptions were made for the coupling calculations:

- The couplers were rectangular, identical and phased matched

- The coupling was mainly due to the parallel region of the waveguides. Coupling in the bent region leading to the parallel section was ignored.

- The couplers were lossless

- The coupling was unidirectional

- The waveguide was transverse electric (TE) guided

- The bent effects on the guided mode were ignored
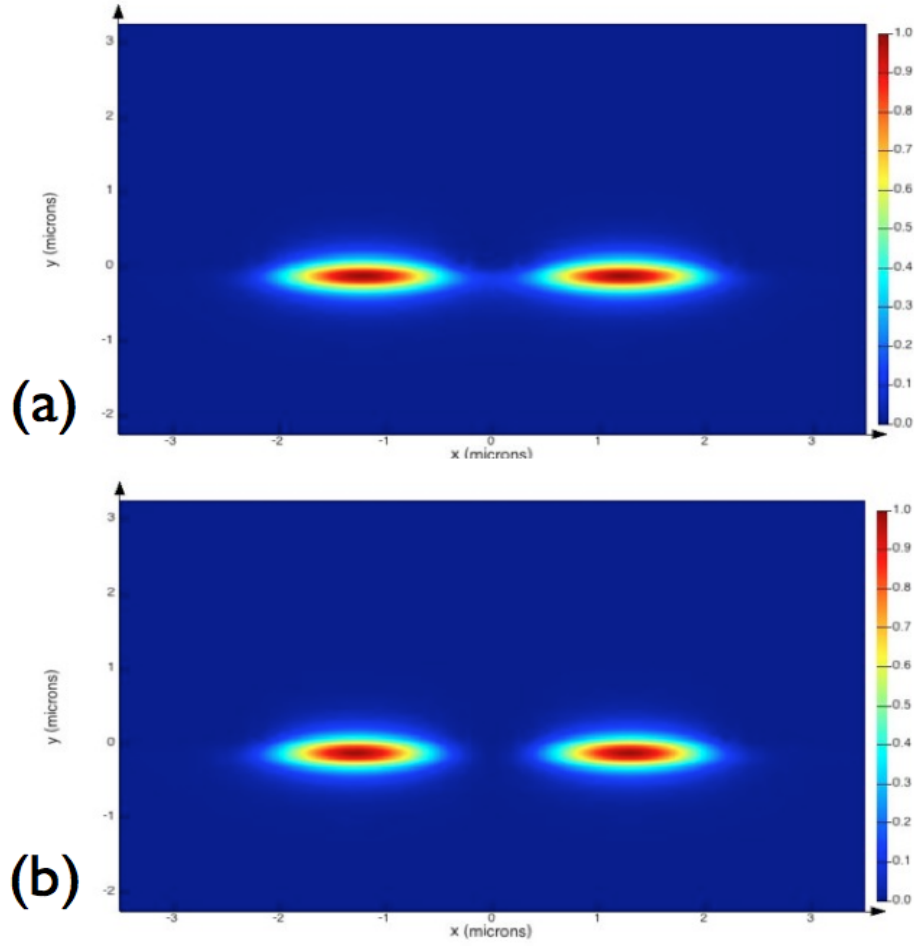
Figure 2.3: The E intensity for the coupler with rectangular waveguides of width=2 μm, gap=0.5 μm, λ=1.55 μm. (a) Symmetric/Even supermode. (b) Anti-symmetric/Odd supermode.

Using the Lumerical software integrated with FDTD mode solver package, the effective indices n_{eff1} and n_{eff2} for the even and odd supermodes were extracted for waveguides of width W = 2 μm and W = 3 μm with varying coupler spacings. Figure 2.3 depicts an example of such simulation for the even and odd modes for a coupler with W = 2 μm and Gap = 0.5 μm. The rectangular waveguide structure used for the effective index simulations has the epi-wafer layer structure of a typical commercial InP epi-wafer which was purchased for our fabrication. This epi-wafer structure details are shown and discussed later in the InP Material Structure section of chapter 2.

Let the two electromagnetic modes with power amplitudes P_a and P_b represent the power in the input coupler waveguide and the power in the coupled waveguide, respectively. The power coupling coefficient κ, equivalent to the square of the field coupling coefficient is defined by

$$\kappa = \frac{P_b}{P_a} \tag{2.3}$$

Once n_{eff1} and n_{eff2} are extracted, using the super-mode theory the crossover length (coupler length at which 100% coupling occurs) L_x, and κ were calculated as [20]:

$$\beta_1 = \frac{2\pi n_{eff1}(\lambda)}{\lambda} \tag{2.4}$$

$$\beta_2 = \frac{2\pi n_{eff2}(\lambda)}{\lambda} \tag{2.5}$$

where β is the propagation constant in units of rad/m. The cross over length

occurs at a distance travelled by the propagating fields where the two fields have a phase difference of π.

$$L_x(\lambda, s) = \frac{\lambda}{2(n_{eff1}(\lambda) - n_{eff2}(\lambda))} \tag{2.6}$$

$$\text{Coupling per length} = \kappa^* = \frac{\pi}{L_x(\lambda, s)} \tag{2.7}$$

$$P_b = P_a \sin(\kappa^* z)^2 \tag{2.8}$$

The exponential dependancy of L_x on the waveguide separation is depicted in Figure 2.4.
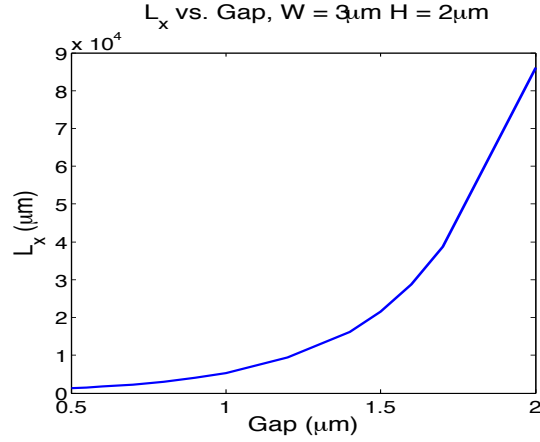
Figure 2.4: L_x as a function of separation between waveguides. This plot was obtained for a 3 µm wide rectangular structure.

Figure 2.5 shows the exponential relationship between the coupled mode
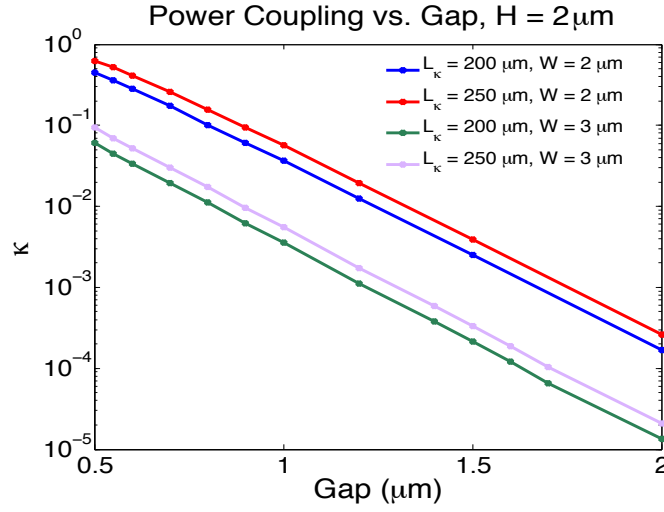
Figure 2.5: The evolution of κ is shown as a function of coupler waveguide spacing for waveguides with coupler lengths 200 µm and 250 µm at 1550 nm wavelength. The case for a constant waveguide height of H = 2 µm with widths of W = 2 µm and W = 3 µm, are shown. The data was obtained using FDTD mode solver and the super mode theory.

power and the waveguide spacing for waveguides of widths 2 μm and 3 μm, with a fixed height of 2 μm at 1550 nm wavelength. Tables 2.2 and 2.3 show the simulated coupling design parameters for the SRLs that were fabricated in this project. These coupling values are rather small, which result in low output power values in the μW ranges (the detectors in the lab are very sensitive and can measure power down to nW ranges). To increase the power coupling (this is analogous to the increase in the effective index difference between n_{eff1} and n_{eff2}), smaller gaps are required (>0.5 μm); however, this is challenging for the fabrication process. These lower coupling factors are advantageous for the initial devices since they result in a lower threshold. After the first devices are fabricated and their lasing characteristics are measured successfully, the mask could be re-designed and the fabrication process improved in order to optimize for power (while satisfying reasonable threshold conditions) by increasing the power coupling coefficient.

Table 2.2: Power Coupling for Rectangular Waveguides W = 2 μm H = 2 μm

Gap (μm)	n_{eff1}	n_{eff2}	κ_a	κ_b	L_x (μm)
0.5	3.257165	3.255365	0.444	0.625	430
1	3.25653	3.256057	0.036	0.056	1638
1.5	3.256362	3.256239	0.00248	0.00388	6301
2	3.256485	3.256453	0.00017	0.00026	24218

Table 2.3: Power Coupling for Rectangular Waveguides W = 3 μm H = 2 μm

Gap (μm)	n_{eff1}	n_{eff2}	κ_a	κ_b	L_x (μm)
0.5	3.264419	3.263803	0.061	0.094	1258
1	3.26417	3.264023	0.0036	0.0055	5272
1.5	3.264131	3.264095	0.00021	0.00033	21527
2	3.26417	3.264161	0.00001	0.00002	86111

As later will be discussed in the wet etching fabrication section of this thesis, the 3 μm wide waveguide devices have a better chance of being successfully fabricated. Moreover, the waveguides end up with a more trapezoidal structure rather than a rectangular structure after the wet etching process. To take into account the wet etching effects, a trapezoidal structure was made in the FDTD solver. The first order mode distribution for the trapezoidal structure is shown in Figure 2.6 and its corresponding refractive index profile and field distribution are depicted in Figure 2.7.

The trapezoidal structure results in even slightly lower coupling values. The coupling could be increased via deposition of a thin dielectric film. This dielectric film deposition will also provide planarization as will be explained in the Fabrication chapter. Considering a roughly 200 nm thick layer of polyimide with a refractive index of 1.7, trapezoidal structures were simulated in the FDTD mode solver to obtain the coupling information by consider-
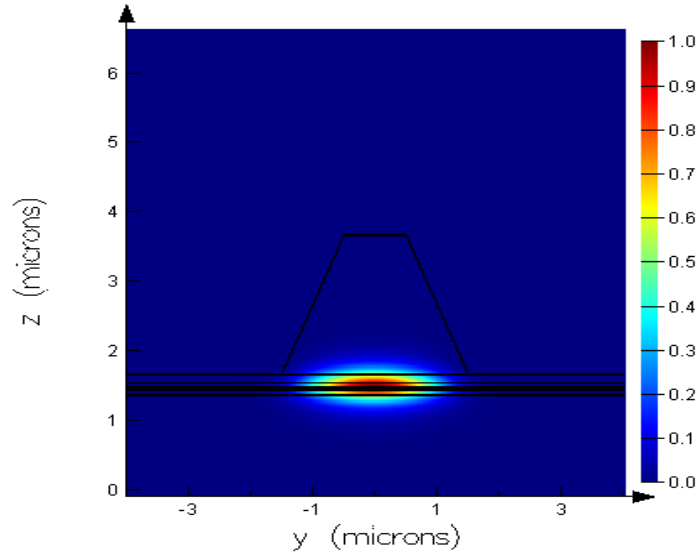
Figure 2.6: The first order mode distribution in the trapezoidal waveguide structure with H = 2 µm, W_{bottom} = 3 µm and W_{top} = 1 µm is shown here.
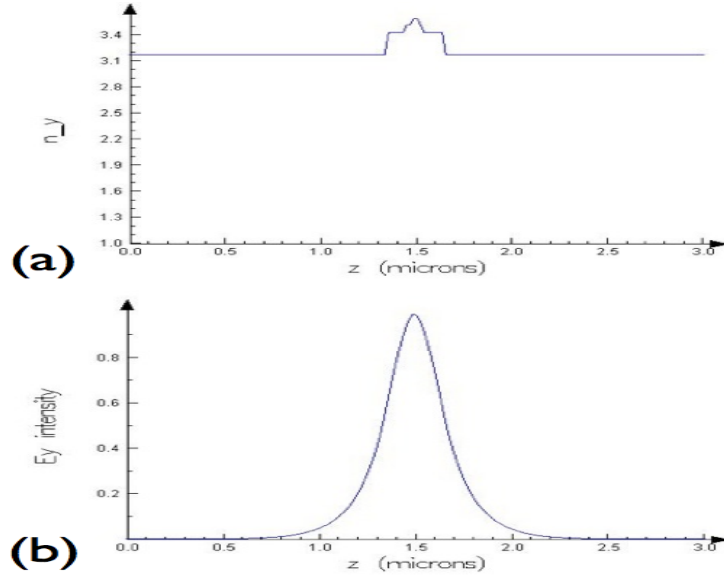
Figure 2.7: Aspects of the trapezoidal waveguide structure with H = 2 µm, W_{bottom} = 3 µm and W_{top} = 1µm : (a) the refractive index profile; (b) the electric field profile for a mode traveling in the y-direction.

ing the wet etching fabrication process. Figure 2.8 shows this waveguide structure for the case of a coupler with a 0.5 μm waveguide spacing.
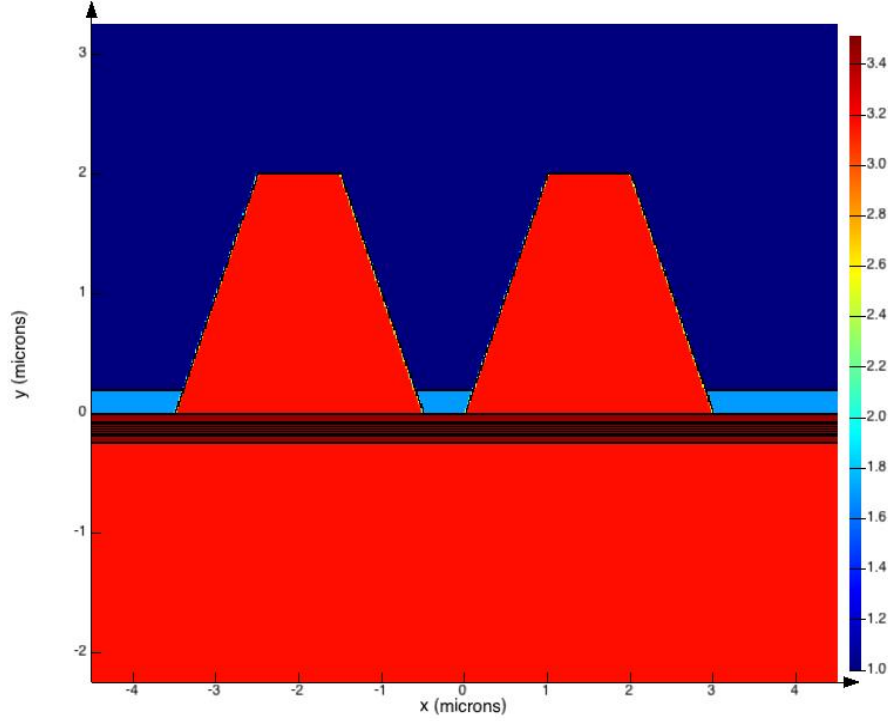
Figure 2.8: Trapezoidal waveguide structure with a uniform 200 nm thick polyimide layer. The refractive index distribution for a coupler with a 0.5 μm spacing is shown here.

Table 2.4 gives a summary of the extracted coupling information and Table 2.5 gives a summary of the expected device performance for the largest possible cavity design with bend radius R = 300 μm when biased at a current of 100 mA (this value is higher than the threshold current). Table 2.6 gives a summary of the expected device performance for the largest possible cavity design with bend radius R = 50 μm when biased at a current of 100 mA. In

27

the Tables, the subscripts a and b refer to a coupler length $L_{\kappa a} = 200$ μm and a coupler length $L_{\kappa b} = 250$ μm, respectively.

Table 2.4: Power Coupling for Trapezoidal Waveguide with 200 nm Thick Polyimide $W_{bottom} = 3$ μm, $W_{top} = 1$ μm

Gap (μm)	$\mathbf{n}_{eff1}$	$\mathbf{n}_{eff2}$	κ_a	κ_b	$\mathbf{L}_x$ (μm)
0.5	3.264004	3.263390	0.061	0.094	1260
1	3.263763	3.263606	0.004	0.0063	4936
1.5	3.263763	3.263679	0.0012	0.0018	9226
2	3.263763	3.263753	0.00002	0.00003	77500

Table 2.5: Predicted Performance for Trapezoidal Waveguide $W_{bottom} = 3$, μm $W_{top} = 1$ μm, R = 300 μm and a 200 nm Thick Polyimide Planarization, Biased @ 100 mA

	I_{th} (mA)		P_{out} μW	
Gap (μm)	1_a	1_b	a	b
0.5	89	85	365	430
1	81	84.5	25	30
1.5	80	84	7	9
2	80	84	1	2

One of the parameters for the SRL that can be measured is the free spectral range (FSR). Taking into consideration the effect of wavelength on the effective index the FSR is [19] :

Table 2.6: Predicted Performance for Trapezoidal Waveguide $W_{bottom} = 3$ μm $W_{top} = 1$μm R = 50μm and a 200nm Thick Polyimide Planarization, Biased @ 100mA

Gap (μm)	I_{th} (mA)		P_{out} μW	
	1_a	1_b	a	b
0.5	26	30	4300	5500
1	25	29	300	400
1.5	25	29	140	100
2	25	29	15	19

$$FSR = \Delta\lambda = \frac{\lambda^2}{n_g d} \tag{2.9}$$

where d is defined as the total cavity length of the racetrack resonator in Equation 2.10 [19], R is the radius of curvature and L_κ is the parallel length in the coupler region.

$$d = 2\pi R + 2L_\kappa \tag{2.10}$$

The parameter n_g is called the group index and it takes into account the effective index dependence on the wavelength. For further information on FSR and n_g please refer to the reference [19]. FDTD simulations show approximately a linear dependency of the effective index and the group index on wavelength. Figure 2.9 shows this result.

2.4 Racetrack Laser Resonator Design

We are primarily interested in the LI characteristic of the SRL. First, the effect of coupling (κ) and resonator length (d) on the output power and
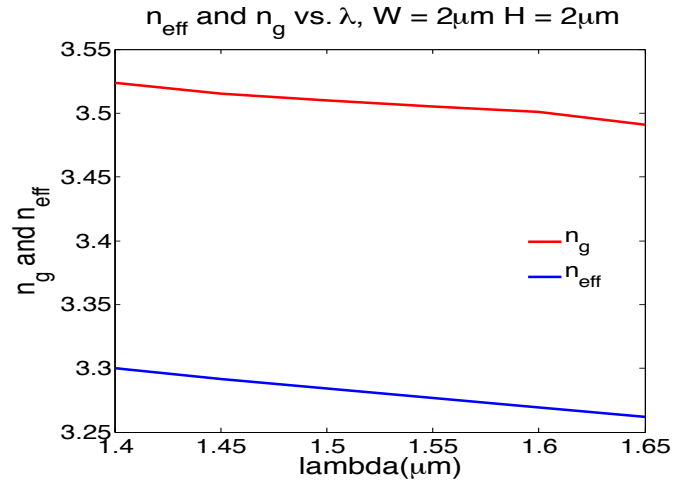
Figure 2.9: Effective index and group index as a function of wavelength. The calculations for group index here take into account the waveguide dispersions and the bulk InP material dispersion.

threshold current were investigated. Then, an estimated LI curve was predicted for the designed SRLs. These analyses were all carried out using Matlab. Table 2.7 lists the parameter values used.

Table 2.7: Simulation Parameters. Data taken from Lecture Notes of Dr.Lukas Chrostowski and Ref [1]

Symbol	Boiling Point (Description)	Value or Range
λ	Wavelength	1550 nm
B	Gain slope (near transparency)	$1.5 \times 10^{-16} \text{cm}^2$
ϵ	Gain compression	2×10^{-7}
η_i	Quantum efficiency	0.9
N_{tr}	Transparency carrier density	$3.3 \times 10^{18} \text{cm}^{-3}$
τ_s	Carrier lifetime	2 ns

The equivalent for the mirror reflectivity R (as normally seen for a Fabry-Perot Etalon) for the racetrack resonator is (1-κ). Thus, the output coupling loss was calculated [5]:

$$\alpha_m = (\frac{1}{d})ln\sqrt{(1-\kappa)} \qquad (2.11)$$

The additional propagation losses were roughly chosen to be 5 cm^{-1}. This is a pessimistic value based on taking a higher value compared to reported values such as 0.34 cm^{-1}[21].

The threshold and output power for the laser can be expressed [5].

$$I_{th} = \frac{\frac{n_g}{c(\Gamma B \tau_p)} + N_{tr}}{\tau_s \eta_i} qV \tag{2.12}$$

$$P_{out} = \eta_i \frac{\alpha_\kappa}{\alpha + \alpha_\kappa} \frac{h\nu}{q} (I - I_{th}) \tag{2.13}$$

Where τ_p is the photon lifetime and α is the propagation loss here taken to be 5 cm^{-1}.

$$\tau_p = \frac{n_g}{c[\alpha - \alpha_m]} \tag{2.14}$$

Figure 2.10 shows the threshold current as a function of κ for fixed ring radii. τ_p increases for larger ring radii given a fixed κ, which in turn reduces the threshold Ith; however, at the same time the volume is increasing for larger ring radii, which will increase I_{th}. Overall the increase in volume overcomes the increase in τ_p resulting in a linear relationship between the ring radii and the threshold current I_{th}. Increasing κ for a fixed ring radius allows more photons to escape in the coupling region; in other words, it reduces the photon lifetime; for high κ, this reduction in τ_p is followed by an exponential increase in I_{th}.

Increasing the input current results in an increase in the unsaturated gain and the intensity inside the laser; this increase in the bias effectively shifts the P_{out} vs. κ curve to higher values as depicted in figure 2.11. The peak of each curve corresponds to the optimum output coupling (κ). For higher bias points the output coupling needs to shift to slightly higher values
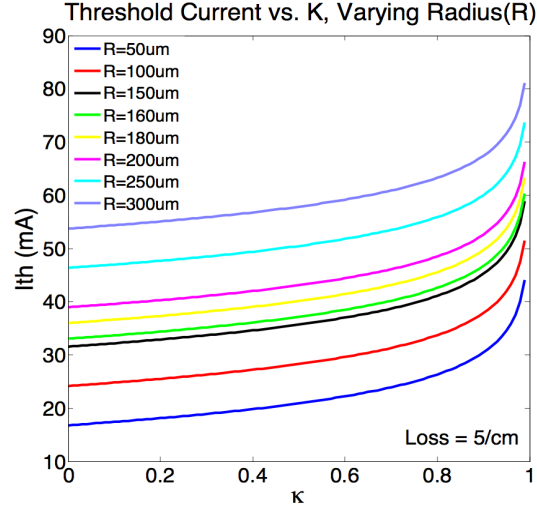
Figure 2.10: I_{th} of the laser is plotted as a function of κ for an increasing ring radius and a coupler length of 200μm. I_{th} has an exponential dependency on κ and almost a linear dependency with the ring radius. Round trip losses are taken to be 5cm^{-1}
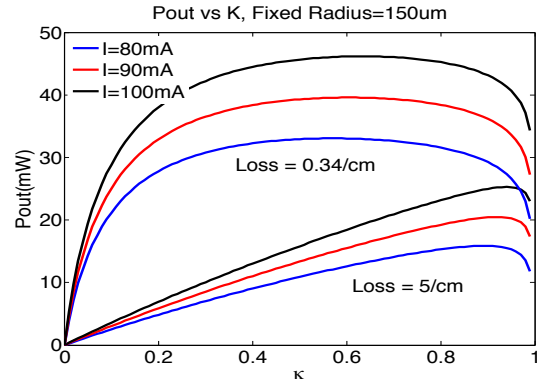
Figure 2.11: P_{out} of the laser is plotted as a function of κ at 3 different bias conditions for a device wtih a coupler length of 200 μm and radius of 150 μm. Round trip losses are taken to be 5cm^{-1}

in order to track the peak power. Moreover, Figure 2.11 shows the effect of increased losses from a low loss value of 0.34 cm^{-1} [21] to a higher value of 5 cm^{-1}. Increase in losses could be due to poor fabrication, high bending losses and/or mode conversion losses amongst other possibilities. From these plots it is observed that for lower losses (excluding coupling losses), the peak of the power shifts to lower coupling values at the same time allowing a wide range of couplings to be used for delivering high values very close to the peak output power. Thus, reducing losses plays a major roll in the performance of the device.

Figure 2.12 shows the relationship between the output power, coupling efficiency κ and ring radius R. The output power has a rollover behaviour with respect to κ for a fixed R. Increasing κ allows more photons to escape/couple out of the ring, resulting in a higher output power; however, too much coupling will prevent the intensity inside the ring from recovering, resulting in a net decrease of intensity inside the ring and thus a drop in the output power. The output power decreases for larger SRLs. Figure 2.13 shows that with higher losses, the output power is more sensitive to κ; moreover, higher coupling is required to output more power from the laser.

Finally we can predict the LI curve using the laser rate Equations [5]. Figure 2.14 shows the LI curve for a SRL with the following specs: W = 3 μm, H = 2 μm, G = 1 μm, R = 150 μm, L_κ = 250 μm.
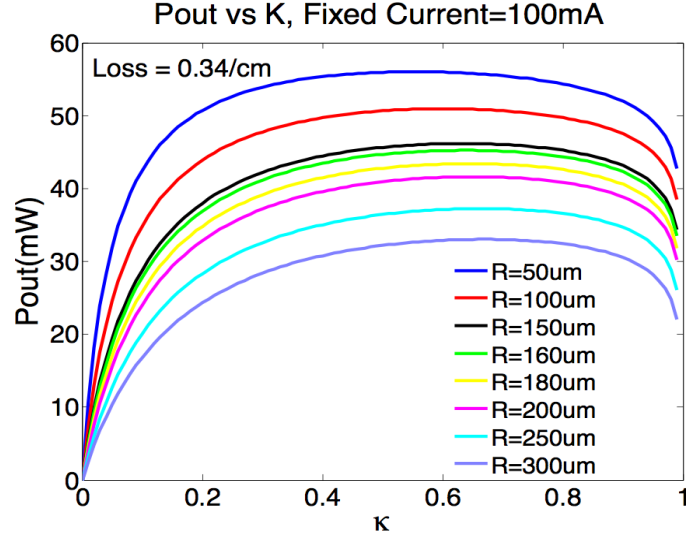
Figure 2.12: Output power of the laser is plotted as a function of κ for a varying ring radius and a coupler length of 200 μm. Round trip losses are approximate to be 0.34 cm^{-1}.
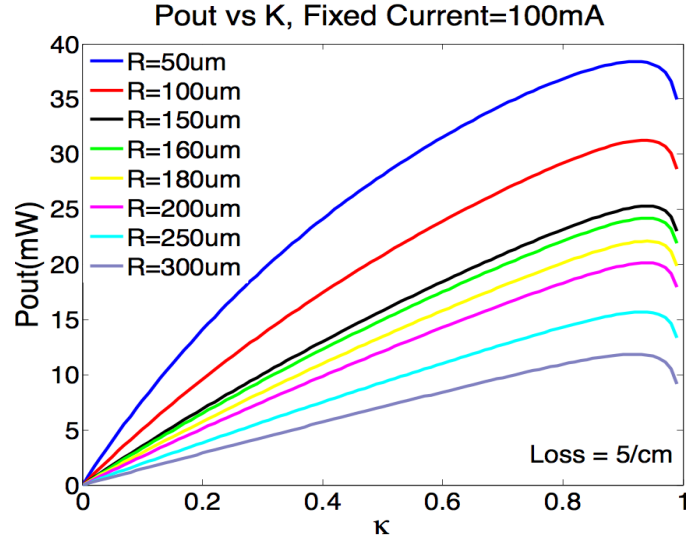
Figure 2.13: Output power of the laser is plotted as a function of κ for a varying ring radius and a coupler length of 200 μm. A higher round trip loss is taken to be 5 cm^{-1} in the case of poor fabrication, bending losses, and mode conversion losses amongst others.
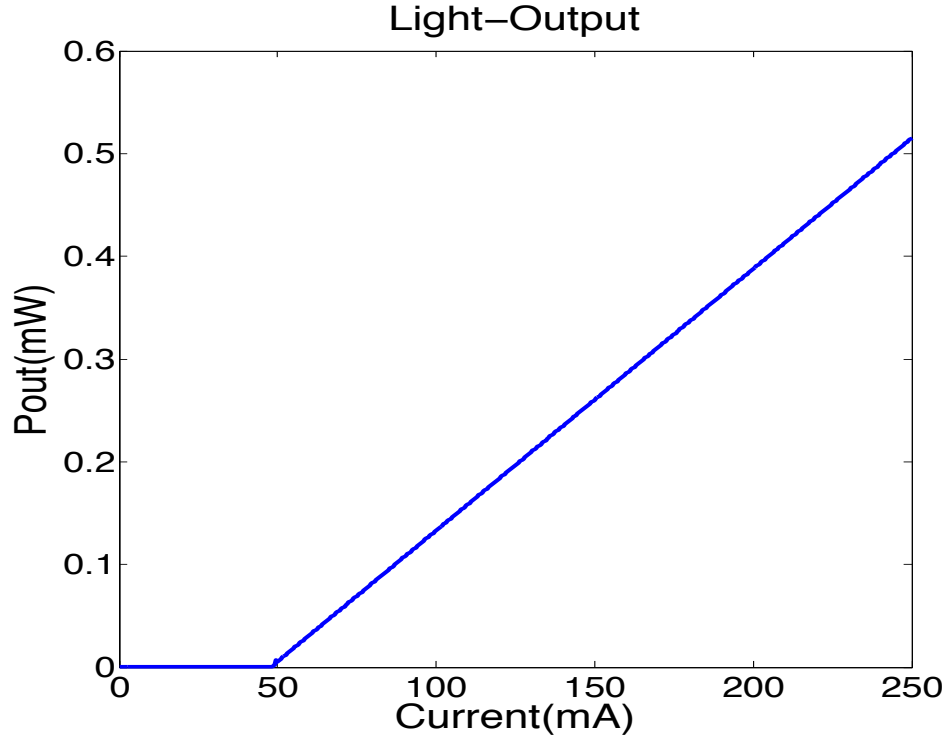
Figure 2.14: Output power is plotted as a function of input current for a SRL with the following specs: W = 3 μm, H = 2 μm, G = 1 μm, R = 150 μm, L_κ = 250 μm. Round trip losses are approximate to be 5 cm^{-1}. This device has a threshold of 49 mA and a slope efficiency of 2.5 μW/mA.

2.5   Double Bus Passive Resonator

The purpose of this section is to further study the racetrack resonator structure, test the design process and develop a parameter extraction method.

Passive racetrack resonators were designed in silicon on insulator (SOI) technology and fabricated by Interuniversity Microelectronics Centre (IMEC). Racetrack resonators were chosen instead of ring resonators in order to enhance coupling as well as allowing more control over the coupling.The waveguide height is fixed to 0.22 µm according to IMEC fabrication steps and the width of the waveguide is determined to be 0.4 - 0.6 µm to ensure single mode operation at TE polarization. The buried oxide box is 2 µm thick. Dosage sweeping during the photolithography step provided a variation in the designed waveguide widths and spacings. To facilitate light coupling, vertical fiber couplers are chosen, as there is no need for cleaving, and although aligning is still challenging they are relatively easier to align. Couplers used here should have a coupling efficiency of 30%, with a 3 dB bandwidth of 60 nm around 1550 nm as designed by IMEC. SOI racetrack resonators were designed with add and drop coupler waveguides [19]. An optical image of a fabricated design is shown in Figure 2.15.

A 2D finite difference methode integrated with Matlab developed by the Photonics Research Lab at the University of Maryland is used to estimate n_{eff1}, n_{eff2} from which the coupling was calculated using the super-mode approach.

The equations [19] to predict the add and drop port responses are as follows:
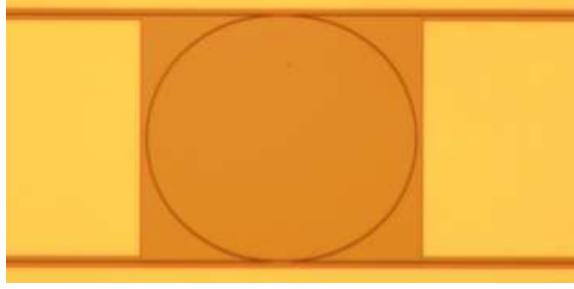
Figure 2.15: Depicted here is the optical image of a fabricated SOI device.

$$Add : |\sigma_{t1}|^2 = \frac{t_1^2 + t_2^2 a^2 - 2t_1 t_2 a cos(\delta)}{1 + t_1^2 t_2^2 a^2 - 2t_1 t_2 a cos(\delta)} \tag{2.15}$$

$$Drop : |\sigma_{t2}|^2 = \frac{(1 - |t_1|^2)(1 - |t_2|^2)a}{1 + t_1^2 t_2^2 a^2 - 2t_1 t_2 a cos(\delta)} \tag{2.16}$$

,where t_1 and t_2 are the straight through field coefficients, $\delta = \omega d/c$ [rad] with c [m/sec] being the phase velocity and ω [rad/sec] the angular frequency [19].

High quality factor (Q) devices with varying parameters were designed. In the Double Bus design, the response at the drop port is similar to the response expected from the SRL output. Figure 2.17 shows the drop port measurement for a device with the following specifications: $L_x = 391$ μm, $L_y = 75$ μm, radius = 4 μm. Using both the Lumerical FDTD mode solver and the Maryland Matlab mode solver, coupling was calculated to compare the two methods:

- κ from FDTD mode solver = 0.07

- κ from Matlab 2-D FDTD = 0.1

A set up was originally built by Dr. Nicolas Rouger and Nadai Makan, which was then improved to include polarization maintaining lensed fibres, a wider fiber movement range and a 3D microscope movement. A picture of the setup is shown in Figure 2.16.
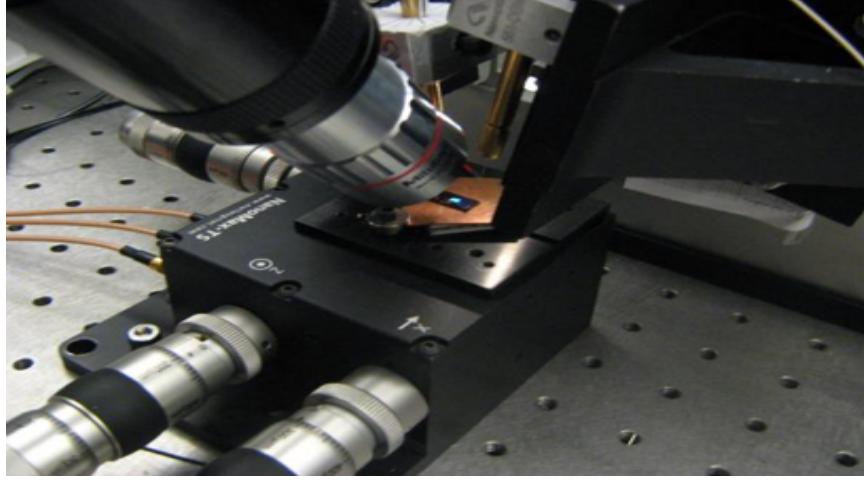
Figure 2.16: SOI Measurement Setup [22].

κ, n_g, and FSR were extracted by curve fitting as shown in Figure 2.17. The extracted values were:

- κ from curve fitting = 0.14

- n_g = 4.474622

- FSR = 0.56 nm

The κ extracted from measurements is higher than both predictions. This is expected since in the coupling predictions it was assumed that all the power coupling is from the parallel length region of the couplers and the contributions from the bent waveguide were ignored. The measured FSR is

matches 99% to the prediction by Equation 2.9. The device shows a Q of 47000 and a 22 dB extinction ratio. The loss values extracted from these measurements were used in publications by other students. This design approach has been used for several silicon-on-insulator projects, some of which have been published and presented at conferences [23] [24] [25].
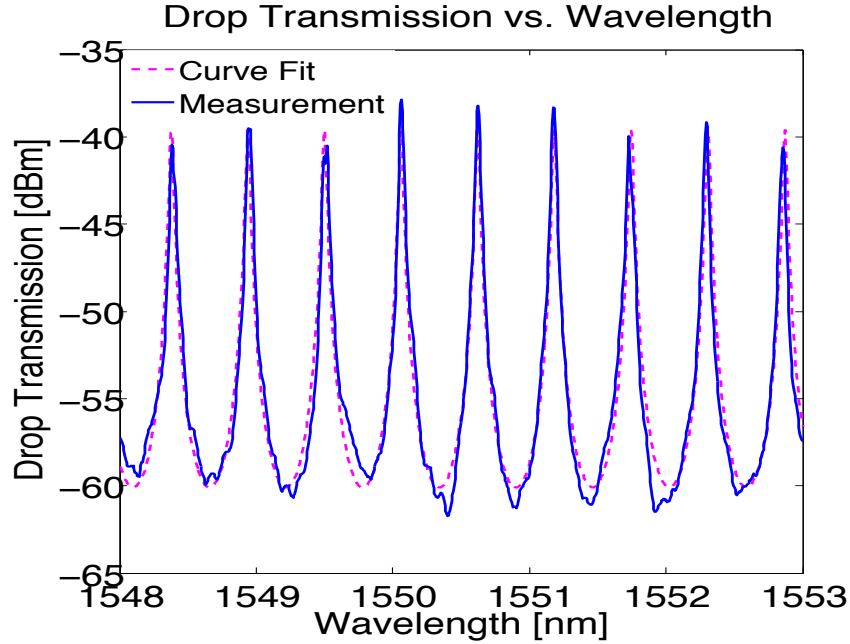
Figure 2.17: Drop port response of a SOI racetrack resonator with $L_x = 391$ µm, $L_y = 75$ µm, R = 4 µm. The solid line is the measurement data and the dotted line is the curve fitted function from which the parameters κ, FSR and n_g were extracted to be 0.14, 0.56 nm, and 4.474622, respectively.

Chapter 3

Fabrication Via Wet Etching

3.1 Introduction

This chapter presents the experiments and results of the investigation of fabrication techniques via wet etching utilized for SRLs and ridge waveguide RWG edge emitting lasers in InP based material systems. The objective is to develop a new fabrication process via the wet etching approach for SRLs. To the best of our knowledge, there has been no publication on SRLs made via wet etching in InP based materials.

The preferred laser fabrication method used in industry for regular RWG edge emitters and VCSELS is wet etching or a combination of dry and wet etching. Wet etching techniques are preferred due to their lower processing costs, lower processing time and lower optical losses [7–10]. In order to achieve completely anisotropic sidewall profiles and zero in-plane etching, plasma and dry etching techniques have been mainly utilized for the fabrication of SRLs; these processes are usually very expensive, more complex, can leave relatively rough surfaces and may even damage the sample. This project investigates the fabrication steps for InP semiconductor ring laser using simpler, less costly, wet etching techniques with the aim of achieving smoother sidewalls/surfaces in order to reduce the scattering from the rough

surface typically present from plasma etched ring lasers. This would improve the efficiency of the laser and reduce the threshold. The wet etch process requires some optimization of the process conditions in order to achieve: isotropic etch rate in the x and y cross section, flat surfaces, maximize the etch rate ratio of orthogonal etching to in-plane etching (for higher sidewall verticality) and reduced under cuts.

There are 3 major sections in this chapter: InP Material Structure, InP Edge Emitter Racetrack Resonator Laser, InP Edge Emitter Ridge Waveguide Laser. In the first section the InP epi-wafer structure details are introduced; the same epi-wafer was used for the fabrication investigation of both the SRLs and RWGLs. The analysis of the SRLs fabricated via wet etching revealed a set of possible areas for improvements in the fabrication and design. To pin point the main challenge in the SRL fabrication a simpler design was made to fabricate RWG edge emitting lasers via wet etching. Finally we started processing dry etched SRLs in collaboration with the fabrication facility at Sherbrooke. The mask designs and fabrication processes for each of the devices are described in this chapter. Figure 3.1 show a flow diagram for the fabrication steps required. Table 3.1 shows an overview of the material and equipments used for the fabrication processes.
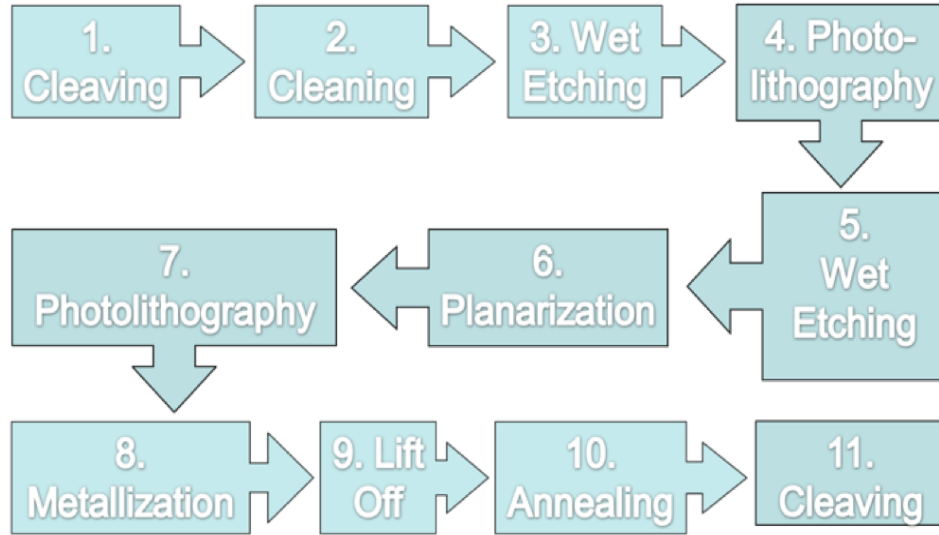
Figure 3.1: Depicts the fabrication steps required to process an SRL.

Table 3.1: Overview of The Fabrication Steps

Process	Materials	Equipments	Settings/Action
Solvent Cleaning	Sample	Hotplate	
	Acetone	Microscope	
	Isopropanol	Waste Beaker	
	DI Water, Compressed N_2 gas		
			Continued on next page

Table 3.1 – continued from previous page

Process	Materials	Equipments	Settings/Action
Wet Etch	Sample, H_3PO_4:HBr:H_2O, DI Water, Compressed N_2 gas	2 Beakers tweezers	Etch ~150nm of u-InP
Spinning	Sample AZ P4110	Spinner	1min @ 3000rpm
Soft Bake	Sample	Hotplate	7min @ 100 C
Optical Patterning	Sample Mask	320nm Optics Karl Suss Mask Aligner	0 Gap contact mode 1 min exposure
Pattern Developing	Sample, Beakers AZ400k Developer 1 : 4 DI Water,	Microscope	90 sec
Wet Etch	Sample, Compressed N_2 gas, DI Water, H_2SO_4:H_2O_2:H_2O	4 Beakers	Etch InP and In-GaAs/InGaAsP for a total etch depth of ~2μm
			Continued on next page

Table 3.1 – continued from previous page

Process	Materials	Equipments	Settings/Action
	H_3PO_4:HBr:H_2O	Dektak Pro-filometer	

3.2   InP Material Structure

The basic layered structure is grown epitaxially on a crystalline InP substrate by metal organic vapour phase epitaxy (MOCVD) at LandMark Optoelectronics Corp. in Taninan, Taiwan. The orientation of the substrate used is (100) +/- 0.1 deg. Table 3.2 shows the epi-wafer structure in detail. This design is a commercial product used for edge emitting lasers and we use this proven design as a starting point for our fabrication.

The substrate is n^+ Sulphur doped InP with layers grown on top as follows: a lower cladding including a 500 nm n-type InP layer and a 185 nm transition quaternary layer; a 100 nm waveguide core; an upper cladding including a 75 nm InAlGaAs transition quaternary layer, a 50 nm InAlAs etch stop layer, a total of 72 nm transition quaternary layers, a 1.8 μm P-type InP layer, 50 nm of InGaAsP transition quaternary layers and finally a p-type InGaAs contact layer.

For 1550 nm emission:

$$Eg = \frac{1.24eV}{1.55\mu m} = 0.8eV \qquad (3.1)$$

Therefore, the bandgap of the QW is 0.8 eV. The bandgap energy is gradually increased as we move away from the QW with changes in the x and y composition ratios. Using InP as substrate a range of lattice-matched quaternaries extending from InP to the InGaAs ternary line are accommodated. Here the quaternary is specified by an x and y value, i.e., $In_{1-x}Ga_xAs_yP_{1-y}$. Choosing x equal 0.46 y results in approximate lattice matching to InP [2].

This structure includes 6 InAlGaAs QW layers each 6 nm thick, alternating with 7 barriers each 9 nm thick (In mode calculations the barriers are not included), sandwiched between two regions of varying layers (for simplicity of mode calculations here considered to be just InP).

LandMark provided some test data of this epi-wafer including a photo-luminescence (PL) measurement reporting a peak wavelength of 1512.5±5 nm. The PL was measured again at UBC by Ph.D student Wei Shi and the data are shown in Figure 3.2.

Table 3.2: R2 - 1550 nm FP-LD Epi-wafer Structure[2]

#	Name	Value	Unit	Thickness Accuracy
0	InP Substrate	S-Doped $2-8 \times 10^{18}$	cm^{-3}	
1	N-InP Buffer Layer (Concentration)	0.5 1×10^{18}	μm cm^{-3}	±10% ±20%
2	$N - In_{0.53}Al_xGa_{0.47-x}As$	0.01	μm	±10%
				Continued on next page

Table 3.2 – continued from previous page

#	Name	Value	Unit	Thickness Accuracy
	(x:0.31→0.44) (Concentration)	1×10^{18}	cm^{-3}	$\pm 20\%$
3	$N - In_{0.52}Al_{0.48}As$ (Concentration)	0.1 1×10^{18}	µm cm^{-3}	$\pm 10\%$ $\pm 20\%$
4	$U - In_{0.53}Al_xGa_{0.47-x}As$ (x:0.44→0.3)	0.075	µm	$\pm 10\%$
5	$6\times$ InAlGaAs QW $(+1.0 \sim +1.15\%$ CS$)/$ $7\times$ InAlGaAs Barrier $(-0.45 \sim -0.55\%$ TS$)$ (λ_{PL})	$5.5 \sim 6/$ 9 (1512.5)	nm nm nm	 $\pm 10\%$ $\pm 5\%$
6	$U - In_{0.53}Al_xGa_{0.47-x}As$ (x:0.3→0.44)	0.075	µm	$\pm 10\%$
7	$U - In_{0.52}Al_{0.48}As$	0.05	µm	$\pm 10\%$
8	P-InP Layer (Concentration)	0.05 $5 \sim 8 \times 10^{17}$	µm cm^{-3}	$\pm 10\%$
9	P-InGaAsP Layer (Concentration)	0.022 $5 \sim 8 \times 10^{17}$	µm cm^{-3}	$\pm 10\%$
10	P-InP Layer (Concentration)	1.8 $1 \to 1.5 \times 10^{18}$	µm cm^{-3}	$\pm 10\%$
				Continued on next page

Table 3.2 – continued from previous page

#	Name	Value	Unit	Thickness Accuracy
11	P-InGaAsP Layer (Concentration)	0.025 $> 3 \times 10^{18}$	μm cm^{-3}	±10%
12	P-InGaAsP Layer (Concentration)	0.025 $> 3 \times 10^{18}$	μm cm^{-3}	±10%
13	P-InGaAs Layer (Concentration)	0.15 $> 1 \times 10^{19}$	μm cm^{-3}	±10%
14	U-InP Layer	0.15	μm	±10%
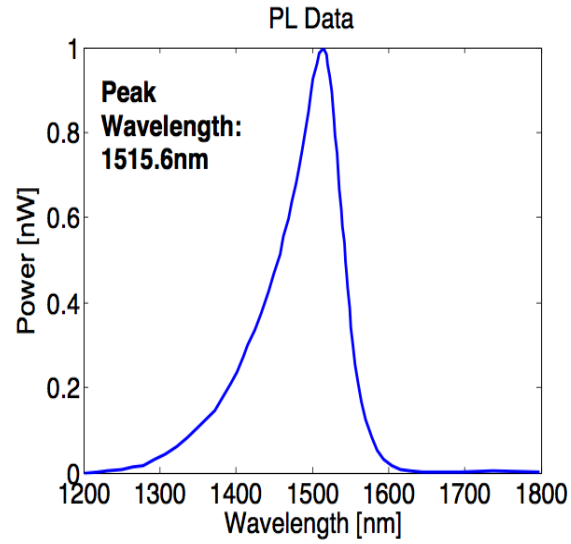
Figure 3.2: The epi-wafer PL data at room temperature is shown here. Courtesy of Wei Shi.

3.3 InP Edge Emitter Racetrack Resonator Laser

3.3.1 Mask

Overview

Once a range of possible SRL design parameters was determined, the required mask was designed using a Matlab program integrated with Clewin (a drawing software). Mask was done using a script to facilitate varying the parameters.

The mask was purchased from the Infrastructure of Nanosctructures and Femtosciences (INRS) Centre in Quebec.

At INRS two types of direct writing techniques were available: a laser writer, an e-beam writer. The e-beam mask was chosen because it provides the highest possible resolution and that is necessary to obtain the 0.5 μm gaps in our design.

The mask patterns were defined in chromium on a 5" × 5" glass plate with a thickness of 0.09". The mask was later on cut down into a 4" × 4" plate in-order to fit the Karl Suss mask aligner used at the UBC AMPEL Nanofabrication facility. Figure 3.3 shows the mask design.

The fabrication required two photolithography steps thus two mask layers: Layer 1 to form the waveguide ridge (both the coupler waveguide and the racetrack waveguide), Layer 2 to define the contact opening before metallization. For Layer 1, two designs were printed on the mask. Design of Layer 1(a) as shown in Figure 3.4 is simple and appropriate for wet etching techniques; however, the exposed area in this design is very large for dry
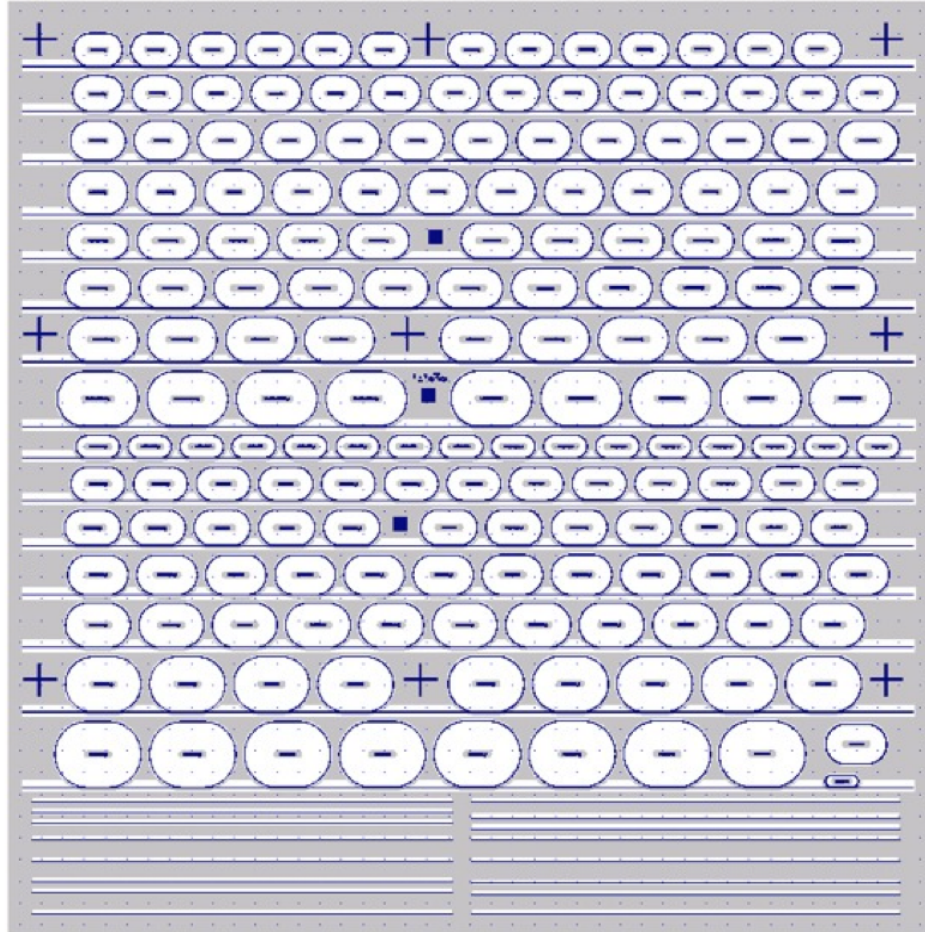
Figure 3.3: The SRL mask layout. This is the final version of the mask submitted. The metal layer is inverted.
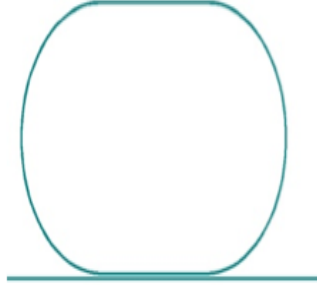
Figure 3.4: Layer 1(a) shows the etch mask layout used for wet etching.
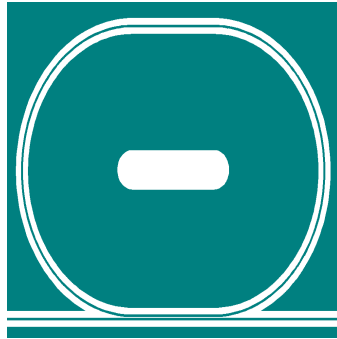
Figure 3.5: Layer 1(b) shows the etch mask layout. A trench design is applied for the case of dry etching.

Figure 3.6: Layer 2 shows the top contact mask layout. This is before inversion, thus the coloured region would be the contact area.

etching techniques and causes reduction in the uniformity throughout the wafer. In order to reduce the exposed area and increase the reliability of uniformity throughout the processed sample specially when dry etching, a second design Layer 1(b) using trenches was drawn as shown in Figure 3.5. Figure 3.6 shows the layer 2 design before inversion.

SRL Design Variation

Due to the approximations in modelling (for example ignoring coupling due to the bend region, estimating the overall losses, etc.), potential unexpected imperfections and/or limitations in the fabrication process, and also for the purpose of device characterization, the SRLs were designed with varying parameters. The coupling is a function of the effective index, coupling spacing and coupler length. In order to study the coupling behaviour and its effects on quality factor, output power, resonance frequency, bandwidth and sensitivity, different coupling lengths each with several varying coupling gaps were designed. Over 80 different designs were included on the mask with a combination of the following parameters:

- Bent Region Radius: 150 μm, 160 μm, 180 μm, 200 μm, 250 μm, 300 μm

- Coupling Gap: 0.5 μm, 1 μm, 1.5 μm, 2 μm, 2.5 μm

- Coupler Lengths: 200 μm, 250 μm

- Waveguide Width: 2 μm, 3 μm

Every device included a label to identify its parameters. The labels have a format of LxxxRxxWxGxxx. As an example a label reading L200R150W2G1, identifies a device with coupler length 200 μm, bent radius of 150 μm, waveguide width of 2 μm and coupling gap of 1 μm.

Alignment Marks

There are two important alignment steps required with the current mask design. First, when using Layer1 of the mask, the mask patterns should be aligned to the edge of the sample in such a way so that the waveguides run parallel to an edge of the sample. This alignment is necessary for the cleaving step required to achieve the output facet of the laser. If the patterns are misaligned with the edge of the sample, when the sample is cleaved along its crystallographic orientation, many devices can be damaged and thus the fabrication yield is reduced. The second critical alignment is between Layer 1 and Layer 2 of the mask. This alignment has a large tolerance, roughly ±10 μm since the metal pattern is very large. Large cross like alignment markers were placed throughout the mask to assist with coarse alignment. For finer alignment, vernier scales were designed with 6 μm to 6.2 μm spacings to improve the alignment accuracy up to ±2 μm.

3.3.2 Sample Preparation

InP is very brittle; compared to Si it is a few times easier to break or shatter InP. The cleaving process was done manually. A tip of a diamond cutter was used to apply pressure to a point on the InP wafer. Once enough pressure was applied, the sample broke along its crystallographic orientation. The 2"

epi-wafer was cleaved into small pieces of roughly 1 cm by 1 cm.

3.3.3 Photolithography

Cleaning

InP based fabrication is costly; high yields are demanded for making products more affordable. Cleanliness is a critical factor in achieving reliable, reproducible results with a high yield in all micro-fabrication processes including semiconductor laser fabrication. The cleaning process refers to the removal of any undesirable material from the sample surface prior to any further processing. Examples of such undesirable materials include chemical residues from previous steps, debris from cleaving or particles due to poor environmental control. Insufficient cleanliness leads to degradation of the process quality or sample integrity (because it can crack during alignment). Photoresist (PR) spin-coating and patterning, wet or dry etching, polymer application and oxidation for passivation and planarization, and metal adhesion are all affected by the initial cleanliness conditions of the sample surface. The environment cleanliness is defined by the size and number of particles present in the fabrication environment. The UBC yellow room facility is a class 1000, which means the maximum concentration of airborne particles larger than 0.5 µm in diameter is controlled to be less than 1000 particles/ft^3. Moreover, the cleanroom atmosphere is both temperature and humidity controlled [26].

Organic solvents were used to remove any organic material such as PR and oil, grease or wax residues from the InP surface. Acetone was used

to rinse the sample surface; unfortunately it may also leave some residue behind. Isopropanol or methanol was used to rinse away any residues left behind after the acetone rinse, then the sample was rinsed by de-ionized water and dried with a compressed nitrogen gas. Some properties of the solvents used are shown in Table 3.3.

Table 3.3: Solvent and Properties (Data from [3])

Solvent	Boiling Point ($°C$)	Flash Point($°C$)	Water Solubility	Safety
Acetone	56.3	-16	100%	Flammable
Propanol-2 (Isopropyl alcohol)	82.3	22	100%	Flammable
Methanol	64.7	12	100%	Flammable

The solvents used were disposed of in the appropriate non-halogenated waste containers [27].

After rinsing the sample surface and drying with the nitrogen gun, the sample was heated at 100°C on a hotplate for 2 minutes to ensure that the surface was perfectly dried before the PR spinning step. After drying the sample on the hotplate, the sample was left for 2 minutes to cool before PR spinning. The sample surface was then observed under the microscope to ensure that it was sufficiently clean. The solvent cleaning procedure was

repeated as many times as necessary until the surface was acceptably clean.

Photoresist Spin-coating

The next step in the process of photolithography involves PR, a photosensitive organic material that is applied to sample surfaces a thin film. It is selectively subjected to UV light that creates exposed areas. Photolithography in short is a patterning technique used in semiconductor processing. There are two general types of PR, negative and positive. When positive resist is exposed to UV light, it gains enough energy to change its chemical structure. This chemical change makes the resist sensitive to chemical etchants and more soluble in the developer. Therefore, any areas where the positive resist is exposed to UV light are being washed away in the developer, exposing the underlying InP layer. Negative PR works in the opposite way. Exposure to UV polymerizes the PR and therefore the exposed areas become resistant to chemical etchants and do not dissolve easily in the developer. In the negative resist, it is the unexposed portions that are removed during the developing process. In our fabrication a positive PR was used.

A thin layer of roughly 1.4 μm thick PR was applied uniformly on the die surface via spin coating. The final thickness of the PR film is determined by the material of the stage surface, the viscosity of the PR and the speed at which the wafer spins. Given the spinning speed, spinning longer than a certain amount of time will not change the final thickness of the PR. The thickness was determined by a profilometer.

After making sure that the sample was completely clean, dry and cool, the wafer was placed onto a spinner. A pipette was used to dispense 2-3 PR

drops onto the sample which covered the entire surface. The PR was spun at 3000 rpm for 1 min.

A successful spin coat should result in a uniform layer of PR. If the layer was non-uniform or there were dots, lines or areas that were not covered by PR, the process was started from the beginning.

Soft Bake

The amount of water present in the PR film determines how soluble the UV exposed area becomes in the developing step. Optical exposure causes a chemical reaction in the PR film to form a ketone. If water is present, the ketone will react to form a product (indene carboxylic acid)which is highly soluble in the developer. In the absence of water, the degraded components form cross-linkages with other molecules and solubility decreases. Soft baking removes some of the water and organics in the PR film which is critical to the PR exposure and developing steps. Some baking is required to harden the film, reduces its thickness and improves its adhesion. If the PR is over baked, it loses its sensitivity to light and thus degrades its solubility in the basic developer. However, if it is under-baked and there is still a significant amount of organics remained, PR resistance in the developer would degrade resulting in overdevelopment [28] and the sample's PR can stick to the mask during the subsequent contact lithography step. Recipe for soft baking is given in the steps below[29]:

- Adjust the hotplate temperature to 100 C

- Place sample on the hotplate for 7 mins

- Remove sample from hotplate and keep away from UV light sources

- Allow 3 minutes for the surface to cool before exposure

Optical Patterning

The AZ P4110 PR absorption spectrum is matched to the emission spectrum of mercury. When the PR is exposed to Hg emission, it gains energy which causes a chemical reaction necessary for the developing process. Using the appropriate photon energy and H_2O concentration in the resist after soft bake, the PR development rate increases. For the positive PR the transparent patterns on the mask are the parts that will be exposed and later removed in the developing process [28].

The Karl Suss mask aligner used at the UBC fabrication facility is a manual system with 320 nm optics, which focuses UV light produced by a mercury lamp via a system of lenses onto the mask. This machine is limited to a maximum wafer diameter of 3" and a maximum mask plate size of 4" by 4". The distance between the mask and the wafer, the intensity of the UV light, and the exposure time could all be adjusted to achieve the desired results [30].

The lateral resolution is limited by the emission wavelength and the gap between the mask and the sample. The lateral resolution d of an image transferred from the mask pattern to the PR has a relationship with the wavelength λ and the distance between the mask and PR g as shown in Equation 3.2 [28]. Figure 3.7 shows the relationship of Equation 3.2.

$$d = (\lambda g)^{\frac{1}{2}} \tag{3.2}$$
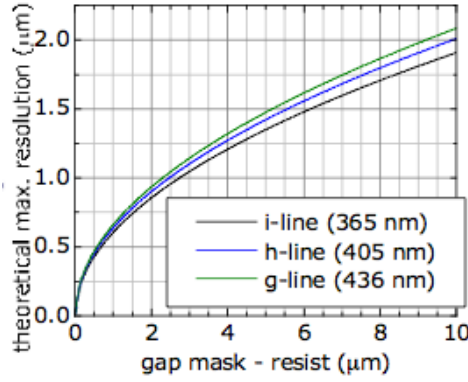
Figure 3.7: Theoretical maximum resolution that can be achieved as a function of the distance between the mask and the PR surface is shown here.[28]

Since the mask has a high resolution demand on the lithography (smallest coupling gap is 0.5 μm), it is very critical to reduce the distance between the mask and the PR surface sufficiently ($g < 0.5$ μm). Profilometer data revealed that the PR height close to the edges of the sample could be as much as roughly 1 μm to 1.5 μm higher than the uniform PR height everywhere else on the sample. This height difference becomes an issue for patterns requiring lateral resolutions below 2 μm. To resolve this issue, before transferring the mask patterns onto the PR surface a pre-exposure step was applied to remove the PR from the edges and corners of the sample. The sample was exposed in contact mode (the gap between the wafer and the mask was manually closed), for 1min.

Pattern Developing

A low concentration developer solution was prepared with 1 part AZ400k developer and 4 parts DI water[29]. Developing refers to the process of agitating the sample in the developer solution for the appropriate amount of time needed for the exposed PR to dissolve in the solution. Developing for 1 min was found sufficient. Thanks to the corner and edge bead removal step as shown in Figure 3.8 a resolution of 1um was achieved.
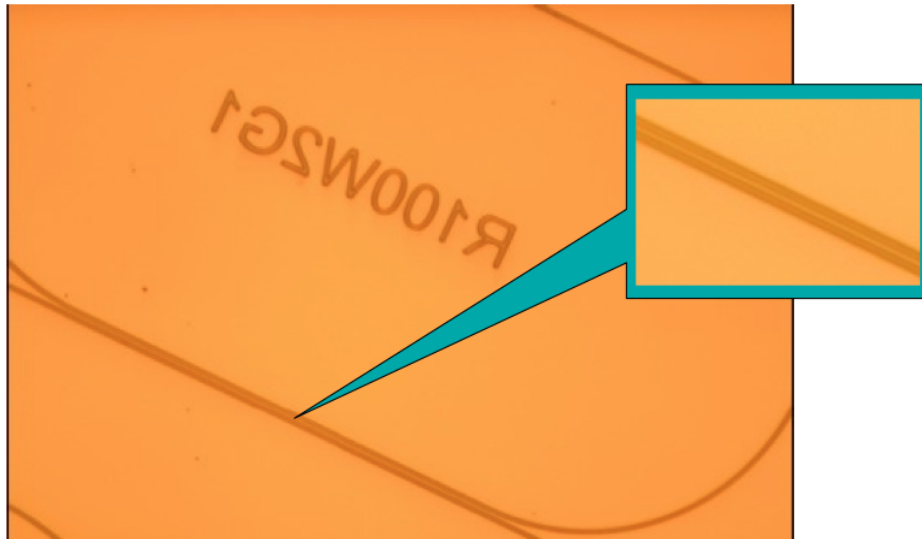
Figure 3.8: Shows a 1µm resolution achieved by optical lithography using the manual Karl Suss mask aligner and applying the edge beading compensation technique.

Yeild Ananlysis

With no unexpected issues in the above steps, a 100 percent yield was achieved on devices with 1µm resolution and higher. Since a near perfect

lithography step is possible under expected conditions, if any defects were observed at this point in the fabrication the sample was cleaned and the process was repeated once the occurred defects were investigated. Here are some factors that may contribute to defects and lower the yield:
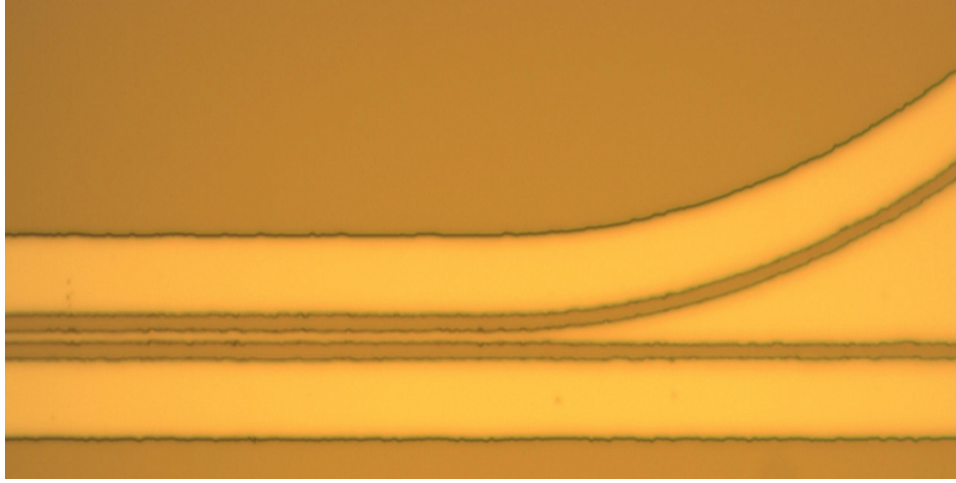
Figure 3.9: Defect revealed after developing due to rough edges present on the mask. Some of these mask damages were present originally due to the mask fabrication quality and some damages developed over time through usage.

Particles in the PR due to contaminated substrate(insufficient cleaning or inherent defects), insufficient cleanroom conditions, contaminated PR container or pipette (PR dries very quickly and even reusing the same pipette could introduce some dry chunks), expired PR, mask contamination(by particles or previous PR), bubbles introduced when dispensing the PR droplets onto the surface, edge bead. These problems will cause a $g > 0$. Also over or under baking and exposure would effect the developing results. Figures 3.10, 3.9 and 3.11 show optical images of some different defects.

Figure 3.10: Defect revealed after developing due to presence of impurities in the PR. This problem was resolved by using fresh PR and also ensuring that the sample surface was cooled before PR spinning.

Figure 3.11: PR residue left over after cleaning including the following approaches: over-flooding the PR with the UV and developing, two-solvent process at room temperature, two-solvent process at close to boiling temperature. This is most likely due to expired PR and/or over-baking the PR. A PR stripper solution can usually remove the residues.

3.3.4 Wet Etching

Wet etching refers to the process of removing layers from the epi-wafer sample through chemical reactions that occur at the surface of the material when exposed to liquid etchants. Once the sample has been patterned during the photolithography process, some areas are protected by PR from the etchant while the unprotected areas are exposed to the etchant and could be removed. Wet etching is used here to form mesa structures for device isolation, to define the waveguide structures, and to remove the protective u-InP layer.

The wet etch requirements for the SRL fabrication are:

- High selectivity: An acceptable selectivity allows the etchant to perfectly remove the desired layer without damaging the underlying layers or completely removing the mask layer. In other words, the etch rate for the layer to be removed must be higher than that of the mask and the underlying layers. Selective etchants are needed to control the etch depth.

- In-plane isotropy: Perfect isotropic in-plane etching results in equal erosion of the material in the x and y cross-sections. This is important for achieving the same waveguide dimensions everywhere on the SRL including the bend regions. Typical InP wet etchants are anisotropic.

- Orthogonal to in-plane anisotropy: Ideally, a perfectly straight sidewall profile is desired with no undercuts, however, that is impossible with wet etching techniques. It is desired to maximize the etch rate

ratio of orthogonal to in-plane etching.

Suitable Etchants

The approach was to adjust the etchant concentrations in already reported InP etchant recipes to find the most suitable etchant recipe. A suitable recipe should achieve:

- The highest possible in-plane isotropy

- Flat bottom

- Smooth surfaces

- Maximize the sidewall verticality

- Minimize the amount of mask undercut

There are various wet etching recipes previously reported by other researchers including defect revealing etchants, material selective etchants or etchants for applications that were not highly sensitive to in-plane isotropy as reported in the review paper of Ref. [31] and Ref. [32].These recipes were tested on dummy InP wafer with the help of Dr. Mark Greenberg in order to determine the most suitable recipe for our application.

Table 3.4 shows a summary of a number of approaches taken to achieve the wet etching requirement; the table lists the different etchant systems that were tried and the observations made during fabrication testing.

Table 3.4: Etchants Tried

	Etchant System	**Etched Material**	**Selective**	**Observations**
1	H_2SO_4/ H_2O_2/ H_2O	InP	No	Large undercut
2	H_3PO_4/HCl	InP	No	in-plane anisotropy
3	HCl/ CH_3COOH/H_2O_2	InP	No	In-plane isotropy achieved but very slanted sidewall profile
4	HBr/H_2O_2/H_2O/HCl	InP	No	in-plane isotropy achieved but non-flat bottom profile
5	H_3PO_4/HBr/ H_2	InP	Yes, <4	in-plane isotropy achieved,
6	H_2SO_4/H_2O_2/H_2O	InGaAsP and In-GaAs	Yes, <4	smooth surfaces

Figures 3.12 to 3.15 show optical images of test samples etched with the etchants of approach 1 to 4 listed in Table 3.4.

It was initially decided that Approach 4 listed in Table 3.4 , the HBr/H_2O_2/H_2O/HCl system, was the most suitable for SRL fabrication. However, after the first batch of devices were fabricated, no light was observed from the cavity. Using the Dektak profilometer, the etching profile revealed that there is a

Figure 3.12: $3H_2SO_4$: H_2O_2 : H_2O system is highly corrosive (etch rate mainly proportional to Sulphuric acid concentration) and results in large amount of undercut. Not suitable for our masking patterns.
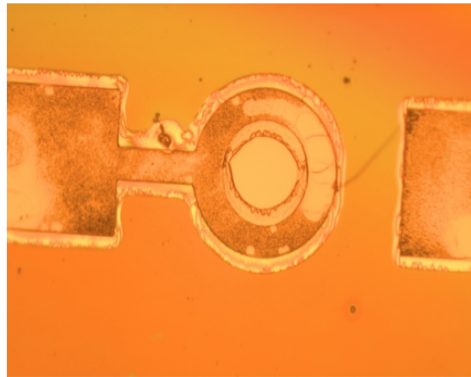
(a)40 H3PO4 : HCl   (b)7 H3PO4 : HCl

Figure 3.13: H_3PO_4/HCl systems are not suitable for our masking patterns. (a) High concentrations of phosphoric acid seems to result in holes and nonplanar bottoms. (b)Reducing the phosphoric acid concentration seems to result in smoother surfaces.

(a)3HCl:6CH3COOH:H2O2   (b)HCl:6CH3COOH:2H2O2
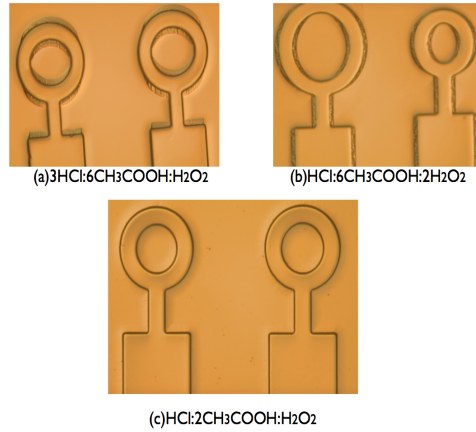
(c)HCl:2CH3COOH:H2O2

Figure 3.14: Etching results with HCl/ CH_3COOH/H_2O_2 systems (a)High HCl and acetic acid concentrations enhance the in-plane anisotropic etching behaviour. (b)Reducing the HCl concentration improved the in plane isotropy. (c) Reducing the acetic acid concentration to the HCl and hydrogen peroxide concentration by a factor of 2 resulted in perfect in-plane isotropy; however, the sidewall profile was very slanted.

(a)20HBr:H2O2:10H2O:10HCl   (b)20HBr:H2O2:72H2O:10HCl
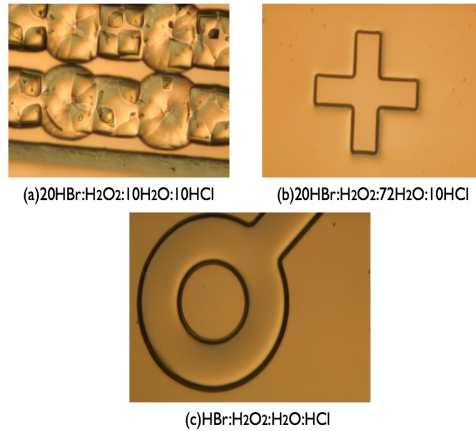
(c)HBr:H2O2:H2O:HCl

Figure 3.15: Etching results with HBr/H_2O_2/H_2O/HCl systems. (a) Reveals very non-flat bottom and sidewall profiles with high undercuts.(b)Diluting the recipe reduced the etch rate and the undercut behaviour; however, the bottom and sidewall profile is still very non flat. (c)The HBr concentration was reduced to help improve the flatness issue and then the recipe was diluted 12 times. This recipe was still inappropriate for our masking patterns due to the bottom and sidewall non-flatness.

higher etch rate near the waveguide edges, as shown in Figure 3.16. This non uniform etch depth is due to a higher concentration of Br_2 molecules near the edges compared to far away from the edges. Br_2 molecules diffuse to the mask corners since they can't react with the substrate in the masked regions; moreover, due to their low mobility they have a higher probability of consumption near the mask corner rather than far away from the corners as shown in Figure 3.17 [33]. The $HBr/H_2O_2/H_2O/HCl$ systems are commonly used for spherical lens formation and are not suitable for the SRL fabrication.
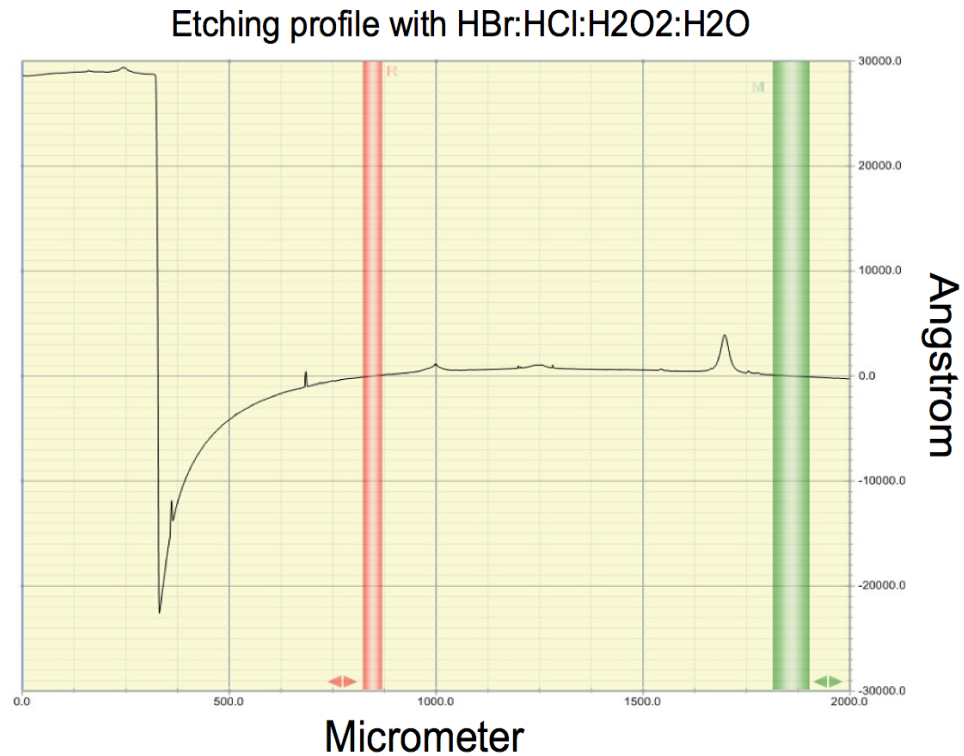
Figure 3.16: Etching profile with $HBr/H_2O_2/H_2O/HCl$ system shows the Br_2-based diffusion limited etching effect observed from the higher etch depth near the mask boundary relative to far away from it.

68
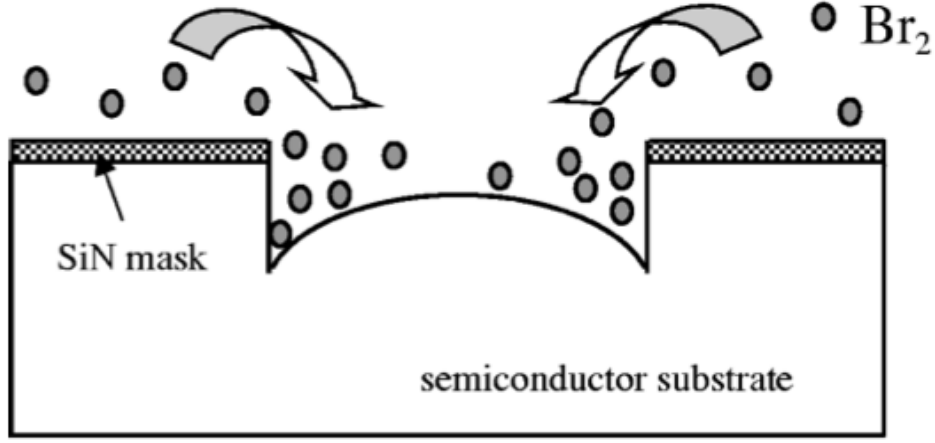
Figure 3.17: A schematic illustration of the semiconductor microlens fabrication process using Br_2-based diffusion-limited etching [33].

The most suitable selective (higher etch rate of InP to InGaAs and InGaAsP) recipe for wet etching InP was observed to be approach 5 of Table 3.4, H_3PO_4 : HBr : H_2O solution. It resulted in a vertical etch rate that was twice as fast as the in-plane etch rate. Similar to approach 4, approach 5 system also uses HBr; however, it does not have the non-uniform etch depth problem of approach 4 since there are no H_2O_2 molecules oxidizing HBr molecules and thus no Br_2 molecules are introduced into the solution.

The epi-wafer includes some InP layers alternating with InGaAs/InGaAsP layers. For removing the InGaAs and InGaAsP layers selectively and stopping at the InP layer, approach 6 of table 3.4 was used [34] [35]. This approach resulted in very smooth surfaces as observed with optical microscopy and profilometer measurements.

The wet etching process for the epi-wafer of Table 3.2 required switching between approach 5 and approach 6 solutions for a total of 5 steps in order

to selectively remove the 3 InP layers (including the protective layer on top) and the 2 InGaAs/InGaAsP layers and stop at the InAlGaAs layer above the QWs. This switching makes use of etch stop layers to allow more control over the etch depth. Etch depth measurements with the Dektak profilometer after each etch step was carried out to further monitor the etching process. Table 3.5 shows an example of the data collected to monitor the wet etching process. As seen in table 3.5 the typical total etch time was roughly 5 minutes + 40 seconds for the desired etch depth of $\sim$ 2 μm. However, it was observed that for every 2 μm etched in the vertical direction, there was a 1 μm undercut from each side of the mask. This places a limit on the minimum width of our structures for the desired etch depth, as well as resulting in relatively low steep sidewall profiles (ideally straight sidewalls are desired: slope of infinity). The side profile in the SEM image of a wet etched InP sample in Figure 3.18 shows this 1:2 ratio. Figure 3.19 shows the device condition as the wet etching time is increased for both 2 μm wide waveguides and 3 μm wide waveguides.

Table 3.5: Wet Etch Monitor Table for Sample : R2 epiwafer, ID: D04 Date: Jul19/2010

Dektak Setting [μm/sample]	Etch Time [min]	PR+Metal Height [μm]	Etchant	Step's Etch Rate [μm/min]
0.128	0	1.582		
				Continued on next page

Table 3.5 – continued from previous page

Dektak Setting [μm/sample]	Etch Time	PR+Metal Height [μm]	Etchant	Step's Etch Rate [μm/min]
0.128	2.5	1.763	H_2SO_4:H_2O_2:H_2O	0.076
0.128	2.5	3.502	H_3PO_4:HBr:H_2O	0.698
0.128	0.5	3.53	H_2SO_4:H_2O_2:H_2O	0.03
0.128	0.117	3.593	H_3PO_4:HBr:H_2O	0.53

$$\text{Overall Etch Rate} = \frac{\text{Total Etch Depth}}{\text{Total Etch Time}} = \frac{2.01}{5.62} = 0.36 \mu\text{m/min}.$$

H_2SO_4:H_2O_2:H_2O and H_3PO_4:HBr:H_2O Etch System Results

With no unexpected issues in the above etching steps, roughly a 30% yield was achieved; devices with a 3 µm waveguide width and coupling gaps of 1 µm and higher survive. Here are some factors that may contribute to defects and lower the yield further:

- The PR lifting from the the 2 µm wide devices introduces PR strips that are free to move around the sample and sit anywhere on the surface for a random amount of time during the etching process. This causes additional undesired masking effects and could be reduced by avoiding drying the sample with a nitrogen gun (or via applying very low pressure) in between etching steps.
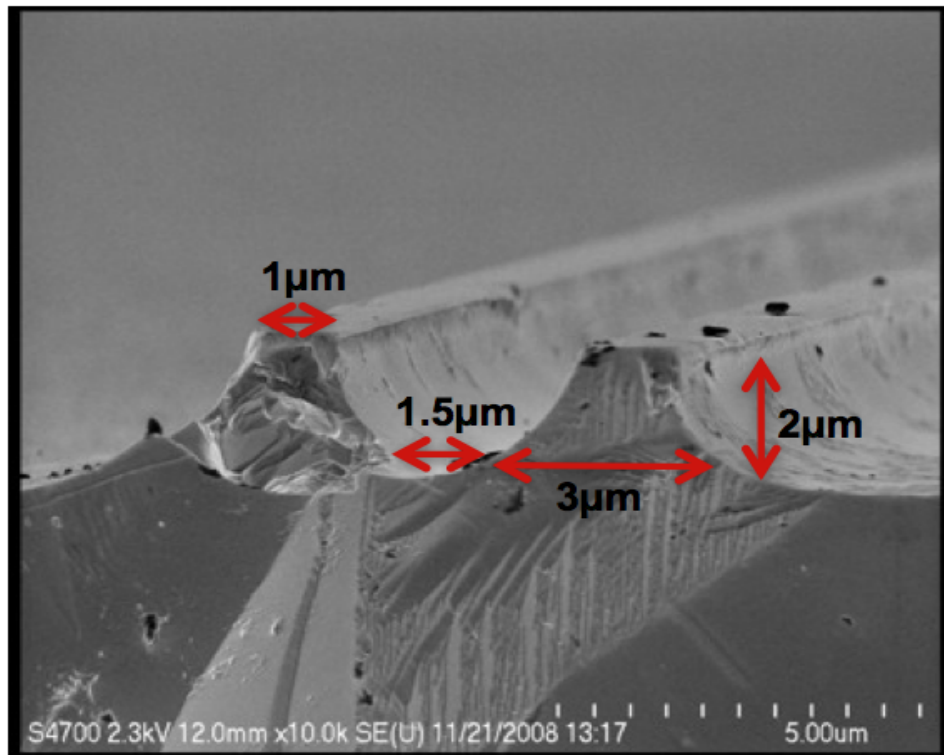
Figure 3.18: SEM image showing the side wall profile of InP after wet etching.

2um width

3um width
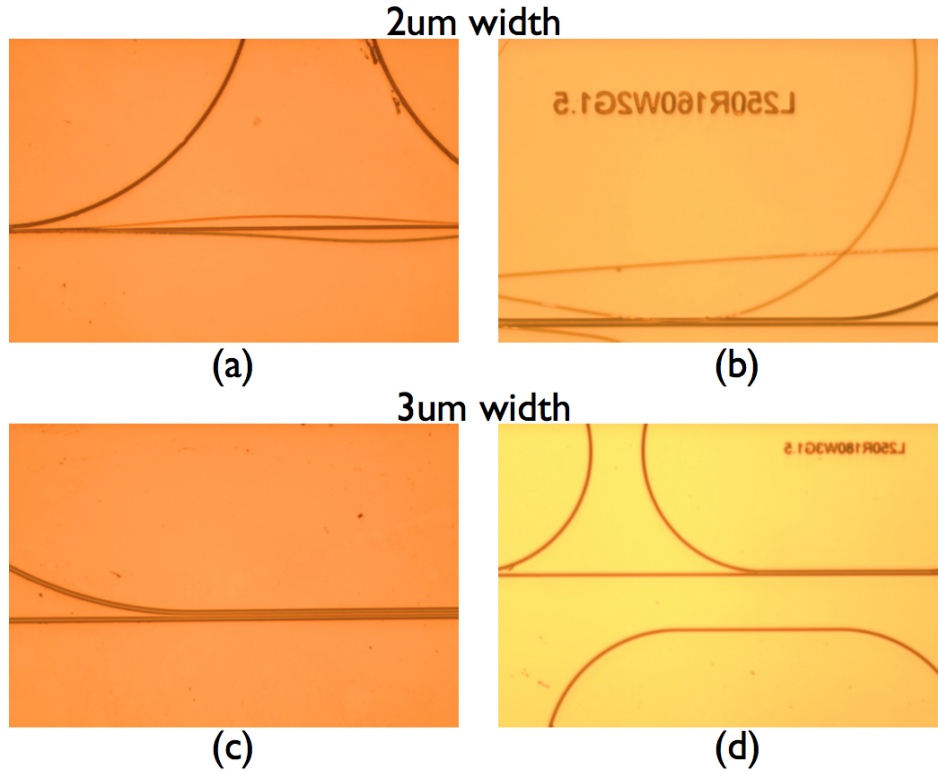
Figure 3.19: Shows the PR lifting effect due to increasing under cuts as the sample is etched for a longer time. (a)Shows the start of PR lifting at time 1 for waveguides of width 2µm. (b) Shows complete PR lifting at time 2 > time 1for waveguides of width 2µm. (c)Shows no PR lifting problems at time 1 for waveguides of width 3µm. (d) Shows no PR lifting problems at time 2> time 1for waveguides of width 3µm.
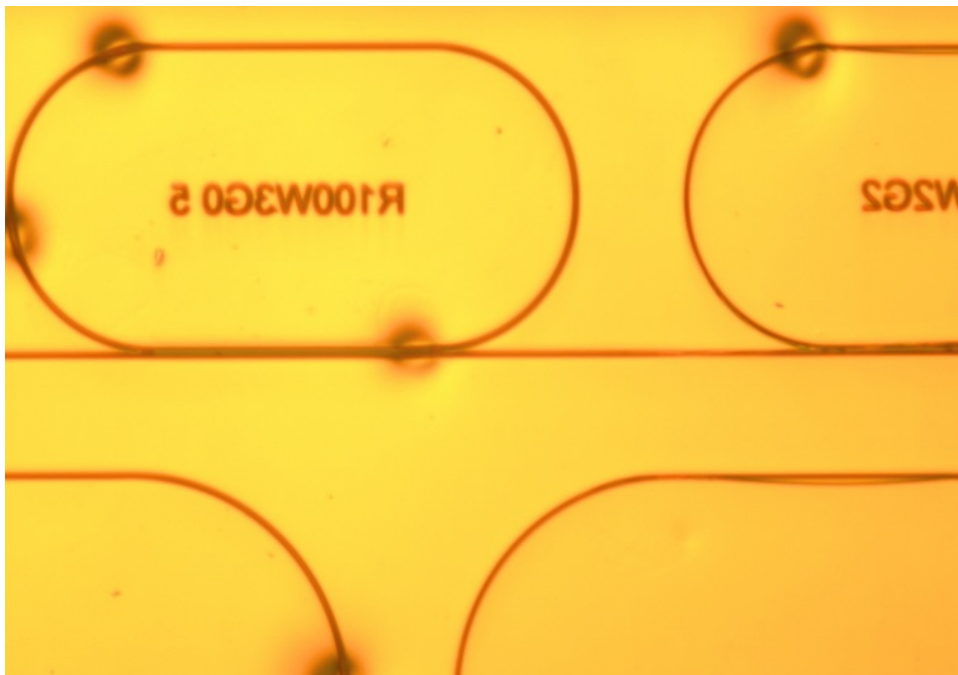
Figure 3.20: Shows defects due to formation of bubbles during wet etching. Also the PR lifting effect is observed in the 2μm wide devices.

- Bubbles forming when using some etchants containing hydrogen peroxide may cause non uniform etching and introduce undesired masking effects as seen in Figure 3.20. This problem can be reduced by agitation.

- HBr oxidation occurs in a solution that has been used and kept for a relatively longer time. This oxidation results in non uniform etching observed due to Br_2-based diffusion-limited etching. A change in the color of this solution from clear to more reddish is an indicator of this problem. A fresh solution of H_3PO_4:HBr:H_2O should always be used.

3.3.5   Planarization

The aim here is to develop a planarization technique. A successful planarization step must satisfy the following requirements:

- Provide device isolation: The dielectric film should prevent un-intended electrical connections. Thus the film must provide coverage without any cracks and sufficiently low porosity.

- Provide contact support: The dielectric film should minimize the height mismatches throughout the sample to increase contact stability.

At first, SiN_x and SiO_2 dielectric film growth followed by an etch back step was considered for the planarization and passivation process. SiO_2 film growth and etch processes were successfully developed using the PECVD machine at the UBC AMPEL Nanofabrication facility. However, this approach required an additional mask layer with an alignment tolerance better

than 1 μm and it was due to this fabrication limitation that this technique was not applied.

An alternative to the dielectric film solution is the use of polyimide. Polyimide is a photosensitive dielectric. It has been reported that UV sensitive polyimide can be lithographically masked as a dielectric film for planarization usage. However, an additional mask layer would be required, also aligning this mask layer to the small coupler gap would be very challenging and not reliable with the current mask aligner available. Instead of the traditional masking of polyimide, a new 'etch-back' process in a developer without UV irradiation was developed. Figure 3.25 shows an image of a sample planarized with Polyimide.

The process steps are the following:

Polyimide HD8220:

- Spinning: (1) 60 sec, 500 rpm, (2) 60 sec, 5000 rpm

- Softbake: 3 min at 120C on a hotplate

- Developing: ~ 5min in 10% TMA developer for the 'etch back' process, in a few steps, checked under microscope until the top of the waveguides were exposed as monitored by the colour change

- Hardbaking; 30 min at 320 C at a hotplate

Polyimide spinning process allows a non-uniform film deposition in such a way that a higher thickness of polyimide is deposited in the trenches compared to the thickness deposited on top of the waveguides. Spinning polyimide allows sidewall coverage and partial filling of gaps. This 'filling

effect' reduces the height difference throughout the sample, although it does not result in a perfectly flat surface. Figure 3.21 shows a flow diagram of the planarization step.

3.3.6   Metalization

Ohmic contacts are needed to allow the flow of electrical current into and out of the laser. A good contact is one that contributes very little to resistance, it is stable and has a linear I-V characteristic. The contact compositions chosen for the n-type InP and p-type InGaAs layers for our laser were chosen based on previously reported results by other groups[36] [37][38]. A summary of the ohmic contact data used for n-type InP and p-type InGaAs are shown in Table 3.6.

Table 3.6: Summary of Ohmic Contact Data

Metalization	**Anneal**	**Doping (cm^{-3})**	$\rho_c(\Omega\mathbf{cm}^2)$
N-InP Ni(30nm), Au/Ge(60nm), Au (80nm)	10min @ 400C in 5%H$_2$ 95%N$_2$	$2 - 8 \times 10^{18}$	2×10^{-7} [36]
P-InGaAs Pd(10nm), Ti(35nm), Pd(35nm), Au(80nm)	10min @ 400C in 5%H$_2$ 95%N$_2$	1×10^{19}	7.7×10^{-6} [37] [38]
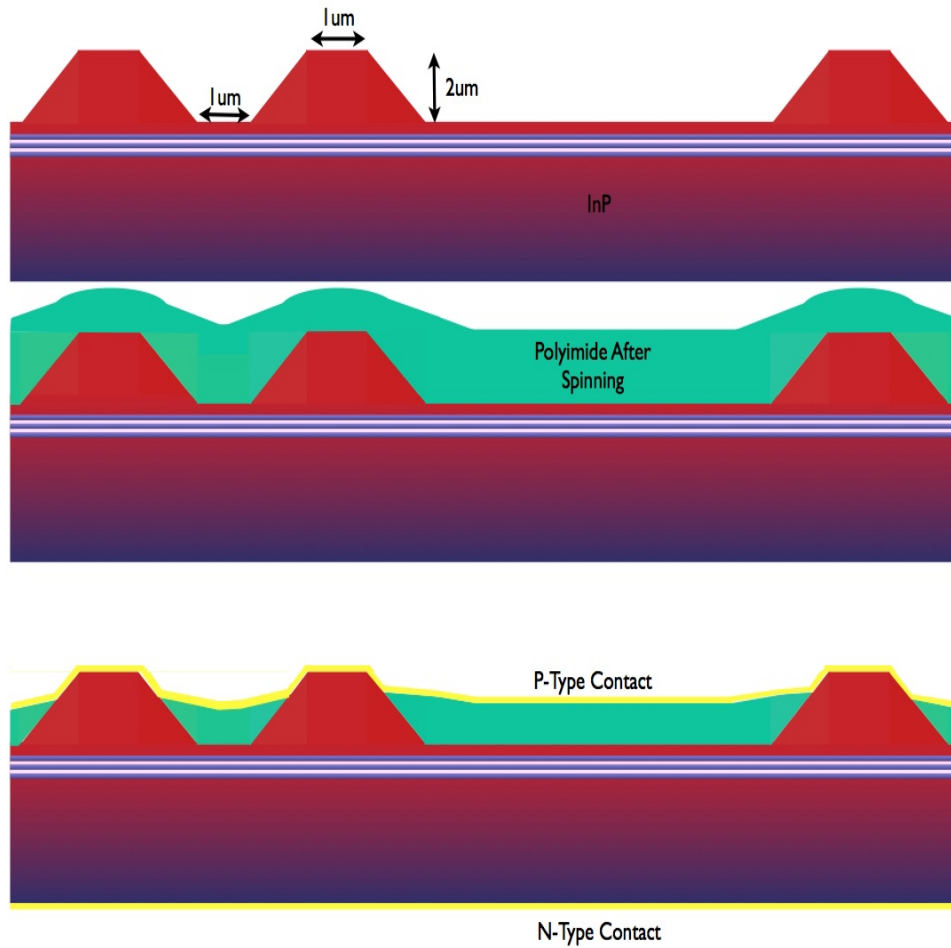
Figure 3.21: A flow diagram showing the polyimide planarization step. Once the polyimide was spinned onto the sample, an etch back process in the developer solution exposed the top of the waveguides. The next step was to evaporate the contacts.

The metal contacts were applied to the device by the e-beam evaporator available at the UBC cleanroom facility. A crystal thickness monitor was used to control the film thickness during the evaporation process [39]. The contacts were then annealed for 10 min at 400 C in $5\%H_2$ $95\%N_2$.

The contact quality was tested by measuring the IV characteristics of two separated contact regions. The contact geometry was a large circle of roughly 600 μm^2 area and the current path was as follows: Probe 1 $\rightarrow$ metal/substrate(doped InP) interface layer $\rightarrow$ substrate(doped InP) $\rightarrow$ Probe 2

Thus, the measured resistance was a total resistance R_T including resistance from the wirings R_w, probes R_p, contacts R_c and the InP material R_{InP}.

The N-type back side contact quality was tested by probing two separated metal strips and measuring the IV characteristic as shown in Figure 3.22. A total resistance of $R_T = 1.7$ Ω was obtained. The P-type top contact was tested in the same way after removal of the U-InP protective layer; the IV characteristic is shown in Figure 3.23. A total resistance of $R_T = 1.5$ Ω was obtained.

The achieved contact quality was acceptable since it satisfied the following conditions:

- The contacts exhibited reasonably low resistances, $R_T < R_{diode}$, where $R_{diode} = 37$ Ω is shown in Figure 3.27.

- The contact characteristics were ohmic
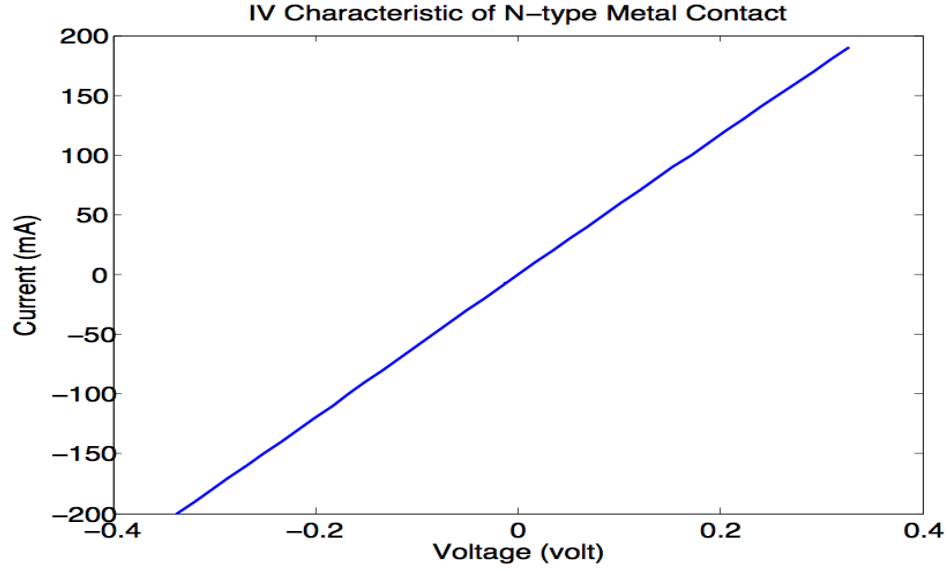
Figure 3.22: The IV characteristic of the N-type ohmic contact evaporated on the InP contact layer is shown here. A resistance of roughly 1.7 Ω.
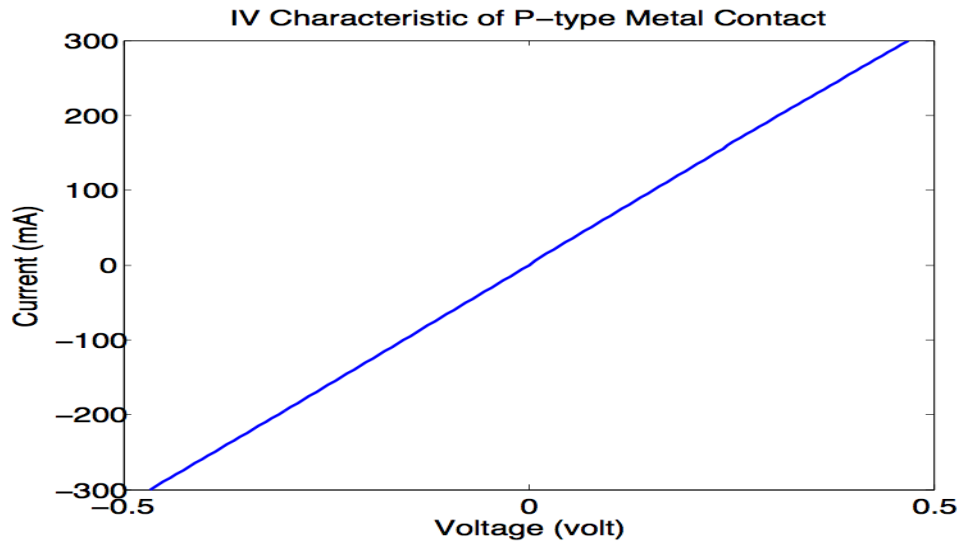
Figure 3.23: The IV characteristic of the p-type ohmic contact evaporated on the InGaAs contact layer is shown here. A resistance of roughly 1.5 Ω.

3.3.7   Cleaving

Since these devices are edge emitters, the samples need to be cleaved in-order to provide an output port for measurements. The cleaving requirements for our mask and design are:

- Provide a smooth and flat facet free of any damages such as scratches or cracks

- Separate devices, which means a cleaving pitch of about 200 μm

The cleaving process was done manually. Similar to when the wafer was cleaved into small die pieces during the sample preparation step, a tip of a diamond cutter was used to brake the sample along its crystallographic orientation line. Placing a damper such as clean wipes underneath the sample when cleaving helps the process.

Looking at the side wall of the cleaved samples as shown in the optical images of Figure 3.24 and cleaved facets in the SEM image of Figure 3.18, many defects and damages are observed as the result of the cleaving technique and process.

The device yield after the final cleaving step is very low for the following reasons:

- Cleaving location is not well controlled and results in destruction of devices,

- Coupler waveguides are damaged and/or terminated before the cleaved output edge

- Due to large cleaving pitch and limited location control, a number of resonators maybe left coupled to the same coupler waveguide. Testing devices away from the cleaved facet allows more losses due to defects (such as other devices coupled to the same output waveguide or damages to the output waveguide) along the path to the output.

- The cleaved facet has a poor quality as observed in Figure 3.18 and Figure 3.24

- A good cleaved output facet would significantly improve the amount of light coupled out as well as easing the task of fiber alignment when doing measurements.

A good facet is specially critical for the RWG edge emitter lasers since it forms the cavity as further discussed in Section 5.4. Suggestions and current efforts to improve and to replace this manual cleaving technique are explained in the final analysis section.

3.3.8   Results

Figure 3.25 shows an optical image of the fabricated devices.

A suitable setup was made with the help of Wei Shi, in order to measure the diode and laser characteristics of t he edge emitting devices. A picture of the setup is shown in Figure 3.26. After cleaving, the samples were fixed using a carbon tape onto a 4 cm × 4 cm × 2 mm copper sheet which was placed on top of a 3-axis stage. The temperature of the copper sheet was controlled by a temperature controller through a Peltier cooler. The bus top
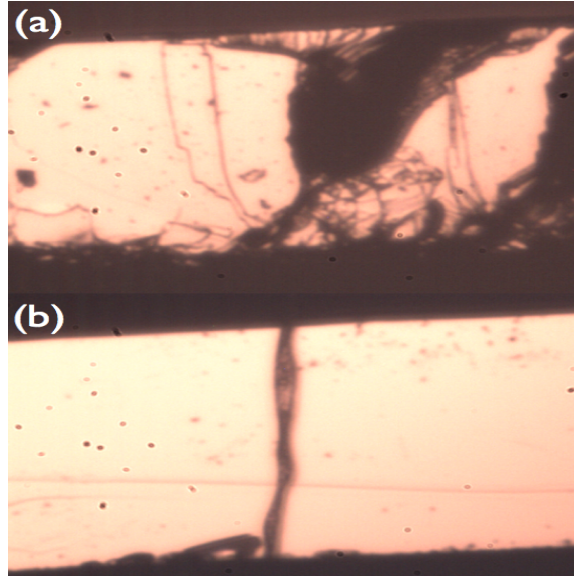
Figure 3.24: Optical images showing the side view of the wafer after cleaving. These samples were not thinned.
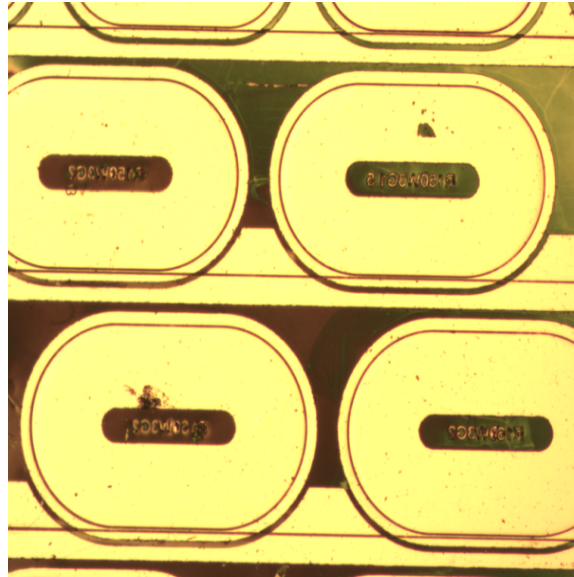
Figure 3.25: The final fabricated SRLs are displayed before cleaving. The waveguides, top contacts and the polyimide regions are all shown in this Figure.

contact was kept at a fixed low bias while the ring contact current was swept. A Matlab program (LIVdownloader.m) was used to retrieve the data.
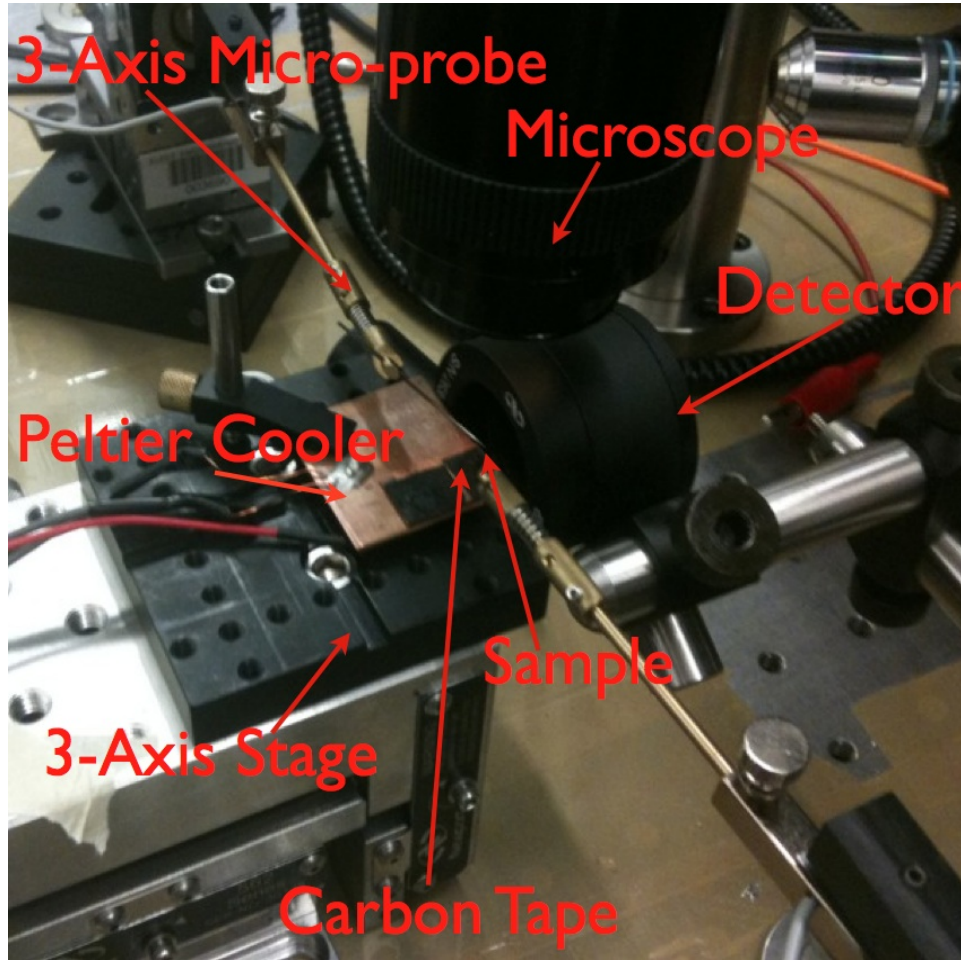
Figure 3.26: The set up used for measuring edge emitter lasers.

The IV and LI measurements of Figures 3.27(a) and 3.27(b) show that a good IV characteristic as well as light emission was successfully achieved.

The device's optical spectrum behaviour for varied bias conditions was measured using an optical spectrum analyzer (OSA), an example of such
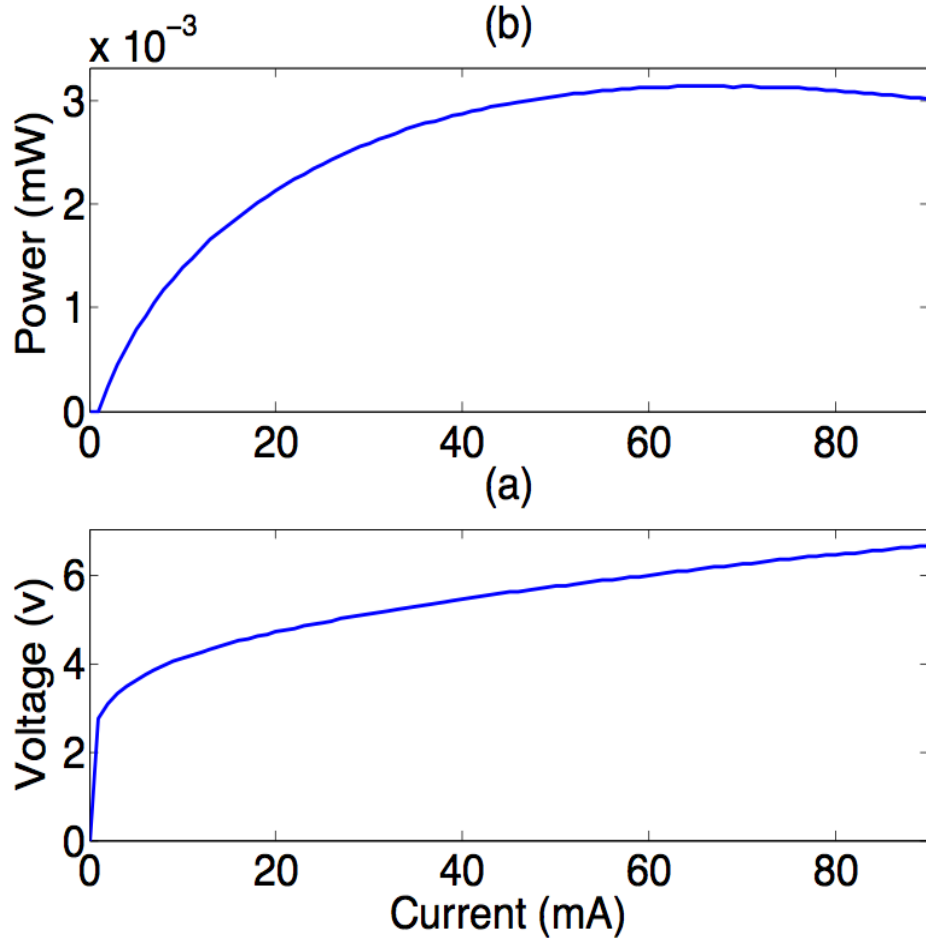
Figure 3.27: (a)IV Characteristic of a fabricated SRL with a diode resistance $R_{diode} = 37\Omega$(b)LI characteristic of a fabricated SRL.
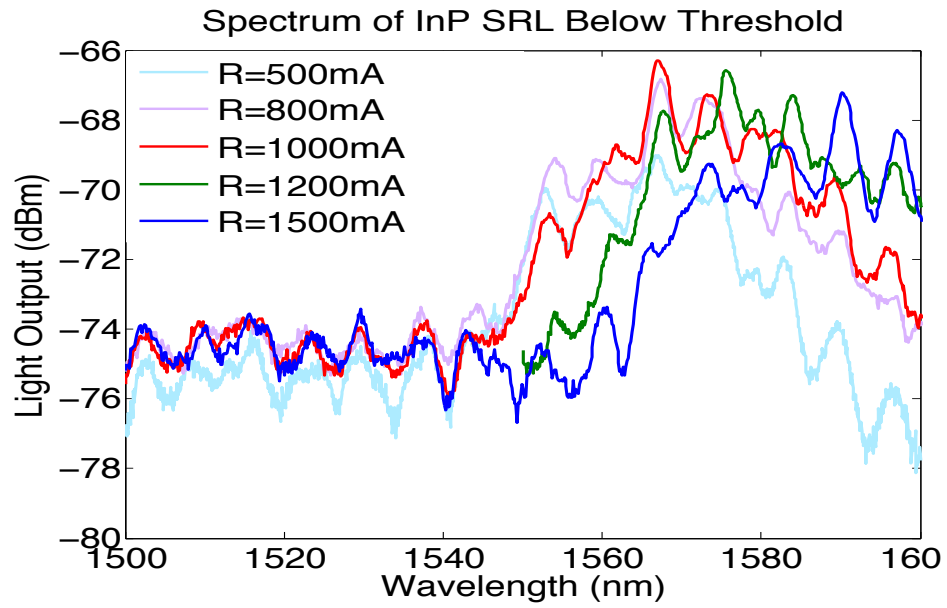
Figure 3.28: (a)Optical spectrum of a fabricated SRL biased at 500 mA, 800 mA, 1000 mA, 1200 mA, and 1500 mA. The sample was cooled to roughly 5 degrees.

measurement is shown in Figure 3.28. Lasing, however was not observed. Going to higher currents showed that the device overheated and the power rolled off before lasing could occur.

The voltage at 500mA was 6 V. Thus the power consumed by the device was:

$$P_{consumed} = IV = (1500mA)(6V) = 9W \tag{3.3}$$

The output power as measured by the OSA was:

$$P_{out} = IV = 10^{-65dBm/10} = 0.3nW \tag{3.4}$$

Device area:

$$Area = (3\mu m)(2\pi 200\mu m + 2 \times 250) = (3\mu m)(1756.6\mu m) \approx 5300\mu m^2 \tag{3.5}$$

The lasing wavelength shifts with a varying bias current. The lasing wavelength is dependent on the length (d) of the cavity and the index of refraction (n).

$$\lambda = \frac{n_g d_0}{m}(m = 1, 2, 3, 4...) \tag{3.6}$$

The gain-peak shows a shift of $\approx$ 20 nm. This shift is due to the high temperature effects.

3.3.9   Analysis

The spectrum measurements of Figure 3.28 show the gain spectrum, some resonances and the effect of increasing the bias current on the emission spectrum below threshold. Below threshold, increases in bias current contribute mostly to spontaneous emission, as also shown in the LI curve of Figure 3.27(b); there is almost no stimulated emission. An increase in the pumping rate directly contributes to an increase in the population inversion and the amplitude of the gain spectrum increases, but since there is no lasing, the emission spectrum is wide. Below threshold, the cavity losses exceed the gain coefficient, which means none of the emissions in the spectrum can experience a large enough gain to start lasing. The losses mainly due to fabrication have resulted in a very large threshold.

Some sources contributing to the cavity losses could be:

- Defects along the ring waveguide such as dirt and scratches could cause too much scattering or completely interfere with the light propagation.

- Polyimide residues leftover on some areas of the ring waveguide (before the contact evaporation step) would result in areas where there is no pumping and thus no inversion occurs.

- Metal deposition on the waveguide sidewalls could result in increased propagation losses, specially if the metal is closer to the bottom of the waveguide where it can have a higher affect on the field distribution.

- Losses due to bending, mode conversion losses

- Self-heating effect: the device's resistance could lead to heating, which would reduce the optical gain.

- Another possibility could be problems with the epitaxy. The PL and the contacts are reasonable, so there is no evidence for this hypothesis, but it has not been ruled out.

The major limiting step in the fabrication process was the cleaving. Due to the very low yield after cleaving, many devices did not have the chance to be properly tested. This process is currently under improvement. The common industry practice is to thin the wafers from their typical roughly 1 mm thickness down to 100 μm - 200 μm thickness before cleaving. We have tested the thinning idea, by manually thinning a sample on a sand paper and much better cleaving results were observed. However, doing this manually takes several hours of sanding by hand and it is not a reliable method. This wafer thinning process is done with automatic equipment in industry. We are currently putting parts together to test a wafer thinning machine at UBC.

Once the wafer is thinned, still a better cleaving tool is required. The diamond tips are too wide, a better choice are surgery knives. Surgery knives are not the common option for cleaving InP wafers, however after thinning not much force is required and the surgery knife can easily be used to cleave devices.

3.4 InP Edge Emitter Ridge Waveguide Laser

Demonstrating a RWG edge emitting laser in InP would be a step closer towards fabricating InP SRLs. The same epi-wafer used to fabricate the SRLs was used for the fabrication of the RWG lasers. A mask was designed using Clewin's Matlab script; the mask patterns consisted of long straight rectangular waveguides with varying waveguide widths. There were 2 mask layers: Layer 1 for etching and Layer 2 for contact evaporation. The etch mask was drawn wider in order to compensate for the under-etch effect. The etch mask included the following variations:

Waveguide width [μm]: 6, 8, 12, 17, 22, 27, 32, 37, 47

Waveguide contact [μm]: 2, 4, 8, 10, 15, 20, 25, 30, 40

The fabricated devices were tested and LED characteristics similar to the SRL results were obtained; however, lasing was not observed. This is again most likely due to the cleaving technique leaving a poor quality facet which is very critical for the RWG laser since the cleaved facets form the cavity mirrors. Moreover, the cleaving pitch is also currently limited to roughly 1 mm and higher. Thus the cavity lengths are large, providing a larger area for inversion and thus having higher threshold currents.

3.5 Conclusion

A commercial 1550 nm epi-wafer was purchased. The required mask was designed and purchased. The following fabrication steps were successfully achieved:

- A semi-automated mask drawing script

- A photolithography process with a resolution better than 1 µm thanks to edge bead removal

- A selective wet etching recipe giving smooth surfaces, in-plane isotropy, and an orthogonal to in-plane etch rate ratio of 2

- A planarizing technique via polyimide spinning, which does not require any extra masking step

- Reasonably low resistance, ohmic contacts for n and p contacts

An appropriate setup was made for testing edge emitters. The diode characteristics of the device was successfully measured. Light emission was also measured. The spectrum measurements were performed and the gain spectrum and some resonances were observed. However, the output power was very low, in the tenths of nWs, and lasing did not occur. The cleaving process is being improved in order to allow further testing.

Chapter 4

Fabrication Via Dry Etching

Dry etching techiques used for SRL fabrication are well published and more mature, thus we wanted to make some SRLs via dry etching to test the designs. We originally planned to pursue dry and wet etching techniques in parallel at the UBC Nanofabrication facility.

The most common dry etching techniques are reported to be high temperature Cl_2 based or hydrocarbon-based plasma. Usually the hydrocarbon-based dry etching is preferred for InP laser fabrication. The main reason for which hydrocarbon-based plasma is preferred over Cl2-based electron cyclotron resonance (ECR) plasma is that Cl2 etching rate of InP is temperature dependent [40]. In low temperatures of 80deg etching rate is <0.05 μm/min (this is due to the nonvolatile InCl reaction products, which also result in grassy-roughened surfaces), for higher temp of 230deg the rate is saturated at more than 1 μm/min [40]. This higher temperature requires a hard mask (SiO_2/or SiN). To achieve smoother side-walls and bottom surfaces high ion voltage of 900 V is reported and Cl_2 gas pressure of 7E-5 torr [40]. Meanwhile the CH_4 plasma etching is done at room temperature and it has been reported that addition of O2 decreases the etch rate but it gives selectivity of 60 (higher etching rate of InP over InAlAs) [40]. This

selectivity is explained by the oxidation of InAlAs layer, forming a thin layer of Al2O3 which could also provide electrical passivation. Addition of O2 also improves the side-wall verticality because it partially removes the polymer, which forms during the InP etching[40].

The UBC AMPEL Nanofabrication facility has an ECR machine in working condition. This machine was not suitable for CH_4 gas; however, it has Cl_2 gas available but the machine was not able to provide the required high temperatures. Investigation was done to replace the heating chuck in order to supply higher temperatures but this turned out to be an overly expensive task.

The UBC facility also has an reactive ion etcher (RIE) machine which could be used for the preferred CH_4 etching; however, this machine is not in working conditions. The machine was being repaired for over 1.5 years but it was decided that it was not going to reach working conditions. Thus we started to look dry etching fabrication outside UBC.

Dry etching fabrication of the InP SRL has started at CRN2 facility of University of Sherbrooke funded by CMC. The high resolution SRL mask was redesigned in order to take into account the dry etching approach and include a planarization step. The planarization step will be done via SiO2 deposition and etch back process instead of the previous polyimide spinning technique. Figure 4.1 shows the 3 different mask layers with layer 1 for dry etching process, layer 2 for planarization and layer 3 for metal evaporation. Figure 4.2 shows a cartoon like cross section of the epi-wafer and SRL via dry etching.

They already have a recipe developed for InP etching using a plasma

L200R150W3G2

Trench for dry etching —
Contact opening for planarization —
Top metal location —
This color shows the overlap regions —
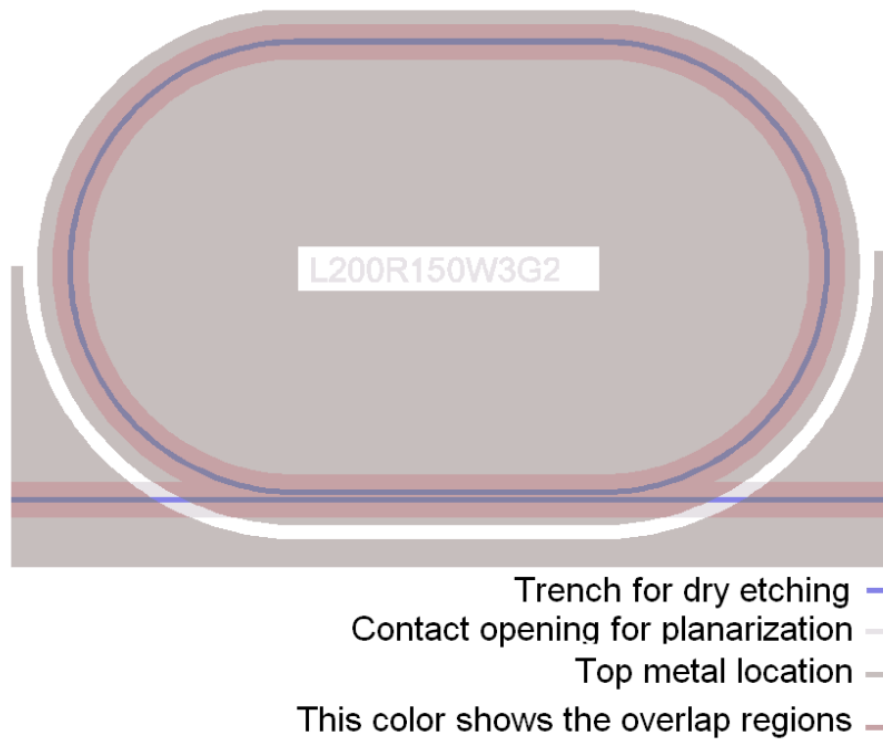
Figure 4.1: The three different mask layers used to first define the trench for dry etching, next to make a contact opening for the oxide planarization process and finally to define the metalization region for the top p-type contacts. The n-type contact is evaporated on the backside.
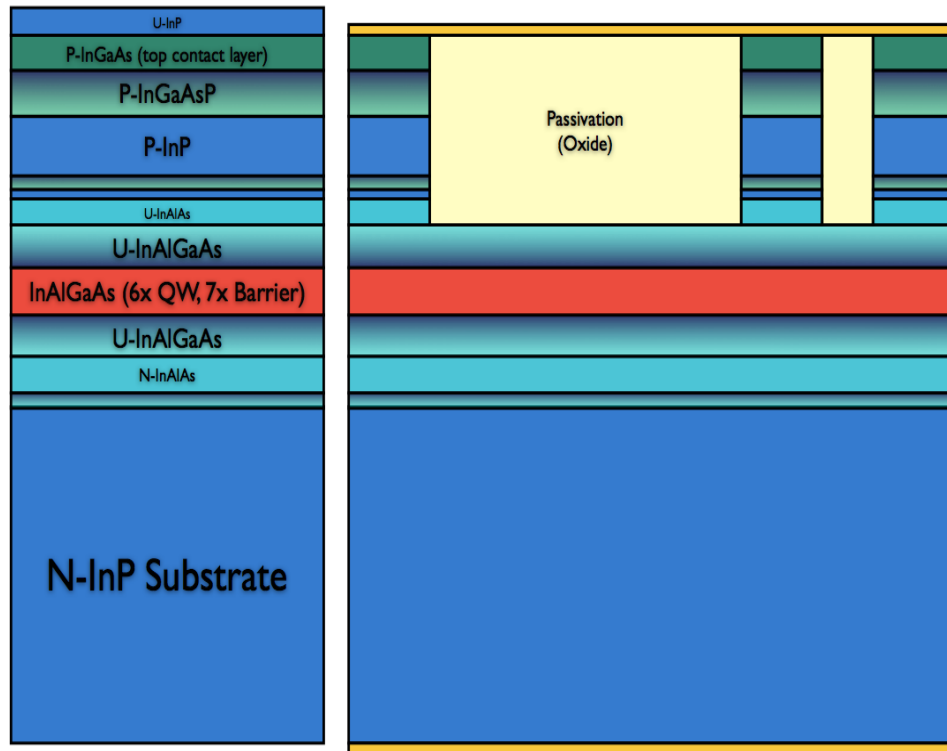
Figure 4.2: Cartoon of the epi-wafer structure and the side view of a dry etched SRL.

etcher STS ICP III-V. They have completed the first dry etching tests and tuned their recipe for our heterostructure; the etch depth is monitored with a laser end point detection system. An aspect ratio dependent etching (ARDE) was observed as depicted in Figure 4.3, which shows an SEM image of the cross section for the latest sample that was dry etched with their system.

Signal A = InLens   EHT = 3.00 kV   Mag = 3.00 K X   2 µm   CRN2   Aperture Size = 30.00 µm   Tilt Angle = 0.0 °   Date :5 Aug 2010
F600agb_17.tif   WD = 6.0 mm   ⊢——⊣   Stage at T = 3.0 °   Tilt Corrn. = Off   Time :14:53:19
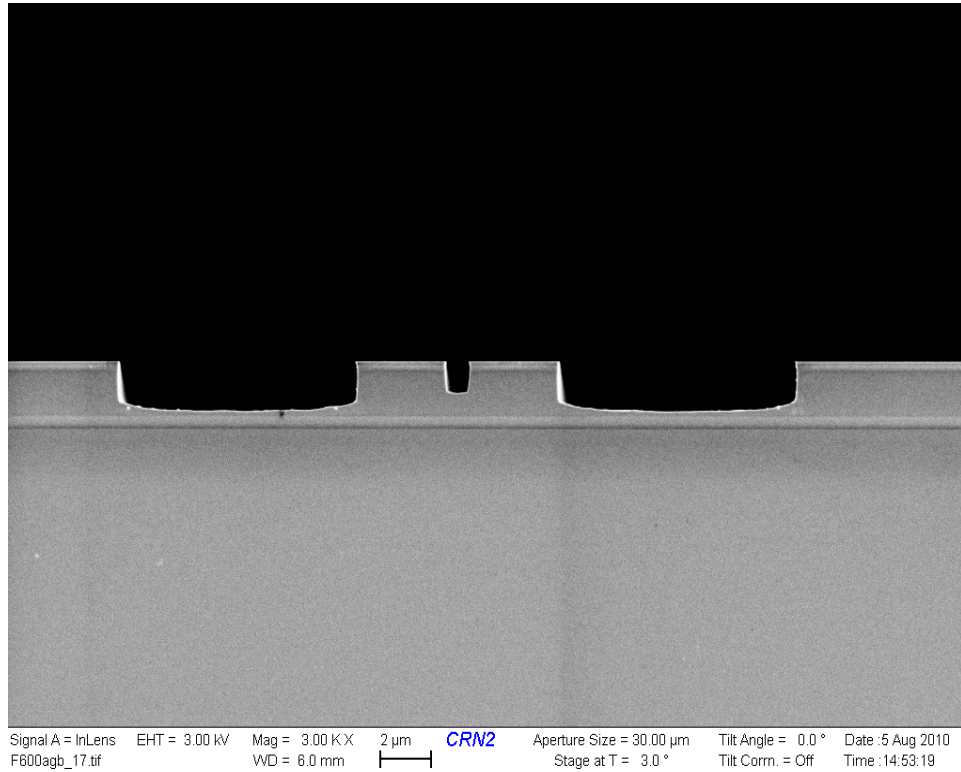
Figure 4.3: SEM image revealing the etch profile and etch depth in the coupler region and the trench region. Courtesy of Sherbrooke.

The ARDE was summarized in Figure 4.4. The ARDE can be translated in terms of the thickness between the bottom of the etched trench and the etch stop layer.
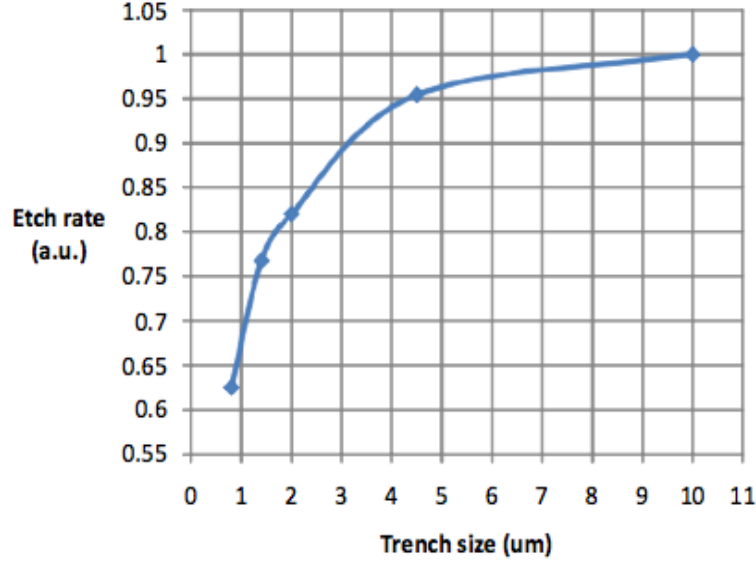
Figure 4.4: A plot of etching rate as a function of the trench size is shown here to capture the ARDE for the dry etching of the InP samples. Courtesy of Sherbrooke.

A study was done to analyze the designs etch depth tolerance. Structures were simulated in FDTD mode solver and the corresponding coupling behavior was then extracted for the etch depths predicted by the graph of Figure 4.4. The results show much stronger field interaction between the waveguides and thus much shorter crossover coupling lengths as depicted in the data of Table 4.1 and Table 4.2. In the Tables, the subscripts a and b refer to a coupler length $L_{\kappa a} = 200$ μm and a coupler length $L_{\kappa b} = 250$ μm respectively. The corresponding threshold current and output power values for the devices of Table 4.1 are predicted and presented in Table 4.3 for a device with a bend region of radius R $= 300$ μm. The etch rate dependence of the dry etching on the gap size results in much shorter crossover lengths. However these L_x values are now shorter than the current designed coupler

lengths which could make the coupling determination more challenging, but it will provide more devices at higher powers to measure and analyze. Comparing the results of Table 4.2 to Table 2.3, the achieved L_x values are very different. These two Tables present results for 3 wide devices, the only differences are the etch depths and the waveguide shapes (rectangular vs. trapezoidal). The L_x value for the trapezoidal device with an etch depth of 2 μm is 86111 μm, meanwhile for the rectangular device of etch depth 1.64 μm it is 171.1 μm. This can be explained by comparing the effect of the etch depth on the mode distributions for the structures. Comparing the first order mode distribution for the trapezoidal structure as shown in Figure 4.5 to the dry etched waveguide of etch depth 1.64 μm as depicted in Figure 4.6, a much stronger field interaction is observed between the coupler waveguides.

They are currently working to improve their recipe and perhaps to change into a selective recipe.

Table 4.1: Etch Depth Analysis, W = 2 μm

Gap (μm)	Etch Depth (μm)	n_{eff1}	n_{eff2}	κ_a	κ_b	L_x (μm)
0.5	1.1	3.268150	3.256780	0.99	0.249	68.16
0.8	1.26	3.268454	3.258455	0.625	0.88	77.51
1	1.36	3.268499	3.259402	0.27	0.99	85.19
						Continued on next page

| 1.5 | 1.54 | 3.267857 | 3.261085 | 0.149 | 0.082 | 114.4 |
| 2 | 1.64 | 3.266478 | 3.261949 | 0.931 | 0.561 | 171.1 |

Table 4.2: Etch Depth Analysis, W = 3 µm

Gap (µm)	Etch Depth (µm)	n_{eff1}	n_{eff2}	κ_a	κ_b	L_x (µm)
0.5	1.1	3.270061	3.264313	0.5	0.052	134.8
0.8	1.26	3.270126	3.264932	0.74	0.238	149.2
1	1.36	3.270069	3.265295	0.873	0.437	162.3
1.5	1.54	3.269434	3.265993	0.97	0.97	225.2
2	1.64	3.268362	3.266283	0.557	0.755	372.8

Table 4.3: Predicted Performance for Waveguide W = 2 µm R = 300 µm

Gap (µm)	I_{th} (mA)		P_{out} (mW)	
	1_a	1_b	a	b
0.5	80	58	9	3
0.8	60	69	8.5	10.5
1	56	83	4	7.9
1.5	55	57	2	1.1
2	71	61	11.8	7.2
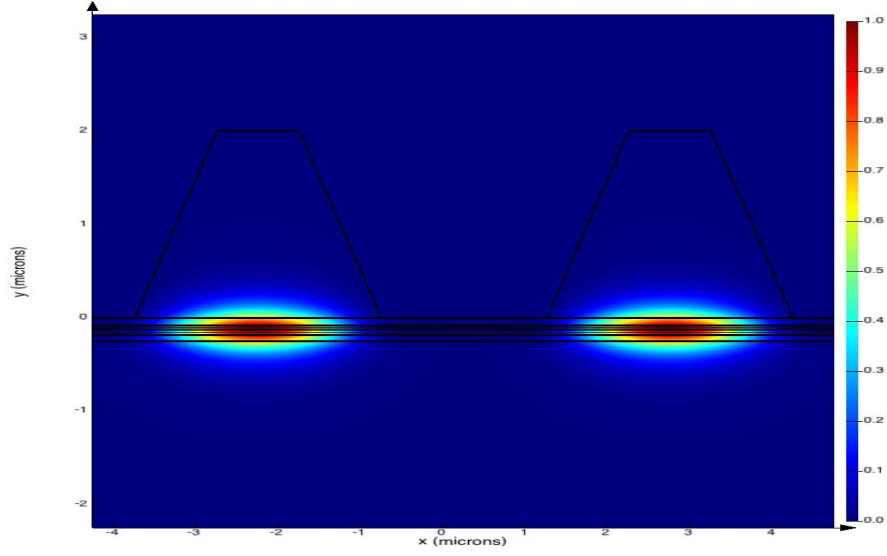
Figure 4.5: The mode distribution is shown for a trapezoidal structure with uniform 2 μm etch depth everywhere.
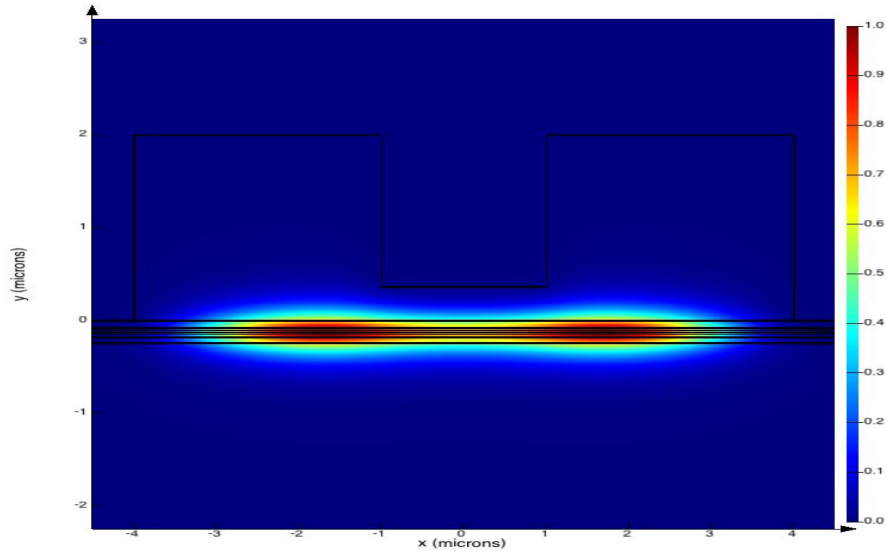
Figure 4.6: The mode distribution is shown for a structure with a 1.64 μm etch depth in the gap region and 2 μm etch depth on the outside walls of the waveguides.

Chapter 5

Conclusion

This thesis discussed the design process and process development for the fabrication of SRLs based on a commercial InP epitaxy. Unlike the well developed dry etching approach taken by other groups, we developed a new selective multi step wet etching technique for the fabrication of SRLs. This wet etching approach is a much simpler, cheaper and faster process compared to the dry etching methods. Moreover, achieving smooth surfaces by dry etching is possible however it adds more complexity to the etching process where as wet etching inherently results in smooth surfaces. Using this wet etching approach SRLs with waveguide widths as small as 3 µm can be fabricated. This limitation on the width of the device is due to the 1 to 2 relationship of the in-plane etch rate to the orthogonal etch rate.

Also a polyimide planarization technique was developed that didn't require any additional masking, UV exposure or plasma exposure.

We were able to measure the spectrum and LED characteristics of the fabricated SRLs.

5.1 Future Work

Further design, fabrication and measurement work are required in future to improve the SRL design model and optimize for device performance.

For a more accurate SRL modelling, a more detailed loss model should be incorporated into the simulations which considers:

- Bending losses: This occurs in the bend waveguide region and is a function of the bend radius.

- Mode conversion losses: This occurs when light travels from the straight waveguide region to the bend waveguide region as well as when light travels into the coupling region. Amongst other parameters, this loss is a function of the effective index difference between the regions along the light's path of travel.

- Scattering losses: This loss is due to interaction of the field at crystal imperfections and surface roughness. It is a function of the amount of field intensity at the waveguide walls as well as the waveguide surface roughness root mean square (rms) amongst other parameters.

Moreover, the power coupling prediction accuracy can be increased by considering power coupling contributions from the bend regions near the coupler region of the SRL device. Other considerations contributing to the SRL modelling accuracy are:

- The refractive index changes due to varying bias conditions since the coupling and the losses are refractive index dependent

- The effect of bias conditions and surface roughness on the dominating resonant mode (CW/CCW/bistable)

- Mode competition analysis and effects

Developing a cleaving process via wafer thinning (thinning the wafers down to 100 µm to 200 µm thickness) that results in high quality facets and allows high cleaving accuracy (allowing device separation) would significantly increase the fabrication yield and reduce the thermal effects to the substrate resistance. Moreover, in order to optimize for output power, higher power coupling coefficients are required. To achieve a higher power coupling coefficient, the higher lithography resolution (better than 300nm) needs to be increased to reduce the coupling gap during fabrication.

Measurement future work:

- Pulsed Measurement, self heating could be reduced by this technique

- Modification of the set up to include a high magnification in order to be able to see 2 µm and 3 µm wide waveguides. This would be helpful for both seeing the waveguide condition (for example damages) as well as seeing the facet, which will help both the alignment and the inspection of facet quality.

- Modifying the experimental set up so that the edge emitting devices could be measured from either one of the cleaved facets. This would allow easier lasing detection, since the device may be operating in clockwise (CW) or counter clockwise (CCW) mode depending on the bias conditions.

Bibliography

[1] *Diode Lasers and Photonic Integrated Circuits.* John Wiley and Sons INC., 1995.

[2] B. Wen, "1550nm fp-ld epiwafer specifications," LandMark, Tech. Rep., 2008.

[3] P. J. T. (Ed.), "Solvent guide," Burdick and Jackson Laboratories, Inc, Tech. Rep., 1980.

[4] L.Chrostowski and W.Shi, "Monolithic injection-locked high-speed semiconductor ring lasers," *Lightwave Technology*, vol. 26, 2008.

[5] A. ariv and P. Y. eh, *Photonics,OpticalElectronicsInModern Communications*, 6th ed. Oxford University Press, 2007.

[6] R. K.Amarnath and R.Ho, "Electrically pumped InGaAsP-InP microring optical amplifiers and lasers with surface passivation," *Photonics Technology Letters*, vol. 17, no. 11, 2005.

[7] Y. Fedoryshyn, P. Strasse, P. Ma, F. Robin, and H. Jäckel, "Optical waveguide structure for an all-optical switch based on intersubband transitions in InGaAs/AlAsSb quantum wells," *Optics Letters*, vol. 32, no. 18, 2007.

[8] T.-C. Peng, C.-C. Yang, Y.-H. Huang, M.-C. Wu, C.-L. Ho, and W.-J. Ho, "Self-terminated oxide polish technique for the waveguide ridge laser diode fabrication," *Journal of American Vacuum Society*, 2005.

[9] K. K. Masaki Yanagisawa, T. Kawasaki, R. Yamabi, S. Yaegassi, and H. Yano, "A robust all-wet-etching process for mesa formation of ingaas–inp hbt featuring high uniformity and high reproducibility," *IEEE Transactions On Electrom Devices*, vol. 51, no. 8, 2004.

[10] K. Shinoda, K. Nakahara, and H. Uchiyama, "InGaAlAs/InP ridge-waveguide lasers fabricated by highly selective dry etching in CH4/H2/02 plasma," *IEEE*, 2003.

[11] M. Sorel, P. J. R. Laybourn, G. Giuliani, and S. Donati, "Unidirectional bistability in semiconductor waveguide ring lasers," *Applied Physics Letters*, vol. 80, no. 17, 2002.

[12] J. P. R. L. Bach, Member, A. Forchel, J. L. Gentner, and L. Goldstein, "Wavelength stabilized single-mode lasers by coupled micro-square resonators," *IEEE Photonics Technology Letters*, vol. 15, no. 3, 2003.

[13] K. Amarnath, R. Grover, Member, S. Kanakaraju, and P.-T. Ho, "Electrically pumped IGaAsP–InP microring optical amplifiers and lasers with surface passivation," *IEEE Photonics Technology Letters*, vol. 17, no. 11, 2005.

[14] S. F. rst, M. Sorel, A. Scire', G. Giuliani, and S. Yu, "Technological challenges for cw operation of small-radius semiconductor ring lasers," *Proc. of SPIE*, vol. 6184, 2006.

[15] S. Park, S.-S. Kim, L. Wang, and S.-T. Ho, "InGaAsP–InP nanoscale waveguide-coupled microring lasers with submilliampere threshold current using Cl–N-based high-density plasma etching," *IEEE Journal Of Quantum Electronics*, vol. 41, no. 3, 2005.

[16] A. W. Fang, R. Jones, H. Park, O. Cohen, O. Raday, M. J. Paniccia, and J. E. Bowers, "Integrated AlGaInAs-silicon evanescent racetrack laser and photodetector," *Optical Society of America*, 2007.

[17] O. Tadanaga, K. Tateno, H. Uenohara, T. Kagawa, and C. Amano, "An 850-nm InAlGaAs strained quantum-well vertical-cavity surface-emitting laser grown on GaAs (311)b substrate with high-polarization stability," *IEEE Photonics Technology Letters*, vol. 12, no. 8, 2000.

[18] S. F. rst, M. Sorel, A. Scire', G. Giuliani, and S. Yu, "Technological challenges for cw operation of small-radius semiconductor ring lasers," *Proc. of SPIE*, vol. 6184, 2006.

[19] R. Vafaei, "Silicon on insulator add-drop racetrack resonators," sOI Paper Report.

[20] A.Yariv and P.Yeh, *Photonics, Optical Electronics In Modern Communications*, 6th ed. Oxford University Press, 2007.

[21] R. et al, "Low loss GaAs/AlGaAs optical waveguides on InP substrates," *IEEE Photonics Technology Letters*, vol. 2, 1990.

[22] [Online]. Available: www.mina.ubc.ca/course_nanophotonics2010

[23] W. Shi, R. Vafaei, M. A. G. Torres, N. A. F. Jaeger, and L. Chrostowski, "Design and characterization of microring reflectors with a waveguide crossing," *Optics Letters*, vol. 35, 2010.

[24] ——, "Design and characterization of microring reflectors with a waveguide crossing," in *2010 International Conference on Optical MEMS and Nanophotonics*, 2010.

[25] N. Rouger, L. Chrostowski, and R. Vafaei, "Temperature effects on silicon on insulator (soi) racetrack resonators: a coupled analytic and 2d finite difference approach," *Lightwave Technology*, vol. 28, 2010.

[26] [Online]. Available: www.nanofab.ubc.ca/content/about-facility

[27] [Online]. Available: http://www.nanofab.ubc.ca/process_view

[28] [Online]. Available: www.microchemicals.eu/technical-information

[29] [Online]. Available: www.nanofab.ubc.ca/process-photolithography

[30] [Online]. Available: http://www.nanofab.ubc.ca/equipment_view

[31] A.R.Clawson, "Guide to references on iii-v semiconductor chemical etching," *Material Science and Engineering*, 2001.

[32] S. Adachi and H. Kawaguchi, "Chemical etching characteristics of (001)lnP," *J. Electrochem. Soc.: Solid-State Science And Technology*, vol. 128, no. 6, 1981.

[33] Y.-S. Kim, J. Kim, J.-S. Choe, Y.-G. Roh, H. Jeon, J. Kim, J.-S. Choe, Y.-G. Roh, H. Jeon, and J. C. Woo, "Semiconductor microlenses fabri-

cated by one-step wet etching," *IEEE PHOTONICS TECHNOLOGY LETTERS*, vol. 12, no. 5, 2000.

[34] F. Fiedler, A. Schlachetzki, and G. Klein, "Material-selective etching of InP and an InGaAsP alloy," *Journal of Materials Science*, vol. 17, 1982.

[35] P. H.Holloway and G. E.McGuire, Eds., *Handbook Of Compund Semiconductors Growth, Processing, Characterization and Devices*. Noyes Publications, 1995.

[36] J. R. ABELSON, T. W. SIGMON, G. BAHIR, and J. L. MERZ, "Rapid thermal alloyed ohmic contact on inp," *Journal of Electronic Materials*, vol. 16, no. 4, 1987.

[37] E. F. Chor, W. K. Chong, and C. H. Heng, "Alternative Pd,Ti,Au contacts to Pt,Ti,Au contacts for In0.53Ga0.47As," *JOURNAL OF APPLIED PHYSICS*, vol. 84, no. 5, 1998.

[38] E. Chor, D.Zhang, H.Hong, W. Chong, and S. Ong, "Electrical characterization, metallurgical investigation, and thermal stability studies of (pd, ti, au)-based ohmic contacts," *JOURNAL OF APPLIED PHYSICS*, vol. 87, no. 5, 2000.

[39] Evaporator. [Online]. Available: http://www.nanofab.ubc.ca/ equipment_view

[40] Wada and Hasegawa, Eds., *InP-based Materials and Devices*. Wiley-Interscience, 1999.

Appendix A

Clewin Matlab Script Used for the Mask Layout

```
%This script will create the etch mask layer
% Due to Clewin file script size limitation, separate scripts had to be written and positioned
%after each other to make the whole mask.
% Each of the scripts titled Script 01a to Script 01f will make 3 rows of the mask.
%All scripts are the same except for varying ring\radius and gaps.
%%%%%%%%%%%%%%%%%%%%%%% Script 01a %%%%%%%%%%%%%%%%%%%%%%%%%
%Create an angle vector between -90deg to 90deg, ex:100 angles
angle = linspace(-pi/2,pi/2,100);
offset = 80;
yshift = 0;
yshiftNext = 0;
xshift = 0;
%Create a radius vector giving a radius for each angle:
rInner = [300,250,200,180,160,150,100];%Radius for the inner circle
lenR = length(rInner);
width = [2,3];%rOuter-rInner;
lenw = length(width);
gapArray1 = [0.5,0.5,1,1,1.5,1.5,2,2,1,1,1.5,1.5,2,2];
gapArray2 = [1.5,1.5,2,2,2,1.5,1,1];
```

```
CouplingL = 200;

LofDye=6500;

x1Shift_init=0;

    for iR = 1:3;%lenR

        iG=1;

                for iw = 1:lenw

                w = width(iw);

                if w==2

                    gapArray=gapArray1;

                    lenG = length(gapArray);

                else

                    gapArray = gapArray2;

                    lenG = length(gapArray);

                end

                rOuter = width(iw)+rInner; %Radius for the outer circle for a given width

                %Calculate the nodes of a inner circle and an outer circle,

                nodesInnery = rInner(iR).*sin(angle)+yshift;

                nodesOutery = rOuter(iR).*sin(angle)+yshift;

                lenN = length(nodesInnery);

                Rnodes = [];

                Lnodes = [];

                LofRaceTrack = rOuter(iR)*2+CouplingL+offset;

                CurrentNumofRaceTracks= round(LofDye/(LofRaceTrack));

                %Calculate the nodes of a half ring,

                %i.e. a matrix with 2 columns and 1000 rows:

                for iRx = 1:CurrentNumofRaceTracks/2+1

                    if iRx < CurrentNumofRaceTracks/2 && iR==2 && iRx==1

                        xshift = xshift+50;

                    end

                     gap = gapArray(iRx);
```

```
  if gap == 0.5 && w==2
      shiftUp = (gap - 0.5)+2*w;
 else
      shiftUp = (gap - 0.5)+2*w;
 end
nodesInnerx = rInner(iR).*cos(angle)+xshift;
nodesOuterx = rOuter(iR).*cos(angle)+xshift;
for index = 1:lenN
    if (nodesOuterx(index)-nodesInnerx(index))>= 0
        nodesy(index) = nodesOutery(index)+shiftUp;
        Rnodesx(index) = nodesOuterx(index)+CouplingL/2;
        Rnodes = [Rnodesx(:), nodesy(:)];
        Lnodesx(index) = nodesOuterx(index) - 2.*nodesOuterx(index)
        - CouplingL/2+2*xshift;
        Lnodes = [Lnodesx(:), nodesy(:)];
    end
    lenNr = length(Rnodes(:,1));
    %calculate nodes of coupling length
    x2couplingT = Rnodes(lenNr,1);
    x1couplingT = x2couplingT - CouplingL;
    y2couplingT = Rnodes(lenNr,2)+w/2;
    y1couplingT = y2couplingT - w;
    x2couplingB = Rnodes(1,1);
    x1couplingB = x2couplingB - CouplingL+ x1Shift_init;
    y2couplingB = Rnodes(1,2)+w/2;
    y1couplingB = y2couplingB - w;
    x1Line_init = -400;
    x1Line = x1Line_init + xshift;
    x2Line = x1Line_init+LofRaceTrack+10; %*CurrentNumofRaceTracks;
    y2Line = y1couplingB - gap;
```

```
                    y1Line = y2Line- w;

                    iG = iG+1;

            end

            if iRx > CurrentNumofRaceTracks/2 && iR == 2  && w==2

                rectangle(x1couplingB-rOuter(iR)-offset*0.5, y1Line,x2couplingB-100,y2Line);

                rectangle(x2couplingB-100, y1Line-0.5,x2couplingB+rOuter(iR)+offset,y2Line+0.5);

                xshiftNext = 2*rOuter(iR)+CouplingL+offset-400;

                xshift = xshift+xshiftNext;

            else

                wire(1,w,Rnodes); %Right half ring

                rectangle(x1couplingT,y1couplingT,x2couplingT,y2couplingT);

                rectangle(x1couplingB,y1couplingB,x2couplingB,y2couplingB);

                wire(1,w,Lnodes); %Left half ring

                rectangle(x1couplingB-rOuter(iR)-offset*0.5, y1Line,x2couplingB

                +rOuter(iR)+offset*0.5,y2Line);

                xshiftNext = 2*rOuter(iR)+CouplingL+offset;

                xshift = xshift+xshiftNext;

            end

             if iRx==1 && w==2

                  rectangle(-700, y1Line,x1couplingB-rOuter(iR)-offset*0.5,y2Line);

                  elseif iRx>=CurrentNumofRaceTracks/2 && w==3

                  rectangle(x2couplingB+rOuter(iR)+offset*0.5, y1Line,7600,y2Line);

             end

        end

    end

     xshift = 0;

     if iR<lenR

     yshiftNext = rOuter(iR)+ rOuter(iR+1)+gap+2*w+offset;

     yshift = yshift + yshiftNext;

end
```

```
end


%%%%%%%%%%%%%%%%%%%%%% Script 01b %%%%%%%%%%%%%%%%%%%%%%%%%

Create an angle vector between -90deg to 90deg, ex:100 angles

angle = linspace(-pi/2,pi/2,100);

offset = 80;

yshift = 0;

yshiftNext = 0;

xshift = 0;

%Create a radius vector giving a radius for each angle:

rInner = [180,160,150,100];%Radius for the inner circle

lenR = length(rInner);

width = [2,3];%rOuter-rInner;

lenw = length(width);

gapArray1 = [0.5,0.5,1,1,1.5,1.5,2,2,1,1,1.5,1.5,2,2];

gapArray2 = [1,1.5,1.5,1.5,2,2,1,1];

CouplingL = 200;

LofDye=6730;

x1Shift_init=0;

    for iR = 1:3;%lenR

        iG=1;

                for iw = 1:lenw

                w = width(iw);

                if w==2

                    gapArray=gapArray1;

                    lenG = length(gapArray);

                else

                    gapArray = gapArray2;

                    lenG = length(gapArray);

                end
```

```
rOuter = width(iw)+rInner; %Radius for the outer circle for a given width
%Calculate the nodes of a inner circle and an outer circle,
nodesInnery = rInner(iR).*sin(angle)+yshift;
nodesOutery = rOuter(iR).*sin(angle)+yshift;
lenN = length(nodesInnery);
Rnodes = [];
Lnodes = [];
LofRaceTrack = rOuter(iR)*2+CouplingL+offset;
CurrentNumofRaceTracks= round(LofDye/(LofRaceTrack));
%Calculate the nodes of a half ring,
%i.e. a matrix with 2 columns and 1000 rows:
for iRx = 1:CurrentNumofRaceTracks/2+1
    if iRx < CurrentNumofRaceTracks/2 && iR==2 && iRx==1
        xshift = xshift-50 Remove -700 line
    end
     gap = gapArray(iRx);
     if gap == 0.5 && w==2
         shiftUp = (gap - 0.5)+2*w;
     else
         shiftUp = (gap - 0.5)+2*w;
     end
    nodesInnerx = rInner(iR).*cos(angle)+xshift;
    nodesOuterx = rOuter(iR).*cos(angle)+xshift;
    for index = 1:lenN
        if (nodesOuterx(index)-nodesInnerx(index))>= 0
            nodesy(index) = nodesOutery(index)+shiftUp;
            Rnodesx(index) = nodesOuterx(index)+CouplingL/2;
            Rnodes = [Rnodesx(:), nodesy(:)];
            Lnodesx(index) = nodesOuterx(index) - 2.*nodesOuterx(index)
            - CouplingL/2+2*xshift;
```

```
        Lnodes = [Lnodesx(:), nodesy(:)];
    end
    lenNr = length(Rnodes(:,1));
    %calculate nodes of coupling length
    x2couplingT = Rnodes(lenNr,1);
    x1couplingT = x2couplingT - CouplingL;
    y2couplingT = Rnodes(lenNr,2)+w/2;
    y1couplingT = y2couplingT - w;
    x2couplingB = Rnodes(1,1);
    x1couplingB = x2couplingB - CouplingL+ x1Shift_init;
    y2couplingB = Rnodes(1,2)+w/2;
    y1couplingB = y2couplingB - w;
    x1Line_init = -400;
    x1Line = x1Line_init + xshift;
    x2Line = x1Line_init+LofRaceTrack+10; %*CurrentNumofRaceTracks;
    y2Line = y1couplingB - gap;
    y1Line = y2Line- w;
    iG = iG+1;
end
if iRx > CurrentNumofRaceTracks/2 && iR == 2  && w==2
    rectangle(x1couplingB-rOuter(iR)-offset*0.5, y1Line,x2couplingB-100,y2Line);
    rectangle(x2couplingB-100, y1Line-0.5,x2couplingB+rOuter(iR)+offset,y2Line+0.5);
    xshiftNext = 2*rOuter(iR)+CouplingL+offset-250;
    xshift = xshift+xshiftNext;
else
    wire(1,w,Rnodes); %Right half ring
    rectangle(x1couplingT,y1couplingT,x2couplingT,y2couplingT);
    rectangle(x1couplingB,y1couplingB,x2couplingB,y2couplingB);
    wire(1,w,Lnodes); %Left half ring
    rectangle(x1couplingB-rOuter(iR)-offset*0.5, y1Line,x2couplingB
```

```
                        +rOuter(iR)+offset*0.5,y2Line);

                        xshiftNext = 2*rOuter(iR)+CouplingL+offset;

                        xshift = xshift+xshiftNext;

                end

                if iRx==1 && w==2

                        rectangle(-700, y1Line,x1couplingB-rOuter(iR)-offset*0.5,y2Line);

                        elseif iRx>=CurrentNumofRaceTracks/2 && w==3

                        rectangle(x2couplingB+rOuter(iR)+offset*0.5, y1Line,7600,y2Line);

                end

            end

        end

         xshift = 0;

         if iR<lenR

         yshiftNext = rOuter(iR)+ rOuter(iR+1)+gap+2*w+offset;

         yshift = yshift + yshiftNext;

    end

end


%%%%%%%%%%%%%%%%%%%%%%% Script 01c %%%%%%%%%%%%%%%%%%%%%%%%%%
%Create an angle vector between -90deg to 90deg, ex:100 angles

angle = linspace(-pi/2,pi/2,100);

offset = 80;

yshift = 0;

yshiftNext = 0;

xshift = 0;

%Create a radius vector giving a radius for each angle:

rInner = [100];%Radius for the inner circle

lenR = length(rInner);

width = [2,3];%rOuter-rInner;

lenw = length(width);
```

```
gapArray1 = [0.5,0.5,1,1,1.5,1.5,2,2,1,1,1.5,1.5,2,2];

gapArray2 = [0.5,1,1,1.5,1.5,1.5,2,2,1,1];

CouplingL = 200;

LofDye=6730;

x1Shift_init=0;

    for iR = 1:lenR

        iG=1;

            for iw = 1:lenw

            w = width(iw);

            if w==2

                gapArray=gapArray1;

                lenG = length(gapArray);

            else

                gapArray = gapArray2;

                lenG = length(gapArray);

            end

            rOuter = width(iw)+rInner; %Radius for the outer circle for a given width

            %Calculate the nodes of a inner circle and an outer circle,

            nodesInnery = rInner(iR).*sin(angle)+yshift;

            nodesOutery = rOuter(iR).*sin(angle)+yshift;

            lenN = length(nodesInnery);

            Rnodes = [];

            Lnodes = [];

            LofRaceTrack = rOuter(iR)*2+CouplingL+offset;

            CurrentNumofRaceTracks= round(LofDye/(LofRaceTrack));

            %Calculate the nodes of a half ring,

            %i.e. a matrix with 2 columns and 1000 rows:

            for iRx = 1:CurrentNumofRaceTracks/2+1

                if iRx < CurrentNumofRaceTracks/2 && iR==2 && iRx==1

                    xshift = xshift-50;
```

```
          end
 gap = gapArray(iRx);
 if gap == 0.5 && w==2
      shiftUp = (gap - 0.5)+2*w;
 else
      shiftUp = (gap - 0.5)+2*w;
 end
nodesInnerx = rInner(iR).*cos(angle)+xshift;
nodesOuterx = rOuter(iR).*cos(angle)+xshift;
for index = 1:lenN
    if (nodesOuterx(index)-nodesInnerx(index))>= 0
        nodesy(index) = nodesOutery(index)+shiftUp;
        Rnodesx(index) = nodesOuterx(index)+CouplingL/2;
        Rnodes = [Rnodesx(:), nodesy(:)];
        Lnodesx(index) = nodesOuterx(index) - 2.*nodesOuterx(index)
        - CouplingL/2+2*xshift;
        Lnodes = [Lnodesx(:), nodesy(:)];
    end
    lenNr = length(Rnodes(:,1));
    %calculate nodes of coupling length
    x2couplingT = Rnodes(lenNr,1);
    x1couplingT = x2couplingT - CouplingL;
    y2couplingT = Rnodes(lenNr,2)+w/2;
    y1couplingT = y2couplingT - w;
    x2couplingB = Rnodes(1,1);
    x1couplingB = x2couplingB - CouplingL+ x1Shift_init;
    y2couplingB = Rnodes(1,2)+w/2;
    y1couplingB = y2couplingB - w;
    x1Line_init = -400;
    x1Line = x1Line_init + xshift;
```

```matlab
                x2Line = x1Line_init+LofRaceTrack+10; %*CurrentNumofRaceTracks;

                y2Line = y1couplingB - gap;

                y1Line = y2Line- w;

                iG = iG+1;

            end

            if iRx > CurrentNumofRaceTracks/2 && iR == 2  && w==2

                rectangle(x1couplingB-rOuter(iR)-offset*0.5, y1Line,x2couplingB-100,y2Line);

                rectangle(x2couplingB-100, y1Line-0.5,x2couplingB+rOuter(iR)+offset,y2Line+0.5);

                xshiftNext = 2*rOuter(iR)+CouplingL+offset-250;

                xshift = xshift+xshiftNext;

            else

                wire(1,w,Rnodes); %Right half ring

                rectangle(x1couplingT,y1couplingT,x2couplingT,y2couplingT);

                rectangle(x1couplingB,y1couplingB,x2couplingB,y2couplingB);

                wire(1,w,Lnodes); %Left half ring

                rectangle(x1couplingB-rOuter(iR)-offset*0.5, y1Line,x2couplingB

                +rOuter(iR)+offset*0.5,y2Line);

                xshiftNext = 2*rOuter(iR)+CouplingL+offset;

                xshift = xshift+xshiftNext;

            end

             if iRx==1 && w==2

                    rectangle(-700, y1Line,x1couplingB-rOuter(iR)-offset*0.5,y2Line);

                    elseif iRx>=CurrentNumofRaceTracks/2 && w==3

                    rectangle(x2couplingB+rOuter(iR)+offset*0.5, y1Line,7600,y2Line);

             end

        end

   end

 xshift = 0;

 if iR<lenR

 yshiftNext = rOuter(iR)+ rOuter(iR+1)+gap+2*w+offset;
```

```
        yshift = yshift + yshiftNext;

    end

end


%%%%%%%%%%%%%%%%%%%%%%%%%% Script 01d %%%%%%%%%%%%%%%%%%%%%%%%%%%%%
%Create an angle vector between -90deg to 90deg, ex:100 angles
angle = linspace(-pi/2,pi/2,100);
offset = 80;
yshift = 0;
yshiftNext = 0;
xshift = 0;
%Create a radius vector giving a radius for each angle:
rInner = [250,200,180,160,150,100];%Radius for the inner circle
lenR = length(rInner);
width = [2,3];%rOuter-rInner;
lenw = length(width);
gapArray1 = [0.5,0.5,1,1,1.5,1.5,2,2,1,1,1.5,1.5,2,2];
gapArray2 = [1,1.5,1.5,1.5,2,2,1,1];
CouplingL = 250;
LofDye=6600;
x1Shift_init=0;
    for iR = 1:4;%lenR
        iG=1;
                for iw = 1:lenw
            w = width(iw);
            if w==2
                gapArray=gapArray1;
                lenG = length(gapArray);
            else
                gapArray = gapArray2;
```

```
        lenG = length(gapArray);
    end
    rOuter = width(iw)+rInner; %Radius for the outer circle for a given width
    %Calculate the nodes of a inner circle and an outer circle,
    nodesInnery = rInner(iR).*sin(angle)+yshift;
    nodesOutery = rOuter(iR).*sin(angle)+yshift;
    lenN = length(nodesInnery);
    Rnodes = [];
    Lnodes = [];
    LofRaceTrack = rOuter(iR)*2+CouplingL+offset;
    CurrentNumofRaceTracks= round(LofDye/(LofRaceTrack));
    %Calculate the nodes of a half ring,
    %i.e. a matrix with 2 columns and 1000 rows:
    for iRx = 1:CurrentNumofRaceTracks/2+1
        if iRx < CurrentNumofRaceTracks/2 && iR==2 && iRx==1
            xshift = xshift+50;
        end
         gap = gapArray(iRx);
         if gap == 0.5 && w==2
             shiftUp = (gap - 0.5)+2*w;
          else
             shiftUp = (gap - 0.5)+2*w;
          end
        nodesInnerx = rInner(iR).*cos(angle)+xshift;
        nodesOuterx = rOuter(iR).*cos(angle)+xshift;
        for index = 1:lenN
            if (nodesOuterx(index)-nodesInnerx(index))>= 0
                nodesy(index) = nodesOutery(index)+shiftUp;
                Rnodesx(index) = nodesOuterx(index)+CouplingL/2;
                Rnodes = [Rnodesx(:), nodesy(:)];
```

```
          Lnodesx(index) = nodesOuterx(index) - 2.*nodesOuterx(index)

          - CouplingL/2+2*xshift;

          Lnodes = [Lnodesx(:), nodesy(:)];

      end

      lenNr = length(Rnodes(:,1));

      %calculate nodes of coupling length

      x2couplingT = Rnodes(lenNr,1);

      x1couplingT = x2couplingT - CouplingL;

      y2couplingT = Rnodes(lenNr,2)+w/2;

      y1couplingT = y2couplingT - w;

      x2couplingB = Rnodes(1,1);

      x1couplingB = x2couplingB - CouplingL+ x1Shift_init;

      y2couplingB = Rnodes(1,2)+w/2;

      y1couplingB = y2couplingB - w;

      x1Line_init = -400;

      x1Line = x1Line_init + xshift;

      x2Line = x1Line_init+LofRaceTrack+10; %*CurrentNumofRaceTracks;

      y2Line = y1couplingB - gap;

      y1Line = y2Line- w;

      iG = iG+1;

  end

  if iRx > CurrentNumofRaceTracks/2 && (iR == 2 || iR ==1 || iR==4)  && w==2

      rectangle(x1couplingB-rOuter(iR)-offset*0.5, y1Line,x2couplingB-100,y2Line);

      rectangle(x2couplingB-100, y1Line-0.5,x2couplingB+rOuter(iR)+offset,y2Line+0.5);

      if iR==1

      AlignmentG=500

      else

      AlignmentG=250;

      end

      xshiftNext = 2*rOuter(iR)+CouplingL+offset-AlignmentG;
```

```
                        xshift = xshift+xshiftNext;
                else
                    wire(1,w,Rnodes); %Right half ring
                    rectangle(x1couplingT,y1couplingT,x2couplingT,y2couplingT);
                    rectangle(x1couplingB,y1couplingB,x2couplingB,y2couplingB);
                    wire(1,w,Lnodes); %Left half ring
                    rectangle(x1couplingB-rOuter(iR)-offset*0.5, y1Line,x2couplingB
                    +rOuter(iR)+offset*0.5,y2Line);
                    xshiftNext = 2*rOuter(iR)+CouplingL+offset;
                    xshift = xshift+xshiftNext;
                end
                 if iRx==1 && w==2
                     rectangle(-700, y1Line,x1couplingB-rOuter(iR)-offset*0.5,y2Line);
                     elseif iRx>=CurrentNumofRaceTracks/2 && w==3
                     rectangle(x2couplingB+rOuter(iR)+offset*0.5, y1Line,7600,y2Line);
                 end
            end
        end
         xshift = 0;
         if iR<lenR
         yshiftNext = rOuter(iR)+ rOuter(iR+1)+gap+2*w+offset;
         yshift = yshift + yshiftNext;
    end
end


%%%%%%%%%%%%%%%%%%%%%%%%%%% Script 01e %%%%%%%%%%%%%%%%%%%%%%%%%%%%%
%Create an angle vector between -90deg to 90deg, ex:100 angles
angle = linspace(-pi/2,pi/2,100);
offset = 80;
yshift = 0;
```

```
yshiftNext = 0;

xshift = 0;

%Create a radius vector giving a radius for each angle:

rInner = [200,180,160,150,100];%Radius for the inner circle

lenR = length(rInner);

width = [2,3];%rOuter-rInner;

lenw = length(width);

gapArray1 = [0.5,0.5,1,1,1.5,1.5,2,2,1,1,1.5,1.5,2,2];

gapArray2 = [1,1.5,1.5,1.5,2,2,1,1];

CouplingL = 150;

LofDye=6600;

x1Shift_init=0;

    for iR = 1:3;%lenR

        iG=1;

                for iw = 1:lenw

                w = width(iw);

                if w==2

                    gapArray=gapArray1;

                    lenG = length(gapArray);

                else

                    gapArray = gapArray2;

                    lenG = length(gapArray);

                end

                rOuter = width(iw)+rInner; %Radius for the outer circle for a given width

                %Calculate the nodes of a inner circle and an outer circle,

                nodesInnery = rInner(iR).*sin(angle)+yshift;

                nodesOutery = rOuter(iR).*sin(angle)+yshift;

                lenN = length(nodesInnery);

                Rnodes = [];

                Lnodes = [];
```

```
LofRaceTrack = rOuter(iR)*2+CouplingL+offset;

CurrentNumofRaceTracks= round(LofDye/(LofRaceTrack));

%Calculate the nodes of a half ring,

%i.e. a matrix with 2 columns and 1000 rows:

for iRx = 1:CurrentNumofRaceTracks/2+1

    gap = gapArray(iRx);

    if gap == 0.5 && w==2

        shiftUp = (gap - 0.5)+2*w;

    else

        shiftUp = (gap - 0.5)+2*w;

    end

nodesInnerx = rInner(iR).*cos(angle)+xshift;

nodesOuterx = rOuter(iR).*cos(angle)+xshift;

for index = 1:lenN

    if (nodesOuterx(index)-nodesInnerx(index))>= 0

        nodesy(index) = nodesOutery(index)+shiftUp;

        Rnodesx(index) = nodesOuterx(index)+CouplingL/2;

        Rnodes = [Rnodesx(:), nodesy(:)];

        Lnodesx(index) = nodesOuterx(index) - 2.*nodesOuterx(index)

        - CouplingL/2+2*xshift;

        Lnodes = [Lnodesx(:), nodesy(:)];

    end

    lenNr = length(Rnodes(:,1));

    %calculate nodes of coupling length

    x2couplingT = Rnodes(lenNr,1);

    x1couplingT = x2couplingT - CouplingL;

    y2couplingT = Rnodes(lenNr,2)+w/2;

    y1couplingT = y2couplingT - w;

    x2couplingB = Rnodes(1,1);

    x1couplingB = x2couplingB - CouplingL+ x1Shift_init;
```

```matlab
            y2couplingB = Rnodes(1,2)+w/2;

            y1couplingB = y2couplingB - w;

            x1Line_init = -400;

            x1Line = x1Line_init + xshift;

            x2Line = x1Line_init+LofRaceTrack+10; %*CurrentNumofRaceTracks;

            y2Line = y1couplingB - gap;

            y1Line = y2Line- w;

            iG = iG+1;

        end

        if iRx > CurrentNumofRaceTracks/2 &&  iR==4  && w==2

            rectangle(x1couplingB-rOuter(iR)-offset*0.5, y1Line,x2couplingB-100,y2Line);

            rectangle(x2couplingB-100, y1Line-0.5,x2couplingB+rOuter(iR)+offset,y2Line+0.5);

            xshiftNext = 2*rOuter(iR)+CouplingL+offset;

            xshift = xshift+xshiftNext;

        else

            wire(1,w,Rnodes); %Right half ring

            rectangle(x1couplingT,y1couplingT,x2couplingT,y2couplingT);

            rectangle(x1couplingB,y1couplingB,x2couplingB,y2couplingB);

            wire(1,w,Lnodes); %Left half ring

            rectangle(x1couplingB-rOuter(iR)-offset*0.5, y1Line,x2couplingB

            +rOuter(iR)+offset*0.5,y2Line);

            xshiftNext = 2*rOuter(iR)+CouplingL+offset;

            xshift = xshift+xshiftNext;

        end

         if iRx==1 && w==2

              rectangle(-700, y1Line,x1couplingB-rOuter(iR)-offset*0.5,y2Line);

              elseif iRx>=CurrentNumofRaceTracks/2 && w==3

              rectangle(x2couplingB+rOuter(iR)+offset*0.5, y1Line,7600,y2Line);

          end

    end
```

```
        end
         xshift = 0;
         if iR<lenR
         yshiftNext = rOuter(iR)+ rOuter(iR+1)+gap+2*w+offset;
         yshift = yshift + yshiftNext;
     end
end


%%%%%%%%%%%%%%%%%%%%%%% Script 01f %%%%%%%%%%%%%%%%%%%%%%%%%%
%Create an angle vector between -90deg to 90deg, ex:100 angles
angle = linspace(-pi/2,pi/2,100);
offset = 80;
yshift = 0;
yshiftNext = 0;
xshift = 0;
%Create a radius vector giving a radius for each angle:
rInner = [150];%Radius for the inner circle
lenR = length(rInner);
width = [2,3];%rOuter-rInner;
lenw = length(width);
gapArray1 = [0.5,0.5,1,1,1.5,1.5,2,2,1,1,1.5,1.5,2,2];
gapArray2 = [0.5,1,1.5,1.5,1.5,2,2,1,1];
CouplingL = 150;
LofDye=6600;
x1Shift_init=0;
    for iR = 1:lenR
        iG=1;
            for iw = 1:lenw
            w = width(iw);
            if w==2
```

```
        gapArray=gapArray1;

        lenG = length(gapArray);

    else

        gapArray = gapArray2;

        lenG = length(gapArray);

    end

    rOuter = width(iw)+rInner; %Radius for the outer circle for a given width

    %Calculate the nodes of a inner circle and an outer circle,

    nodesInnery = rInner(iR).*sin(angle)+yshift;

    nodesOutery = rOuter(iR).*sin(angle)+yshift;

    lenN = length(nodesInnery);

    Rnodes = [];

    Lnodes = [];

    LofRaceTrack = rOuter(iR)*2+CouplingL+offset;

    CurrentNumofRaceTracks= round(LofDye/(LofRaceTrack));

    %Calculate the nodes of a half ring,

    %i.e. a matrix with 2 columns and 1000 rows:

    for iRx = 1:CurrentNumofRaceTracks/2+1

        if iRx < CurrentNumofRaceTracks/2 && iR==2 && iRx==1

            xshift = xshift-50;

        end

         gap = gapArray(iRx);

         if gap == 0.5 && w==2

             shiftUp = (gap - 0.5)+2*w;

         else

             shiftUp = (gap - 0.5)+2*w;

         end

        nodesInnerx = rInner(iR).*cos(angle)+xshift;

        nodesOuterx = rOuter(iR).*cos(angle)+xshift;

        for index = 1:lenN
```

```matlab
            if (nodesOuterx(index)-nodesInnerx(index))>= 0

                nodesy(index) = nodesOutery(index)+shiftUp;

                Rnodesx(index) = nodesOuterx(index)+CouplingL/2;

                Rnodes = [Rnodesx(:), nodesy(:)];

                Lnodesx(index) = nodesOuterx(index) - 2.*nodesOuterx(index)

                - CouplingL/2+2*xshift;

                Lnodes = [Lnodesx(:), nodesy(:)];

            end

            lenNr = length(Rnodes(:,1));

            %calculate nodes of coupling length

            x2couplingT = Rnodes(lenNr,1);

            x1couplingT = x2couplingT - CouplingL;

            y2couplingT = Rnodes(lenNr,2)+w/2;

            y1couplingT = y2couplingT - w;

            x2couplingB = Rnodes(1,1);

            x1couplingB = x2couplingB - CouplingL+ x1Shift_init;

            y2couplingB = Rnodes(1,2)+w/2;

            y1couplingB = y2couplingB - w;

            x1Line_init = -400;

            x1Line = x1Line_init + xshift;

            x2Line = x1Line_init+LofRaceTrack+10; %*CurrentNumofRaceTracks;

            y2Line = y1couplingB - gap;

            y1Line = y2Line- w;

            iG = iG+1;

        end

        if iRx > CurrentNumofRaceTracks/2 && iR == 1  && w==2

            rectangle(x1couplingB-rOuter(iR)-offset*0.5, y1Line,x2couplingB-100,y2Line);

            rectangle(x2couplingB-100, y1Line-0.5,x2couplingB+rOuter(iR)+offset,y2Line+0.5);

            xshiftNext = 2*rOuter(iR)+CouplingL+offset-250;

            xshift = xshift+xshiftNext;
```

```
            else
                wire(1,w,Rnodes); %Right half ring
                rectangle(x1couplingT,y1couplingT,x2couplingT,y2couplingT);
                rectangle(x1couplingB,y1couplingB,x2couplingB,y2couplingB);
                wire(1,w,Lnodes); %Left half ring
                %rectangle(x1Line,y1Line,x2Line,y2Line);
                rectangle(x1couplingB-rOuter(iR)-offset*0.5, y1Line,x2couplingB
                +rOuter(iR)+offset*0.5,y2Line);
                xshiftNext = 2*rOuter(iR)+CouplingL+offset;
                xshift = xshift+xshiftNext;
            end
             if iRx==1 && w==2
                 rectangle(-700, y1Line,x1couplingB-rOuter(iR)-offset*0.5,y2Line);
                 elseif iRx>=CurrentNumofRaceTracks/2 && w==3
                 rectangle(x2couplingB+rOuter(iR)+offset*0.5, y1Line,7600,y2Line);
              end
          end
      end
       xshift = 0;
       if iR<lenR
      yshiftNext = rOuter(iR)+ rOuter(iR+1)+gap+2*w+offset;
      yshift = yshift + yshiftNext;
    end
end
```